Fully mixed virtual element schemes for steady-state poroelastic stress-assisted diffusion

Isaac Bermudez[*] Bryan Gómez-Vargas[†] Andrés E. Rubiano[‡] Ricardo Ruiz-Baier[§]

October 14, 2025

Abstract

We propose a fully mixed virtual element method for the numerical approximation of the coupling between stress-altered diffusion and linear elasticity equations with strong symmetry of total poroelastic stress (using the Hellinger–Reissner principle). A novelty of this work is that we introduce a less restrictive assumption on the stress-assisted diffusion coefficient, requiring an analysis of the perturbed diffusion equation using Banach spaces. The solvability of the continuous and discrete problems is established using a suitable modification of the abstract theory for perturbed saddle-point problems in Banach spaces (which is in itself a new result of independent interest). In addition, we establish optimal a priori error estimates. The method and its analysis are robust with respect to the poromechanical parameters. We also include a number of numerical examples that illustrate the properties of the proposed scheme.

MSC (2010): 65N30; 65N15; 74D05.

Keywords: Coupled elasticity-diffusion; Mixed virtual element methods; Stress-based formulations; Error estimates.

1 Introduction

Scope. Mechanical deformations and the diffusion of solutes occur concurrently in various real-world problems, such as those found in metallurgy, geomechanics, and biomedicine. In certain specific applications, the interaction mechanisms involve stress altering the microstructure of the material. This phenomenon is referred to as stress-assisted diffusion, and a number of contributions are available for the analysis and discretisations of that problem in a variety of forms [27–29]. When the underlying medium is poroelastic the coupling implies that the effective poroelastic stress contains contributions from the fluid pressure and also from the diffusive quantity. The equations of poroelastic stress-assisted diffusion have been analysed numerically with mixed finite element formulations in [33] (see also a similar treatment for poroelasticity-heat equations in the recent work [16], as well as twofold saddle-point formulations for poroelasticity equations with nonlinear permeability [36, 39]).

The present work proposes a momentum and mass conservative, robust, and Biot-locking-free virtual element formulation for poroelastic stress-assisted diffusion systems. It constitutes an extension of the stress-assisted diffusion VEM scheme from [37] to the fully mixed poroelastic setting. The underlying model problem is based on [16, 33], but the formulation is simpler as it is based on the Hellinger–Reissner variational principle and imposing strong symmetry of the total Cauchy stress. For this we follow the similar works [1, 3, 22]. In this context we also mention other recent polytopal discretisations for poroelasticity in mixed form, as proposed in [10, 12, 20, 23, 34, 37, 38, 40, 41, 44].

As the continuous formulation is also novel, we conduct its well-posedness analysis treating the linear diffusion-stress coupling terms as a perturbation of two perturbed saddle-point problems. For the stress-assisted diffusion nonlinearity we use a fixed-point argument based on Banach's contraction mapping theorem, and combine this with two applications of the Babuška–Brezzi theory for perturbed saddle-points in [8, Chapter 4] and the Banach–Nečas–Babuška theory for global inf-sup conditions. The analysis requires uniform Lipschitz continuity on the nonlinearity as well as a small data

[*]Sección de Matemática, Sede de Occidente, Universidad de Costa Rica, San Ramón, Alajuela, Costa Rica. Email: isaac.bermudez@ucr.ac.cr.
[†]Sección de Matemática, Sede de Occidente, Universidad de Costa Rica, San Ramón, Alajuela, Costa Rica. Email: bryan.gomezvargas@ucr.ac.cr.
[‡]School of Mathematics, Monash University, 9 Rainforest Walk, Clayton 3800 VIC, Australia. Email: andres.rubianomartinez@monash.edu.
[§]School of Mathematics, Monash University, 9 Rainforest Walk, Clayton 3800 VIC, Australia; and Universidad Adventista de Chile, Casilla 7-D, Chillán, Chile. Email: ricardo.ruizbaier@monash.edu.

assumption – a byproduct of using Banach fixed-point theory. However, and in contrast to previous analysis for stress-assisted diffusion and nonlinear Biot systems in [27, 36, 37, 39], here we only require the Lipschitz continuity of the inverse stress-assistance in $\mathbb{L}^2(\Omega)$, which is a much more reasonable assumption. The price to pay is that now our diffusive flux trial and test functions are sought in $\mathbf{L}^4(\Omega)$, requiring a slightly more involved inf-sup condition, and to invoke a modified abstract result for saddle-point problems in Banach spaces. However, the specific structure of this perturbed saddle-point problem does not fall in the framework of [19, Theorems 3.1 and 3.4]. These results require the main diagonal block (in our case, the flux-flux bilinear form) to be coercive on the kernel of the off-diagonal operator, and this condition is not met in our case. On the other hand, the recent result in [17, Theorem 3.2] assumes that the main form is elliptic on the entire space, which is also not the case for our flux-flux bilinear form. Nevertheless, we observe that the present formulation possesses a dual structure: the perturbation block (the lower diagonal block) is induced by a bilinear form that is elliptic on the whole space. Therefore we introduce a new abstract stability result—symmetric to [17, Theorem 3.2]—which is tailored for the structure of the present problem.

The proposed formulation for Biot–stress-assisted diffusion is robust and conservative, and at the same time has fewer unknowns than those used in [33]. Another important advantage of the analysis presented herein is that we are able to establish in a straightforward manner the uniqueness of the discrete solution. This is a difficult task as observed in previous works [27–29, 33]. There, the solvability analysis of the continuous fixed-point scheme relies on regularity assumptions on the exact solutions. In particular, in that Hilbert context it was possible to control (under small data assumptions) the diffusive flux in the $\mathrm{L}^\infty-$norm. The same holds in Banach spaces (using a primal formulation for the diffusion equation), but in the $\mathrm{L}^{\frac{2r}{2-r}}-$norm, where r is such that $2d/(d+1) - \varepsilon < r < 2$ with $\varepsilon > 0$. In both situations, such bounds enabled the direct application of Banach's Fixed Point Theorem. In contrast, at the discrete level, the additional regularity was not ensured; and as a result, we could not establish the Lipschitz continuity—and thus the contractivity—of the fixed-point operator in a direct way.

In the present work, by formulating the problem in Banach spaces and introducing a suitable fixed-point operator, we obtain bounds in the associated norms that provide the necessary control on the data. Importantly, these bounds do not rely on additional regularity assumptions and apply both at the discrete and continuous levels, thus allowing the use of more natural smallness conditions and the application of Banach's fixed-point theory.

Outline. The remainder of the paper has been organised in the following manner. In the rest of this section we recall usual notational convention for the domain and the used functional spaces. We also state the governing equations of Biot–stress-assisted diffusion, giving also assumptions on the nonlinear diffusion coefficient and the rest of the model parameters. Section 2 contains the derivation of the weak formulation in double saddle-point structure, it specifies the splitting of kernels of suitable operators, and it examines the properties of all bilinear forms (including stability and boundedness). This section also addresses the unique solvability of the separate Biot and mixed diffusion problems, and proving an auxiliary abstract result for perturbed saddle-point problems in Banach spaces. In Section 3 we construct the virtual element discretisation of the coupled model problem, introducing the needed discrete spaces, polynomial interpolation and projection operators, appropriate stabilisation, and discrete operators. In Section 4 we show that the scheme is well-posed using a similar fixed-point argument as in the continuous case. A priori error estimates are presented in Section 5, and simple numerical tests are provided in Section 6, including the verification of optimal convergence, simulation of classical benchmark tests for poromechanics, and a specific application for stress-assisted diffusion.

Recurrent notation. Let us consider a simply connected bounded and Lipschitz domain $\Omega \subset \mathbb{R}^d$, $d \in \{2,3\}$ occupied by a poroelastic body. The domain boundary $\partial\Omega$ is partitioned into disjoint sub-boundaries where homogeneous displacement and traction-type boundary conditions are imposed $\partial\Omega := \overline{\Gamma_{\mathrm{D}}} \cup \overline{\Gamma_{\mathrm{N}}}$, and it is assumed for sake of simplicity that both sub-boundaries are non-empty $|\Gamma_{\mathrm{D}}| \cdot |\Gamma_{\mathrm{N}}| > 0$. Throughout the text, given a normed space S, by $\mathbf{S}$ and $\mathbb{S}$ we will denote the vector and tensor extensions S^d and $S^{d\times d}$, respectively. We define the Hilbert spaces $\mathbf{H}(\mathrm{div},\Omega) = \big\{\boldsymbol{w} \in \mathbf{L}^2(\Omega) : \mathrm{div}\,\boldsymbol{w} \in \mathrm{L}^2(\Omega)\big\}$ and $\mathbf{H}_{\mathrm{N}}(\mathrm{div},\Omega) := \{\boldsymbol{w} \in \mathbf{H}(\mathrm{div},\Omega) : \boldsymbol{w}\cdot\boldsymbol{n} = 0 \text{ on } \Gamma_{\mathrm{N}}\}$ with its norm $\|\boldsymbol{w}\|^2_{\mathrm{div},\Omega} := \|\boldsymbol{w}\|^2_{0,\Omega} + \|\mathrm{div}\,\boldsymbol{w}\|^2_{0,\Omega}$. We also define the Banach spaces $\mathbf{H}^4(\mathrm{div},\Omega) = \{\boldsymbol{w} \in \mathbf{L}^4(\Omega) : \mathrm{div}\,\boldsymbol{w} \in \mathrm{L}^2(\Omega)\}$ and $\mathbf{H}^4_{\mathrm{N}}(\mathrm{div},\Omega) := \{\boldsymbol{w} \in \mathbf{H}^4(\mathrm{div},\Omega) : \boldsymbol{w}\cdot\boldsymbol{n} = 0 \text{ on } \Gamma_{\mathrm{N}}\}$, both endowed with the norm $\|\boldsymbol{\xi}\|_{4,\mathrm{div};\Omega} := \|\boldsymbol{\xi}\|_{0,4;\Omega} + \|\mathrm{div}\,\boldsymbol{\xi}\|_{0,\Omega}$. Next, we recall the definition of the tensorial Hilbert spaces $\mathbb{H}(\mathbf{div},\Omega) = \{\boldsymbol{\tau} \in \mathbb{L}^2(\Omega) : \mathbf{div}\,\boldsymbol{\tau} \in \mathbf{L}^2(\Omega)\}$, $\mathbb{H}(\mathbf{curl},\Omega) = \big\{\boldsymbol{\tau} \in \mathbb{L}^2(\Omega) : \mathbf{curl}\,\boldsymbol{\tau} \in \mathbb{L}^2(\Omega)\big\}$, with their usual norms $\|\boldsymbol{\tau}\|^2_{\mathbf{div},\Omega} := \|\boldsymbol{\tau}\|^2_{0,\Omega} + \|\mathbf{div}\,\boldsymbol{\tau}\|^2_{0,\Omega}$, $\|\boldsymbol{\tau}\|^2_{\mathbf{curl},\Omega} := \|\boldsymbol{\tau}\|^2_{0,\Omega} + \|\mathbf{curl}\,\boldsymbol{\tau}\|^2_{0,\Omega}$, where the divergence acts on the rows of $\boldsymbol{\tau}$, and the curl of a tensor is here understood as the tensor formed by the curl of the rows of $\boldsymbol{\tau}$. We also define the following tensor space

$$\mathbb{H}^{\mathrm{sym}}_{\mathrm{N}}(\mathbf{div},\Omega) := \left\{\boldsymbol{\tau}\in\mathbb{H}(\mathbf{div},\Omega):\ \boldsymbol{\tau}=\boldsymbol{\tau}^{\mathrm{t}},\ \boldsymbol{\tau}\boldsymbol{n}=\mathbf{0} \text{ on } \Gamma_{\mathrm{N}}\right\},$$

which is Hilbert with the $\mathbb{H}(\mathbf{div})$ norm. Also, given a domain $\mathcal{O}$ (in $\mathbb{R}^d$ or $\mathbb{R}^{d-1}$) we denote the inner product in $\mathrm{L}^2(\mathcal{O})$ (similarly for $\mathbf{L}^2(\mathcal{O})$ and $\mathbb{L}^2(\mathcal{O})$) by $(\bullet,\bullet)_{\mathcal{O}}$. When $\mathcal{O}=\Omega$ we simply write $(\bullet,\bullet)$.

Finally, throughout the paper, when comparing two quantities a and b, we use the notation $a\lesssim b$ to indicate that there exists a constant M, independent of the mesh size h, such that $a\leq Mb$.

Strong mixed form. Let us recall that the steady-state Biot system states momentum and mass balances

$$\begin{aligned} -\mathbf{div}\,\boldsymbol{\sigma} &= \boldsymbol{f} \quad \text{in } \Omega,\\ s_0 p + \alpha\operatorname{div}\boldsymbol{u} - \operatorname{div}(\boldsymbol{\kappa}\nabla p) &= g \quad \text{in } \Omega, \end{aligned}$$

respectively, where $\boldsymbol{\sigma}=2\mu\boldsymbol{\varepsilon}(\boldsymbol{u})+(\lambda\operatorname{div}(\boldsymbol{u})-\alpha p-\beta\varphi)\mathbb{I}$ is the poroelastic Cauchy stress tensor including a modulation due to a diffusing quantity φ, α is the Biot–Willis parameter, β is the modulation intensity, s_0 is the storativity coefficient, $\boldsymbol{\kappa}$ is a symmetric and positive-definite tensor of permeability of the porous media (scaled by the fluid viscosity), i.e., there exist two strictly positive real numbers κ_1 and κ_2 satisfying for a.e. $\boldsymbol{x}\in\Omega$ and all $\boldsymbol{\xi}\in\mathbb{R}^d$ such that $|\boldsymbol{\xi}|=1$

$$0<\kappa_1\leq\boldsymbol{\kappa}(\boldsymbol{x})\boldsymbol{\xi}\cdot\boldsymbol{\xi}\leq\kappa_2.$$

The coefficients λ,μ are the Lamé parameters of Hooke's law, $\boldsymbol{f}:\Omega\to\mathbb{R}^d$ is the vector field of body loads and $g:\Omega\to\mathbb{R}$ is a scalar source/sink of fluid, and $\boldsymbol{\varepsilon}(\boldsymbol{u})=\frac{1}{2}(\boldsymbol{\nabla}\boldsymbol{u}+(\boldsymbol{\nabla}\boldsymbol{u})^{\mathrm{t}})$ is the infinitesimal strain tensor.

In addition to the mixed Biot equations, we also consider the presence of a solvent within the poroelastic domain. We denote its concentration by $\varphi:\Omega\to\mathbb{R}$ and its movement in the body for given volumetric source ℓ is governed by

$$\varphi-\operatorname{div}(\varrho(\boldsymbol{\sigma})\nabla\varphi)=\ell \qquad \text{in } \Omega, \tag{1.1}$$

with mixed boundary condition $\varphi=\varphi_{\mathrm{D}}$ on Γ_{D} and $\varrho(\boldsymbol{\sigma})\nabla\varphi\cdot\boldsymbol{n}=0$ on Γ_{N}. The scalar function $\varrho:\mathbb{R}^{d\times d}\to\mathbb{R}$ is a stress-dependent diffusivity accounting for altered diffusion acting in the poroelastic domain and indicating a change in microstructure due to poroelastic stress generation. We assume that this term takes the form

$$\varrho(\boldsymbol{\sigma})=\eta_0\varrho_0+\exp(-\eta_1[\operatorname{tr}\boldsymbol{\sigma}]^2), \tag{1.2}$$

where $\varrho_0>0$ is the base-line effective diffusion (in the absence of stress assistance) and η_0,η_1 are positive modulation parameters (the treatment can also be modified to accommodate for anisotropy with a tensor-valued diffusivity). For sake of the analysis, we require $\varrho^{-1}(\bullet)$ to be uniformly bounded away from zero and Lipschitz continuous with respect to $\boldsymbol{\sigma}\in\mathbb{L}^2(\Omega)$. More precisely, there exist positive constants ϱ_1, ϱ_2 and L_ϱ, such that

$$0<\varrho_1\leq\varrho^{-1}(\bullet)\leq\varrho_2<\infty \quad \text{and} \quad \|\varrho^{-1}(\boldsymbol{\sigma})-\varrho^{-1}(\boldsymbol{\tau})\|_{0,\Omega}\leq L_\varrho\|\boldsymbol{\sigma}-\boldsymbol{\tau}\|_{0,\Omega}, \tag{1.3}$$

for all $\boldsymbol{\sigma},\boldsymbol{\tau}\in\mathbb{L}^2(\Omega)$. The material properties are described at each point by the compliance tensor (the inverse of the fourth-order linear isotropic stiffness tensor $\mathcal{C}$) $\mathcal{C}^{-1}$, which is identified as a symmetric, bounded, and uniformly positive definite linear operator characterised by its action

$$\mathcal{C}\boldsymbol{\varepsilon}(\boldsymbol{u})=2\mu\boldsymbol{\varepsilon}(\boldsymbol{u})+\lambda(\operatorname{div}\boldsymbol{u})\mathbb{I}, \qquad \mathcal{C}^{-1}\boldsymbol{\sigma}=\frac{1}{2\mu}\left(\boldsymbol{\sigma}-\frac{\lambda}{2\mu+d\lambda}\operatorname{tr}(\boldsymbol{\sigma})\mathbb{I}\right),$$

and $\boldsymbol{\sigma}=\mathcal{C}\boldsymbol{\varepsilon}(\boldsymbol{u})-\{\alpha p+\beta\varphi\}\mathbb{I}$ to obtain $\mathcal{C}^{-1}(\boldsymbol{\sigma}+\{\alpha p+\beta\varphi\}\mathbb{I})=\boldsymbol{\varepsilon}(\boldsymbol{u})$.

The problem is rewritten, considering the elasticity equations with strong symmetric stress imposition, which are coupled with the fluid phase obeying Darcy's law for filtration in porous media, and a mixed form associated with (1.1). The unknowns are the effective poroelastic Cauchy stress tensor $\boldsymbol{\sigma}$, the displacement vector $\boldsymbol{u}$, the filtration flux vector $\boldsymbol{z}$, the fluid pressure p, the diffusive flux $\boldsymbol{\zeta}$, and the concentration φ such that

$$\mathcal{C}^{-1}\boldsymbol{\sigma}=\boldsymbol{\varepsilon}(\boldsymbol{u})-\frac{\alpha p+\beta\varphi}{2\mu+d\lambda}\mathbb{I} \quad \text{in } \Omega, \tag{1.4a}$$

$$
\begin{aligned}
-\operatorname{\mathbf{div}} \boldsymbol{\sigma} &= \boldsymbol{f} && \text{in } \Omega, && \text{(1.4b)}\\
\boldsymbol{\sigma} &= \boldsymbol{\sigma}^{\mathrm{t}} && \text{in } \Omega, && \text{(1.4c)}\\
\boldsymbol{\kappa}^{-1}\boldsymbol{z} + \nabla p &= \mathbf{0} && \text{in } \Omega, && \text{(1.4d)}\\
s_0 p + \alpha \operatorname{tr} \mathcal{C}^{-1}[\boldsymbol{\sigma} + (\alpha p + \beta\varphi)\mathbb{I}] + \operatorname{div} \boldsymbol{z} &= g && \text{in } \Omega, && \text{(1.4e)}\\
\varrho(\boldsymbol{\sigma})^{-1}\boldsymbol{\zeta} + \nabla\varphi &= \mathbf{0} && \text{in } \Omega, && \text{(1.4f)}\\
\varphi + \operatorname{div} \boldsymbol{\zeta} &= \ell && \text{in } \Omega, && \text{(1.4g)}\\
\boldsymbol{u} = \boldsymbol{u}_{\mathrm{D}}, \quad p = p_{\mathrm{D}}, \quad \varphi &= \varphi_{\mathrm{D}} && \text{on } \Gamma_{\mathrm{D}}, && \text{(1.4h)}\\
\boldsymbol{\sigma}\boldsymbol{n} = \mathbf{0}, \quad \boldsymbol{z}\cdot\boldsymbol{n} = 0, \quad \boldsymbol{\zeta}\cdot\boldsymbol{n} &= 0 && \text{on } \Gamma_{\mathrm{N}}, && \text{(1.4i)}
\end{aligned}
$$

(stating a rescaling of the stress constitutive relation, the balance of linear momentum, the balance of angular momentum, Darcy's law, the balance of the total amount of fluid, the constitutive equation for the diffusive flux, the concentration balance, and the mixed-loading boundary conditions of homogeneous type, respectively).

2 Weak formulation and continuous well-posedness analysis

The functional structure of the coupled problem (1.4) is developed next. In particular, the ordering of the unknowns for the fluid part of the problem are reversed from their typical form. This section also contains the analysis of existence and uniqueness of weak solution by means of Banach's fixed-point theorem, complemented by an abstract result required to establish the unique solvability of the diffusion sub-problem.

2.1 Derivation and main properties

We apply algebraic manipulations and multiply the strong form of the balance equations and constitutive relations by suitable test functions, integrate by parts in the constitutive relations and in the diffusion term, and employ the boundary conditions to obtain the weak formulation: for $\boldsymbol{f} \in \mathbf{L}^2(\Omega)$, $g, \ell \in \mathrm{L}^2(\Omega)$, $\boldsymbol{u}_{\mathrm{D}} \in \mathbf{H}^{1/2}_{00}(\Gamma_{\mathrm{D}})$, and $p_{\mathrm{D}}, \varphi_{\mathrm{D}} \in \mathrm{H}^{1/2}_{00}(\Gamma_{\mathrm{D}})$; find $(\boldsymbol{\sigma}, p, \boldsymbol{u}, \boldsymbol{z}, \boldsymbol{\zeta}, \varphi) \in \mathbb{H}^{\mathrm{sym}}_{\mathrm{N}}(\mathbf{div}, \Omega) \times \mathrm{L}^2(\Omega) \times \mathbf{L}^2(\Omega) \times \mathbf{H}_{\mathrm{N}}(\mathrm{div}, \Omega) \times \mathbf{H}^4_{\mathrm{N}}(\mathrm{div}, \Omega) \times \mathrm{L}^2(\Omega)$ such that

$$
\begin{aligned}
(\mathcal{C}^{-1}\boldsymbol{\sigma}, \boldsymbol{\tau}) + \big(\frac{\alpha p}{2\mu + d\lambda}, \operatorname{tr}\boldsymbol{\tau}\big) + (\operatorname{\mathbf{div}}\boldsymbol{\tau}, \boldsymbol{u}) + \big(\frac{\beta\varphi}{2\mu + d\lambda}, \operatorname{tr}\boldsymbol{\tau}\big) &= \langle \boldsymbol{u}_{\mathrm{D}}, \boldsymbol{\tau}\boldsymbol{n}\rangle_{\Gamma_{\mathrm{D}}} && \forall \boldsymbol{\tau} \in \mathbb{H}^{\mathrm{sym}}_{\mathrm{N}}(\mathbf{div},\Omega), && \text{(2.1a)}\\
(\operatorname{tr}\boldsymbol{\sigma}, \frac{\alpha q}{2\mu + d\lambda}) + \big[s_0 + \frac{d\alpha^2}{2\mu + d\lambda}\big](p, q) + (q, \operatorname{div}\boldsymbol{z}) + \alpha\big(\frac{d\beta\varphi}{2\mu + d\lambda}, q\big) &= (g, q) && \forall q \in \mathrm{L}^2(\Omega), && \text{(2.1b)}\\
(\operatorname{\mathbf{div}}\boldsymbol{\sigma}, \boldsymbol{v}) &= -(\boldsymbol{f}, \boldsymbol{v}) && \forall \boldsymbol{v} \in \mathbf{L}^2(\Omega), && \text{(2.1c)}\\
(\boldsymbol{\kappa}^{-1}\boldsymbol{z}, \boldsymbol{w}) - (p, \operatorname{div}\boldsymbol{w}) &= -\langle p_{\mathrm{D}}, \boldsymbol{w}\cdot\boldsymbol{n}\rangle_{\Gamma_{\mathrm{D}}} && \forall \boldsymbol{w} \in \mathbf{H}_{\mathrm{N}}(\mathrm{div},\Omega), && \text{(2.1d)}\\
(\varrho(\boldsymbol{\sigma})^{-1}\boldsymbol{\zeta}, \boldsymbol{\xi}) - (\varphi, \operatorname{div}\boldsymbol{\xi}) &= -\langle \varphi_{\mathrm{D}}, \boldsymbol{\xi}\cdot\boldsymbol{n}\rangle_{\Gamma_{\mathrm{D}}} && \forall \boldsymbol{\xi} \in \mathbf{H}^4_{\mathrm{N}}(\mathrm{div},\Omega), && \text{(2.1e)}\\
-(\psi, \operatorname{div}\boldsymbol{\zeta}) - (\varphi, \psi) &= -(\ell, \psi) && \forall \psi \in \mathrm{L}^2(\Omega), && \text{(2.1f)}
\end{aligned}
$$

where the ordering of the unknowns obeys to the subsequent structure of the analysis. Indeed, we group the Biot function spaces as well as trial and test functions for stress-pressure and displacement-discharge flux as follows

$$
\mathbb{V} := \mathbb{H}^{\mathrm{sym}}_{\mathrm{N}}(\mathbf{div}, \Omega) \times \mathrm{L}^2(\Omega), \quad \mathbf{Q} := \mathbf{L}^2(\Omega) \times \mathbf{H}_{\mathrm{N}}(\mathrm{div}, \Omega),
$$

(endowed with the canonical graph norms of the product spaces) and

$$
\vec{\boldsymbol{\sigma}} := (\boldsymbol{\sigma}, p),\ \vec{\boldsymbol{\tau}} := (\boldsymbol{\tau}, q) \in \mathbb{V}, \quad \text{and} \quad \vec{\boldsymbol{u}} := (\boldsymbol{u}, \boldsymbol{z}),\ \vec{\boldsymbol{v}} := (\boldsymbol{v}, \boldsymbol{w}) \in \mathbf{Q},
$$

respectively. Then, (2.1) consists in finding $(\vec{\boldsymbol{\sigma}}, \vec{\boldsymbol{u}}) \in \mathbb{V} \times \mathbf{Q}$ and $(\boldsymbol{\zeta}, \varphi) \in \mathbf{H}^4_{\mathrm{N}}(\mathrm{div}, \Omega) \times \mathrm{L}^2(\Omega)$, such that

$$
\begin{aligned}
A(\vec{\boldsymbol{\sigma}}, \vec{\boldsymbol{\tau}}) + B(\vec{\boldsymbol{\tau}}, \vec{\boldsymbol{u}}) + D(\varphi, \vec{\boldsymbol{\tau}}) &= F(\vec{\boldsymbol{\tau}}) && \forall \vec{\boldsymbol{\tau}} \in \mathbb{V}, && \text{(2.2a)}\\
B(\vec{\boldsymbol{\sigma}}, \vec{\boldsymbol{v}}) - C(\vec{\boldsymbol{u}}, \vec{\boldsymbol{v}}) &= G(\vec{\boldsymbol{v}}) && \forall \vec{\boldsymbol{v}} \in \mathbf{Q}, && \text{(2.2b)}\\
a_{\boldsymbol{\sigma}}(\boldsymbol{\zeta}, \boldsymbol{\xi}) + b(\boldsymbol{\xi}, \varphi) &= H(\boldsymbol{\xi}) && \forall \boldsymbol{\xi} \in \mathbf{H}^4_{\mathrm{N}}(\mathrm{div}, \Omega), && \text{(2.2c)}
\end{aligned}
$$

$$b(\boldsymbol{\zeta},\psi) - c(\varphi,\psi) = I(\psi) \qquad \forall \psi \in \mathrm{L}^2(\Omega), \tag{2.2d}$$

where the bilinear forms $A : \mathbb{V} \times \mathbb{V} \to \mathbb{R}$, $B : \mathbb{V} \times \mathbf{Q} \to \mathbb{R}$, $C : \mathbf{Q} \times \mathbf{Q} \to \mathbb{R}$, $D : \mathrm{L}^2(\Omega) \times \mathbb{V} \to \mathbb{R}$, $b : \mathbf{H}^4_{\mathrm{N}}(\mathrm{div},\Omega) \times \mathrm{L}^2(\Omega) \to \mathbb{R}$, $c : \mathrm{L}^2(\Omega) \times \mathrm{L}^2(\Omega) \to \mathbb{R}$, and (for a given $\widehat{\boldsymbol{\sigma}} \in \mathbb{L}^2(\Omega)$) the bilinear form $a_{\widehat{\boldsymbol{\sigma}}} : \mathbf{H}^4_{\mathrm{N}}(\mathrm{div},\Omega) \times \mathbf{H}^4_{\mathrm{N}}(\mathrm{div},\Omega) \to \mathbb{R}$, are defined as

$$A(\vec{\boldsymbol{\sigma}},\vec{\boldsymbol{\tau}}) := (\mathcal{C}^{-1}\boldsymbol{\sigma},\boldsymbol{\tau}) + \big(\frac{\alpha p}{2\mu + d\lambda}, \operatorname{tr}\boldsymbol{\tau}\big) + \big(\frac{\alpha q}{2\mu + d\lambda}, \operatorname{tr}\boldsymbol{\sigma}\big) + \left[s_0 + \frac{d\alpha^2}{2\mu + d\lambda}\right](p,q),$$
$$B(\vec{\boldsymbol{\tau}},\vec{\boldsymbol{v}}) := (\boldsymbol{v}, \mathbf{div}\,\boldsymbol{\tau}) + (q, \operatorname{div}\boldsymbol{w}), \quad C(\vec{\boldsymbol{u}},\vec{\boldsymbol{v}}) := (\boldsymbol{\kappa}^{-1}\boldsymbol{z},\boldsymbol{w}), \quad D(\psi,\vec{\boldsymbol{\tau}}) := \big(\frac{\beta\psi}{2\mu + d\lambda}, \operatorname{tr}\boldsymbol{\tau} + \alpha d q\big),$$
$$a_{\widehat{\boldsymbol{\sigma}}}(\boldsymbol{\zeta},\boldsymbol{\xi}) := (\varrho(\widehat{\boldsymbol{\sigma}})^{-1}\boldsymbol{\zeta},\boldsymbol{\xi}), \quad b(\boldsymbol{\xi},\psi) := -(\psi, \operatorname{div}\boldsymbol{\xi}), \quad c(\varphi,\psi) := (\varphi,\psi).$$

Similarly, the linear functionals $F : \mathbb{V} \to \mathbb{R}$, $G : \mathbf{Q} \to \mathbb{R}$, $H : \mathbf{H}^4_{\mathrm{N}}(\mathrm{div},\Omega) \to \mathbb{R}$, and $I : \mathrm{L}^2(\Omega) \to \mathbb{R}$ are

$$F(\vec{\boldsymbol{\tau}}) := \langle \boldsymbol{u}_{\mathrm{D}}, \boldsymbol{\tau}\boldsymbol{n}\rangle_{\Gamma_{\mathrm{D}}} + (g,q), \quad G(\vec{\boldsymbol{v}}) := -(\boldsymbol{f},\boldsymbol{v}) - \langle p_{\mathrm{D}}, \boldsymbol{w}\cdot\boldsymbol{n}\rangle_{\Gamma_{\mathrm{D}}},$$
$$H(\boldsymbol{\xi}) := -\langle \varphi_{\mathrm{D}}, \boldsymbol{\xi}\cdot\boldsymbol{n}\rangle_{\Gamma_{\mathrm{D}}}, \quad I(\psi) := -(\ell,\psi).$$

We proceed to examine the properties of the bilinear forms and linear functionals. As an intermediate step we denote by $\mathbf{B}$ and $\mathbf{B}^*$ the operators induced by the bilinear form $B(\bullet,\bullet)$; and by $\mathbf{b}$ and $\mathbf{b}^*$ of the operators induced by the bilinear form $b(\bullet,\bullet)$. Their kernels admit the following characterisations:

$$\begin{aligned}\mathbb{V}_0 &:= \ker(\mathbf{B}) = \{\vec{\boldsymbol{\tau}} \in \mathbb{V} :\ B(\vec{\boldsymbol{\tau}},\vec{\boldsymbol{v}}) = 0,\ \forall \vec{\boldsymbol{v}} \in \mathbf{Q}\}\\ &=: \mathbb{V}_{01} \times \mathbb{V}_{02} \equiv \{\boldsymbol{\tau} \in \mathbb{H}^{\mathrm{sym}}_{\mathrm{N}}(\mathbf{div},\Omega) :\ \mathbf{div}\,\boldsymbol{\tau} = \mathbf{0} \text{ in } \Omega\} \times \{0\},\end{aligned} \tag{2.3a}$$
$$\begin{aligned}\mathbf{Q}_0 &:= \ker(\mathbf{B}^*) = \{\vec{\boldsymbol{v}} \in \mathbf{Q} :\ B(\vec{\boldsymbol{\tau}},\vec{\boldsymbol{v}}) = 0,\ \forall \vec{\boldsymbol{\tau}} \in \mathbb{V}\}\\ &=: \mathbf{Q}_{01} \times \mathbf{Q}_{02} \equiv \{\mathbf{0}\} \times \{\boldsymbol{w} \in \mathbf{H}_{\mathrm{N}}(\mathrm{div},\Omega) :\ \operatorname{div}\boldsymbol{w} = 0 \text{ in } \Omega\}.\end{aligned} \tag{2.3b}$$

The characterisation of $\mathbb{V}_{02}$ (and similarly for $\mathbf{Q}_{01}$) follows as in [18, Section 3.3]. It is possible to realise that $\nabla q = \mathbf{0}$ in the distributional sense, which gives $q \in \mathrm{H}^1(\Omega)$. Moreover, integrating by parts $(q, \operatorname{div}\boldsymbol{w})$ in (2.3b), we arrive at $\langle \boldsymbol{w}\cdot\boldsymbol{n}, q\rangle_{\Gamma_{\mathrm{D}}} = 0$ for all $\boldsymbol{w} \in \mathbf{H}_{\mathrm{N}}(\mathrm{div},\Omega)$. Next, using the surjectivity of the normal trace from $\mathbf{H}_{\mathrm{N}}(\mathrm{div},\Omega)$ onto $\mathrm{H}^{-1/2}_{00}(\Gamma_{\mathrm{D}})$ (cf. [25, Lemma 51.5]), yields $q = 0$ on Γ_{D}, and hence $q \in \mathrm{H}^1_{\mathrm{D}}(\Omega)$.

In turn, the spaces $\mathbb{V}^{\perp}_{01}$, $\mathbb{V}^{\perp}_{02}$, $\mathbf{Q}^{\perp}_{01}$ and $\mathbf{Q}^{\perp}_{02}$ are characterised as follows:

$$\mathbb{V}^{\perp}_{01} \equiv \{\boldsymbol{\sigma} \in \mathbb{H}^{\mathrm{sym}}_{\mathrm{N}}(\mathbf{div},\Omega) :\ (\boldsymbol{\sigma},\boldsymbol{\tau}) = 0,\ \forall \boldsymbol{\tau} \in \mathbb{V}_{01}\}, \quad \mathbb{V}^{\perp}_{02} \equiv \mathrm{L}^2(\Omega),$$
$$\mathbf{Q}^{\perp}_{01} \equiv \mathbf{L}^2(\Omega), \quad \mathbf{Q}^{\perp}_{02} \equiv \{\boldsymbol{z} \in \mathbf{H}_{\mathrm{N}}(\mathrm{div},\Omega) :\ (\boldsymbol{z},\boldsymbol{w}) = 0,\ \forall \boldsymbol{w} \in \mathbf{Q}_{02}\},$$

and hence $\mathbb{V}^{\perp}_0 = \mathbb{V}^{\perp}_{01} \times \mathbb{V}^{\perp}_{02}$ and $\mathbf{Q}^{\perp}_0 = \mathbf{Q}^{\perp}_{01} \times \mathbf{Q}^{\perp}_{02}$ are closed subspaces of $\mathbb{V}$ and $\mathbf{Q}$, respectively.

For the diffusion block, the well-posedness analysis will rely on an abstract result (to be proven later in Theorem 2.5) for which the main bilinear form $a_{\widehat{\boldsymbol{\sigma}}}(\bullet,\bullet)$ only needs to be positive semi-definite on the whole space $\mathbf{H}^4_{\mathrm{N}}(\mathrm{div},\Omega)$ but the perturbed bilinear term, i.e., $c(\bullet,\bullet)$ is required to be elliptic on the whole space $\mathrm{L}^2(\Omega)$. This new theoretical framework does not require a restriction to the kernel of $\mathbf{b}$, and thus its characterisation is not necessary for the subsequent analysis.

Lemma 2.1 (boundedness of the bilinear forms) *The bilinear forms $A(\bullet,\bullet)$, $B(\bullet,\bullet)$, $C(\bullet,\bullet)$, $D(\bullet,\bullet)$, $a_{\widehat{\boldsymbol{\sigma}}}(\bullet,\bullet)$, $b(\bullet,\bullet)$, and $c(\bullet,\bullet)$ are bounded. That is:*

$$\begin{aligned}
|A(\vec{\boldsymbol{\sigma}},\vec{\boldsymbol{\tau}})| &\le \|A\|\|\vec{\boldsymbol{\sigma}}\|_{\mathbb{V}}\|\vec{\boldsymbol{\tau}}\|_{\mathbb{V}} && \forall \vec{\boldsymbol{\sigma}},\vec{\boldsymbol{\tau}} \in \mathbb{V},\\
|B(\vec{\boldsymbol{\tau}},\vec{\boldsymbol{v}})| &\le \|B\|\|\vec{\boldsymbol{\tau}}\|_{\mathbb{V}}\|\vec{\boldsymbol{v}}\|_{\mathbf{Q}} && \forall \vec{\boldsymbol{\tau}} \in \mathbb{V}, \forall \vec{\boldsymbol{v}} \in \mathbf{Q},\\
|C(\vec{\boldsymbol{u}},\vec{\boldsymbol{v}})| &\le \|C\|\|\vec{\boldsymbol{u}}\|_{\mathbf{Q}}\|\vec{\boldsymbol{v}}\|_{\mathbf{Q}} && \forall \vec{\boldsymbol{u}},\vec{\boldsymbol{v}} \in \mathbf{Q},\\
|D(\psi,\vec{\boldsymbol{\tau}})| &\le \|D\|\|\psi\|_{0,\Omega}\|\vec{\boldsymbol{\tau}}\|_{\mathbb{V}} && \forall \psi \in \mathrm{L}^2(\Omega), \forall \vec{\boldsymbol{\tau}} \in \mathbb{V},\\
|a_{\widehat{\boldsymbol{\sigma}}}(\boldsymbol{\zeta},\boldsymbol{\xi})| &\le \|a\|\|\boldsymbol{\zeta}\|_{4,\mathrm{div};\Omega}\|\boldsymbol{\xi}\|_{4,\mathrm{div};\Omega} && \forall \boldsymbol{\zeta},\boldsymbol{\xi} \in \mathbf{H}^4_{\mathrm{N}}(\mathrm{div},\Omega),\\
|b(\boldsymbol{\xi},\psi)| &\le \|b\|\|\boldsymbol{\xi}\|_{4,\mathrm{div};\Omega}\|\psi\|_{0,\Omega} && \forall \boldsymbol{\xi} \in \mathbf{H}^4_{\mathrm{N}}(\mathrm{div},\Omega), \forall \psi \in \mathrm{L}^2(\Omega),\\
|c(\varphi,\psi)| &\le \|c\|\|\varphi\|_{0,\Omega}\|\psi\|_{0,\Omega} && \forall \varphi,\psi \in \mathrm{L}^2(\Omega),
\end{aligned}$$

where the boundedness constants are given by

$$\|A\| := \max\left\{\frac{1}{2\mu} + \frac{\lambda}{2\mu(2\mu+d\lambda)}, \frac{\alpha\sqrt{d}}{2\mu+d\lambda}, s_0 + \frac{d\alpha^2}{2\mu+d\lambda}\right\}, \quad \|B\| := 1, \quad \|C\| := \frac{1}{\kappa_1},$$
$$\|D\| := \frac{\beta\sqrt{d}(1+\alpha)}{2\mu+d\lambda}, \quad \|a\| := \varrho_2 C_{\mathrm{emb}}^2, \quad \|b\| := 1, \quad \|c\| := 1,$$

and C_{emb} is the constant from the continuous embedding $\mathbf{L}^4(\Omega) \hookrightarrow \mathbf{L}^2(\Omega)$.

Proof. The boundedness of the bilinear forms is a direct consequence of the Cauchy–Schwarz and Hölder inequalities, and thus further details are omitted. $\square$

Lemma 2.2 (symmetry and positive semi-definiteness of diagonal forms) *The bilinear forms $A(\bullet,\bullet)$ and $C(\bullet,\bullet)$ are symmetric and positive semi-definite, and (for a given $\widehat{\boldsymbol{\sigma}} \in \mathbb{L}^2(\Omega)$) also $a_{\widehat{\boldsymbol{\sigma}}}(\bullet,\bullet)$ is positive semi-definite.*

Proof. It is clear that $A(\bullet,\bullet)$ and $C(\bullet,\bullet)$ are symmetric, whereas that $C(\bullet,\bullet)$ is positive semi-definite. To prove that $A(\bullet,\bullet)$ is positive semi-definite, note that given $\vec{\boldsymbol{\tau}} \in \mathbb{V}$, we have

$$A(\vec{\boldsymbol{\tau}},\vec{\boldsymbol{\tau}}) = (\mathcal{C}^{-1}\boldsymbol{\tau},\boldsymbol{\tau}) + \frac{2\alpha}{2\mu+d\lambda}(q,\operatorname{tr}\boldsymbol{\tau}) + \left[s_0 + \frac{d\alpha^2}{2\mu+d\lambda}\right]\|q\|_{0,\Omega}^2.$$

Next, applying suitably Young's inequality in the second term of the above equation with $\varepsilon := \dfrac{2\alpha}{s_0(2\mu+d\lambda)+2d\alpha^2}$ and recalling that

$$(\mathcal{C}^{-1}\boldsymbol{\sigma},\boldsymbol{\tau}) = \frac{1}{2\mu}(\boldsymbol{\sigma}^{\mathrm{d}},\boldsymbol{\tau}^{\mathrm{d}}) + \frac{1}{d(2\mu+d\lambda)}(\operatorname{tr}\boldsymbol{\sigma},\operatorname{tr}\boldsymbol{\tau}) \quad \forall\,\boldsymbol{\sigma},\boldsymbol{\tau} \in \mathbb{H}(\mathbf{div},\Omega),$$

readily yields

$$A(\vec{\boldsymbol{\tau}},\vec{\boldsymbol{\tau}}) \geq \frac{1}{2\mu}\|\boldsymbol{\tau}^{\mathrm{d}}\|_{0,\Omega}^2 + \frac{s_0}{2}\|q\|_{0,\Omega}^2 + \frac{s_0}{d(s_0(2\mu+d\lambda)+2d\alpha^2)}\|\operatorname{tr}\boldsymbol{\tau}\|_{0,\Omega}^2 \geq 0 \quad \forall\vec{\boldsymbol{\tau}} \in \mathbb{V}, \tag{2.4}$$

which shows the desired result. Finally, for a given $\widehat{\boldsymbol{\sigma}} \in \mathbb{L}^2(\Omega)$ since $a_{\widehat{\boldsymbol{\sigma}}}(\boldsymbol{\zeta},\boldsymbol{\zeta}) = (\varrho(\widehat{\boldsymbol{\sigma}})^{-1}\boldsymbol{\zeta},\boldsymbol{\zeta}) \geq \varrho_1\|\boldsymbol{\zeta}\|_{0,\Omega}^2 \geq 0$, the form $a_{\widehat{\boldsymbol{\sigma}}}(\bullet,\bullet)$ is positive semi-definite. $\square$

We proceed similarly to [26, Section 2.3] to show that $A(\bullet,\bullet)$ is $\mathbb{V}_0$-elliptic. To do that, we recall the decomposition

$$\mathbb{H}(\mathbf{div},\Omega) = \mathbb{H}_0(\mathbf{div},\Omega) \oplus \mathbb{R}\,\mathbb{I}, \text{ with } \mathbb{H}_0(\mathbf{div},\Omega) := \left\{\boldsymbol{\tau} \in \mathbb{H}(\mathbf{div},\Omega) : \int_\Omega \operatorname{tr}\boldsymbol{\tau} = 0\right\}.$$

We also recall two useful estimates, whose proofs can be found in [26, Lemma 2.3] and [26, Lemma 2.4]. Specifically, there exists $C_1 > 0$, depending only on Ω, such that

$$C_1\,\|\boldsymbol{\tau}_0\|_{0,\Omega} \leq \|\boldsymbol{\tau}^{\mathrm{d}}\|_{0,\Omega} + \|\mathbf{div}\,\boldsymbol{\tau}\|_{0,\Omega} \quad \forall\,\boldsymbol{\tau} \in \mathbb{H}(\mathbf{div},\Omega), \quad \text{and} \tag{2.5}$$

there exists $C_2 > 0$, depending only on Γ_{N} and Ω, such that

$$C_2\,\|\boldsymbol{\tau}\|_{\mathbf{div},\Omega} \leq \|\boldsymbol{\tau}_0\|_{\mathbf{div},\Omega} \quad \forall\,\boldsymbol{\tau} := \boldsymbol{\tau}_0 + m\mathbb{I} \in \mathbb{H}_{\mathrm{N}}(\mathbf{div},\Omega), \tag{2.6}$$

with $\boldsymbol{\tau}_0 \in \mathbb{H}_0(\mathbf{div},\Omega)$ and $m \in \mathbb{R}$. Then, we have the following result.

Lemma 2.3 (coercivity for the main diagonal forms) *There exist constants $\alpha_A, \alpha_c, \alpha_C > 0$ such that*

$$A(\vec{\boldsymbol{\tau}},\vec{\boldsymbol{\tau}}) \geq \alpha_A\|\vec{\boldsymbol{\tau}}\|_{\mathbb{V}}^2 \quad \forall\,\vec{\boldsymbol{\tau}} \in \mathbb{V}_0 = \ker(\mathbf{B}), \tag{2.7a}$$
$$c(\psi,\psi) \geq \alpha_c\|\psi\|_{0,\Omega}^2 \quad \forall\,\psi \in \mathrm{L}^2(\Omega), \tag{2.7b}$$
$$C(\vec{\boldsymbol{v}},\vec{\boldsymbol{v}}) \geq \alpha_C\|\vec{\boldsymbol{v}}\|_{\mathbf{Q}}^2 \quad \forall\,\vec{\boldsymbol{v}} \in \mathbf{Q}_0. \tag{2.7c}$$

Proof. For (2.7a), we let $\vec{\boldsymbol{\tau}} = (\boldsymbol{\tau}, q) \in \mathbb{V}_{01} \times \mathbb{V}_{02}$. This means, according to (2.4), (2.5) and (2.6), that

$$A(\vec{\boldsymbol{\tau}}, \vec{\boldsymbol{\tau}}) \geq \alpha_A \|\vec{\boldsymbol{\tau}}\|_{\mathbb{V}}^2,$$

with $\alpha_A = \dfrac{C_1\, C_2}{4\mu}$. On the other hand, we observe that (2.7b) is trivially satisfied with $\alpha_c = 1$. Finally, given $\vec{\boldsymbol{v}} \in \mathbf{Q}_0$ (cf. (2.3b)), we have

$$C(\vec{\boldsymbol{v}}, \vec{\boldsymbol{v}}) \geq \frac{1}{\kappa_2} \|\boldsymbol{w}\|_{0,\Omega}^2 = \frac{1}{\kappa_2} \left\{ \|\boldsymbol{w}\|_{0,\Omega}^2 + \|\operatorname{div} \boldsymbol{w}\|_{0,\Omega}^2 + \|\boldsymbol{v}\|_{0,\Omega}^2 \right\},$$

which shows (2.7c) with $\alpha_C = \frac{1}{\kappa_2}$. □

Lemma 2.4 (continuous inf-sup conditions) *There exist positive constants β_B, β_b such that*

$$\sup_{\vec{\boldsymbol{\tau}} \in \mathbb{V} \setminus \{\mathbf{0}\}} \frac{B(\vec{\boldsymbol{\tau}}, \vec{\boldsymbol{v}})}{\|\vec{\boldsymbol{\tau}}\|_{\mathbb{V}}} \geq \beta_B \|\vec{\boldsymbol{v}}\|_{\mathbf{Q}} \qquad \forall\, \vec{\boldsymbol{v}} \in [\ker(\mathbf{B}^*)]^{\perp}, \tag{2.8a}$$

$$\sup_{\psi \in \mathrm{L}^2(\Omega) \setminus \{0\}} \frac{b(\boldsymbol{\xi}, \psi)}{\|\psi\|_{0,\Omega}} \geq \beta_b \|\boldsymbol{\xi}\|_{4,\mathrm{div};\Omega} \qquad \forall\, \boldsymbol{\xi} \in \mathbf{H}_{\mathrm{N}}^4(\mathrm{div}, \Omega). \tag{2.8b}$$

Proof. To prove (2.8a), it suffices to establish the following two independent inf–sup conditions, which follow from the diagonal structure of $B(\bullet, \bullet)$:

$$\sup_{\boldsymbol{\tau} \in \mathbb{H}_{\mathrm{N}}^{\mathrm{sym}}(\mathbf{div}, \Omega) \setminus \{\mathbf{0}\}} \frac{(\boldsymbol{v}, \mathbf{div}\, \boldsymbol{\tau})}{\|\boldsymbol{\tau}\|_{\mathbf{div},\Omega}} \geq \beta_1 \|\boldsymbol{v}\|_{0,\Omega} \quad \forall\, \boldsymbol{v} \in \mathbf{Q}_{01}^{\perp}, \tag{2.9a}$$

$$\sup_{q \in \mathrm{L}^2(\Omega) \setminus \{0\}} \frac{(q, \operatorname{div} \boldsymbol{w})}{\|q\|_{0,\Omega}} \geq \beta_2 \|\boldsymbol{w}\|_{\mathrm{div},\Omega} \quad \forall\, \boldsymbol{w} \in \mathbf{Q}_{02}^{\perp}. \tag{2.9b}$$

For (2.9a), we refer to [26, Lemma 2.2, eq. (14)], whereas (2.9b) holds by virtue of the existence of a constant $\widehat{\beta}_2 > 0$, such that (see, e.g., [15, Lemma 3.2])

$$\sup_{\boldsymbol{w} \in \mathbf{H}_{\mathrm{N}}(\mathrm{div}, \Omega) \setminus \{\mathbf{0}\}} \frac{(q, \operatorname{div} \boldsymbol{w})}{\|\boldsymbol{w}\|_{\mathrm{div},\Omega}} \geq \widehat{\beta}_2 \|q\|_{0,\Omega} \quad \forall\, q \in \mathbb{V}_{02}^{\perp} = \mathrm{L}^2(\Omega),$$

and the identity given by [8, eq. (4.3.18)], which also implies that $\beta_2 = \widehat{\beta}_2$. Thus, the required inequality (2.8a) is obtained with $\beta_B = \frac{\beta_1 + \beta_2}{4}$.

Regarding the inf-sup condition for the bilinear form $b(\bullet, \bullet)$ (cf. (2.8b)) let us first define $\boldsymbol{\gamma} := |\boldsymbol{\xi}|^2 \boldsymbol{\xi} \in \mathbf{L}^{4/3}(\Omega)$, and consider the problem of finding $\widehat{\psi} \in \mathrm{W}_0^{1,4/3}(\Omega)$ such that

$$\nabla \widehat{\psi} = \boldsymbol{\gamma} \quad \text{in } \Omega, \qquad \widehat{\psi} = 0 \quad \text{on } \partial\Omega.$$

Testing against $\nabla \zeta$ for any $\zeta \in \mathrm{W}_0^{1,4}(\Omega)$ we have

$$\int_\Omega \nabla \widehat{\psi} \cdot \nabla \zeta = \int_\Omega \boldsymbol{\gamma} \cdot \nabla \zeta \qquad \forall \zeta \in \mathrm{W}_0^{1,4}(\Omega). \tag{2.10}$$

The bilinear form $\tilde{a} : \mathrm{W}_0^{1,4/3}(\Omega) \times \mathrm{W}_0^{1,4}(\Omega) \to \mathbb{R}$ defined as $\tilde{a}(\psi, \zeta) := \int_\Omega \nabla \psi \cdot \nabla \zeta$ is bounded using Hölder's inequality

$$|\tilde{a}(\psi, \zeta)| \leq \|\nabla \psi\|_{0,4/3;\Omega} \|\nabla \zeta\|_{0,4;\Omega} \leq \|\psi\|_{1,4/3;\Omega} \|\zeta\|_{1,4;\Omega},$$

and it satisfies the inf-sup Banach–Nečas–Babuška condition: for a fixed $\psi \in \mathrm{W}_0^{1,4/3}(\Omega)$,

$$\sup_{\zeta \in \mathrm{W}_0^{1,4}(\Omega) \setminus \{0\}} \frac{\tilde{a}(\psi, \zeta)}{\|\zeta\|_{1,4;\Omega}} = \sup_{\zeta \in \mathrm{W}_0^{1,4}(\Omega) \setminus \{0\}} \frac{\|\nabla \psi\|_{0,4/3;\Omega} \|\nabla \zeta\|_{0,4;\Omega}}{\|\zeta\|_{1,4;\Omega}} \| \gtrsim \|\psi\|_{1,4/3;\Omega},$$

by duality between $\mathbf{L}^{4/3}(\Omega)$ and $\mathbf{L}^4(\Omega)$ and Poincaré inequality. In turn, the linear functional $\tilde{F}: \mathrm{W}_0^{1,4}(\Omega) \to \mathbb{R}$ defined as $\tilde{F}(\zeta) := \int_\Omega \boldsymbol{\gamma} \cdot \nabla\zeta$ is bounded thanks to Hölder's inequality

$$|\tilde{F}(\zeta)| \leq \|\boldsymbol{\gamma}\|_{0,4/3;\Omega}\|\nabla\zeta\|_{0,4;\Omega} \leq \|\boldsymbol{\gamma}\|_{0,4/3;\Omega}\|\zeta\|_{1,4;\Omega},$$

and so we obtain that there exists a unique $\widehat{\psi} \in \mathrm{W}_0^{1,4/3}(\Omega)$ satisfying (2.10). This is a standard consequence of the theory of elliptic operators in reflexive Banach spaces [25, Theorem 2.6]. The continuous dependence on data associated with this problem, in combination with the continuous embedding $\mathrm{W}^{1,4/3}(\Omega) \hookrightarrow \mathrm{L}^2(\Omega)$ (valid for Lipschitz domains in 2D and 3D), then gives

$$\|\widehat{\psi}\|_{0,\Omega} \lesssim \|\widehat{\psi}\|_{1,4/3;\Omega} \lesssim \|\boldsymbol{\gamma}\|_{0,4/3;\Omega}, \tag{2.11}$$

where the hidden constant depends only on the norm of the continuous embedding and the Poincaré constant.

Next, for any $\boldsymbol{\xi} \in \mathbf{H}^4_{\mathrm{N}}(\mathrm{div},\Omega)$ we choose $\psi = \widehat{\psi}$ and exploiting the fact that $\widehat{\psi} \in \mathrm{W}_0^{1,4/3}(\Omega)$, we invoke the integration by parts formula to derive

$$\begin{aligned}\sup_{\psi\in \mathrm{L}^2(\Omega)\setminus\{0\}} \frac{1}{2}\frac{b(\boldsymbol{\xi},\psi)}{\|\psi\|_{0,\Omega}} &\geq \frac{b(\boldsymbol{\xi},\widehat{\psi})}{2\|\widehat{\psi}\|_{0,\Omega}} = \frac{-\int_\Omega \mathrm{div}\,\boldsymbol{\xi}\,\widehat{\psi}}{2\|\widehat{\psi}\|_{0,\Omega}} = \frac{\int_\Omega \nabla\widehat{\psi}\cdot\boldsymbol{\xi}}{2\|\widehat{\psi}\|_{0,\Omega}} = \frac{\int_\Omega \boldsymbol{\gamma}\cdot\boldsymbol{\xi}}{2\|\widehat{\psi}\|_{0,\Omega}} \\ &\gtrsim \frac{\|\boldsymbol{\gamma}\|_{0,4/3;\Omega}\|\boldsymbol{\xi}\|_{0,4;\Omega}}{\|\boldsymbol{\gamma}\|_{0,4/3;\Omega}} = \|\boldsymbol{\xi}\|_{0,4;\Omega},\end{aligned} \tag{2.12}$$

where in the second-last equality we have used (2.10) and in the last inequality we have used the definition of $\boldsymbol{\gamma}$ and (2.11).

On the other hand, and again for any $\boldsymbol{\xi} \in \mathbf{H}^4_{\mathrm{N}}(\mathrm{div},\Omega)$, we can construct $\widetilde{\psi} \equiv -\,\mathrm{div}\,\boldsymbol{\xi} \in \mathrm{L}^2(\Omega)$. This straightforwardly implies that

$$\sup_{\psi\in \mathrm{L}^2(\Omega)\setminus\{0\}} \frac{1}{2}\frac{b(\boldsymbol{\xi},\psi)}{\|\psi\|_{0,\Omega}} \geq \frac{b(\boldsymbol{\xi},\widetilde{\psi})}{2\|\widetilde{\psi}\|_{0,\Omega}} = \frac{-\int_\Omega \widetilde{\psi}\,\mathrm{div}\,\boldsymbol{\xi}}{2\|\widetilde{\psi}\|_{0,\Omega}} = \frac{\|\,\mathrm{div}\,\boldsymbol{\xi}\|^2_{0,\Omega}}{2\|\,\mathrm{div}\,\boldsymbol{\xi}\|_{0,\Omega}} = \frac{1}{2}\|\,\mathrm{div}\,\boldsymbol{\xi}\|_{0,\Omega}. \tag{2.13}$$

Finally, it suffices to add (2.12) with (2.13) to obtain the desired inf-sup condition, with constant $\beta_b > 0$ depending only on the Poincaré and continuous embedding constants. □

Remark 2.1 *It is important to clarify that the unique solvability of the auxiliary problem* (2.10) *is understood in a weak sense and it only needs the Banach–Nečas–Babuška argument in combination with Poincaré's inequality. Note that we are not claiming a classical solution of the Dirichlet Poisson problem with* $\mathrm{L}^{s'}(\Omega)$ *control, which allows (from the sharp result in [35]) a solution integrability only up to* $\mathrm{W}^{1,s}(\Omega)$ *with* $\frac{3}{2} - \epsilon < s < 3 + \epsilon$ *for* $d = 3$ *and* $\frac{4}{3} - \epsilon < s < 4 + \epsilon$ *for* $d = 2$.

The strategy for the analysis of well-posedness of (2.2) is simply to decompose the problem into the poroelasticity equations (first two equations in that system) and the remaining diffusion equation in mixed form. We separate the analysis for each problem in the following sub-section.

2.2 Unique solvability of decoupled Biot equations and mixed diffusion equations

As announced in Section 1, the following result is a *dual* to [17, Theorem 3.2] and it provides the necessary framework to establish the well-posedness of the diffusion subproblem without requiring coercivity of $a_{\widehat{\boldsymbol{\sigma}}}(\bullet,\bullet)$.

Theorem 2.5 (Abstract result for Q-elliptic perturbed saddle-point problems) *Let H and Q be reflexive Banach spaces, and let* $a: H\times H \to R$, $b: H\times Q \to R$, *and* $c: Q\times Q\to R$ *be bounded bilinear forms with boundedness constants denoted by* $\|a\|$, $\|b\|$, *and* $\|c\|$, *respectively. Assume that:*

i) $a(\bullet,\bullet)$ *is positive semi-definite, that is* $a(\tau,\tau) \geq 0$ *for all* $\tau \in H$.

ii) $b(\bullet,\bullet)$ *satisfies a* transposed *continuous inf-sup condition, that is, there exists a constant* $\hat{\beta} > 0$ *such that*

$$\sup_{v\in Q\setminus\{0\}} \frac{b(\tau,v)}{\|v\|_Q} \geq \hat{\beta}\|\tau\|_H \quad \forall \tau \in H.$$

iii) $c(\bullet,\bullet)$ *is* Q*-elliptic, that is, there exists a constant* $\gamma > 0$ *such that*

$$c(v,v) \geq \gamma \|v\|_Q^2 \quad \forall v \in Q.$$

Then, for each pair $(F,G) \in H' \times Q'$*, the problem: Find* $(\sigma,u) \in H \times Q$ *such that*

$$a(\sigma,\tau) + b(\tau,u) = F(\tau) \quad \forall \tau \in H, \tag{2.14a}$$
$$b(\sigma,v) - c(u,v) = G(v) \quad \forall v \in Q, \tag{2.14b}$$

has a unique solution. Moreover, there exists a positive constant C*, depending only on* $\|b\|$*,* $\|c\|$*,* γ *and* $\hat{\beta}$*, such that*

$$\|\sigma\|_H + \|u\|_Q \leq C\{\|F\|_{H'} + \|G\|_{Q'}\}. \tag{2.15}$$

Proof. The proof is symmetric to that of [17, Theorem 3.2]. The argument is driven by the strong Q-ellipticity of the form $c(\bullet,\bullet)$. To begin, we establish existence. Indeed, the Q-ellipticity of $c(\bullet,\bullet)$ (hypothesis iii)) guarantees, by the Banach–Nečas–Babuška theorem, for each $\zeta \in H$, the existence of a unique $u_\zeta \in Q$ such that

$$c(u_\zeta, v) = b(\zeta, v) \quad \forall\, v \in Q, \tag{2.16}$$

as well as a unique $u_0 \in Q$ such that

$$c(u_0, v) = G(v) \quad \forall\, v \in Q. \tag{2.17}$$

The corresponding *a priori* estimates are given, respectively, by

$$\|u_\zeta\|_Q \leq \frac{\|b\|}{\gamma}\|\zeta\|_H \quad \text{and} \quad \|u_0\|_Q \leq \frac{1}{\gamma}\|G\|_{Q'} \quad \forall\, \zeta \in H. \tag{2.18}$$

Next, we use the transposed inf-sup condition ii) to obtain for each $\zeta \in H$

$$\hat{\beta}\|\zeta\|_H \leq \sup_{v \in Q\setminus\{0\}} \frac{b(\zeta,v)}{\|v\|_Q} = \sup_{v \in Q\setminus\{0\}} \frac{c(u_\zeta,v)}{\|v\|_Q} \leq \|c\|\|u_\zeta\|_Q. \tag{2.19}$$

Noting from (2.16) that u_ζ depends on ζ, we define a new form $\Theta : H \times H \to \mathbb{R}$ by

$$\Theta(\zeta,\tau) := a(\zeta,\tau) + b(\tau,u_\zeta) \quad \forall \zeta,\tau \in H.$$

In what follows, we prove that $\Theta(\bullet,\bullet)$ is bilinear. Indeed, for $\zeta_1,\zeta_2 \in H$ and scalars $x,y \in \mathbb{R}$, we use the bilinearity of $b(\bullet,\bullet)$ and $c(\bullet,\bullet)$ to arrive at

$$c(xu_{\zeta_1} + yu_{\zeta_2}, v) = xc(u_{\zeta_1},v) + yc(u_{\zeta_2},v) = xb(\zeta_1,v) + yb(\zeta_2,v) = b(x\zeta_1 + y\zeta_2, v) \quad v \in Q.$$

By the uniqueness of the solution to (2.16), we must have $u_{x\zeta_1+y\zeta_2} = xu_{\zeta_1} + yu_{\zeta_2}$. Thus for the first argument, we have

$$\begin{aligned}
\Theta(x\zeta_1 + y\zeta_2, \tau) &= a(x\zeta_1 + y\zeta_2,\tau) + b(\tau, u_{x\zeta_1+y\zeta_2}) \\
&= xa(\zeta_1,\tau) + ya(\zeta_2,\tau) + b(\tau, xu_{\zeta_1} + yu_{\zeta_2}) \\
&= xa(\zeta_1,\tau) + ya(\zeta_2,\tau) + xb(\tau,u_{\zeta_1}) + yb(\tau,u_{\zeta_2}) \\
&= x\Theta(\zeta_1,\tau) + y\Theta(\zeta_2,\tau),
\end{aligned}$$

which proves the linearity in the first argument. The linearity in the second argument and the boundedness of $\Theta(\bullet,\bullet)$ follow directly from the properties of $a(\bullet,\bullet)$ and $b(\bullet,\bullet)$.

We now demonstrate that $\Theta(\bullet,\bullet)$ is H-elliptic. From the definition of u_ζ in (2.16), we have the identity $c(u_\zeta,u_\zeta) = b(\zeta,u_\zeta)$, which, along with hypotheses i) and iii), yields

$$\Theta(\zeta,\zeta) = a(\zeta,\zeta) + b(\zeta,u_\zeta) = a(\zeta,\zeta) + c(u_\zeta,u_\zeta) \geq c(u_\zeta,u_\zeta) \geq \gamma\|u_\zeta\|_Q^2 \geq \gamma\left(\frac{\hat{\beta}}{\|c\|}\right)^2\|\zeta\|_H^2.$$

This proves that $\Theta(\bullet,\bullet)$ is elliptic on H with a constant $\alpha_\Theta = \frac{\gamma\hat{\beta}^2}{\|c\|^2} > 0$. Thus, applying again the Banach–Nečas–Babuška theorem, we conclude that there exists a unique $\sigma \in H$ such that $\Theta(\sigma,\tau) = F(\tau) + b(\tau, u_0)$ for all $\tau \in H$, that is

$$a(\sigma,\tau) + b(\tau, u_\sigma) = F(\tau) + b(\tau, u_0) \quad \forall \tau \in H,$$

which can be rearranged as

$$a(\sigma,\tau) + b(\tau, u_\sigma - u_0) = F(\tau) \quad \forall \tau \in H. \tag{2.20}$$

Now, letting $u = u_\sigma - u_0 \in Q$, it follows from (2.16) and (2.17) that

$$c(u, v) = c(u_\sigma, v) - c(u_0, v) = b(\sigma, v) - G(v),$$

that is

$$b(\sigma, v) - c(u, v) = G(v) \quad \forall v \in Q,$$

which, together with (2.20), shows that $(\sigma, u) \in H \times Q$ is a solution to (2.14a).

In turn, the a priori estimate for the solution is derived now. First, we establish the bound for σ. From the stability of the bilinear form $\Theta(\bullet,\bullet)$, we have

$$\|\sigma\|_H \leq \frac{\|c\|^2}{\gamma\hat{\beta}^2}\left(\|F\|_{H'} + \|b\|\|u_0\|_Q\right).$$

The above together with the second inequality in (2.18), yields

$$\|\sigma\|_H \leq \frac{\|c\|^2}{\gamma\hat{\beta}^2}\|F\|_{H'} + \frac{\|b\|\|c\|^2}{\gamma^2\hat{\beta}^2}\|G\|_{Q'}. \tag{2.21}$$

Next, we establish the bound for u. Using the triangle inequality and the bounds for u_σ and u_0 in (2.18), we get

$$\|u\|_Q \leq \frac{\|b\|}{\gamma}\|\sigma\|_H + \frac{1}{\gamma}\|G\|_{Q'}.$$

Substituting the estimate (2.21) into this inequality yields

$$\|u\|_Q \leq \frac{\|b\|\|c\|^2}{\gamma^2\hat{\beta}^2}\|F\|_{H'} + \left(\frac{\|b\|^2\|c\|^2}{\gamma^3\hat{\beta}^2} + \frac{1}{\gamma}\right)\|G\|_{Q'}. \tag{2.22}$$

Having proved the existence of a solution (σ, u), it only remains to show the uniqueness, for which we let $(\tilde{\sigma}, \tilde{u}) \in H \times Q$ be such that

$$\begin{aligned} a(\tilde{\sigma},\tau) + b(\tau, \tilde{u}) &= 0 \quad \forall \tau \in H,\\ b(\tilde{\sigma}, v) - c(\tilde{u}, v) &= 0 \quad \forall v \in Q. \end{aligned}$$

Then, taking $\tau = \tilde{\sigma}$ and $v = \tilde{u}$, and then subtracting the resulting equations and using i) and iii), we get

$$0 = a(\tilde{\sigma},\tilde{\sigma}) + c(\tilde{u},\tilde{u}) \geq \gamma\|\tilde{u}\|_Q^2.$$

from which $\tilde{u} = 0$. In addition, it is clear from the second row of the homogeneous system and (2.16) that $u_{\tilde{\sigma}} = \tilde{u}$, which, invoking (2.19), yields $\tilde{\sigma} = 0$, thus confirming the uniqueness of the solution.

Finally, (2.21) and (2.22) imply (2.15) and complete the proof. □

We are now in a position to establish the well-posedness of the decoupled subproblems. To this end, the analysis of the Biot equations is based on the classical theory for perturbed saddle-point problems from [8, Theorem 4.3.1], whereas the well-posedness of the mixed diffusion equations follows from Theorem 2.5.

Firstly, let us assume that $\widehat{\varphi} \in \mathrm{L}^2(\Omega)$ is prescribed. Then, we have the following result.

Theorem 2.6 (well-posedness of the Biot equations) *There exists a unique* $(\vec{\boldsymbol{\sigma}}, \vec{\boldsymbol{u}}) \in \mathbb{V} \times \mathbf{Q}$ *such that*

$$A(\vec{\boldsymbol{\sigma}}, \vec{\boldsymbol{\tau}}) + B(\vec{\boldsymbol{\tau}}, \vec{\boldsymbol{u}}) = -D(\widehat{\varphi}, \vec{\boldsymbol{\tau}}) + F(\vec{\boldsymbol{\tau}}) \qquad \forall \vec{\boldsymbol{\tau}} \in \mathbb{V}, \tag{2.23a}$$
$$B(\vec{\boldsymbol{\sigma}}, \vec{\boldsymbol{v}}) - C(\vec{\boldsymbol{u}}, \vec{\boldsymbol{v}}) = G(\vec{\boldsymbol{v}}) \qquad \forall \vec{\boldsymbol{v}} \in \mathbf{Q}, \tag{2.23b}$$

and moreover

$$\|(\vec{\boldsymbol{\sigma}}, \vec{\boldsymbol{u}})\|_{\mathbb{V}\times\mathbf{Q}} \lesssim \frac{(1+\alpha d)\beta}{2\mu + d\lambda}\|\widehat{\varphi}\|_{0,\Omega} + \|\boldsymbol{f}\|_{0,\Omega} + \|\boldsymbol{u}_{\mathrm{D}}\|_{1/2,00;\Gamma_{\mathrm{D}}} + \|g\|_{0,\Omega} + \|p_{\mathrm{D}}\|_{1/2,00;\Gamma_{\mathrm{D}}}.$$

Proof. It follows from Lemma 2.2, and equations (2.7a), (2.7c), and (2.8a) of Lemmas 2.3 and 2.4 and a straightforward application of [8, Theorem 4.3.1]. □

Similarly, for a prescribed $\widehat{\boldsymbol{\sigma}} \in \mathbb{H}^{\mathrm{sym}}_{\mathrm{N}}(\mathbf{div}, \Omega)$, we have the following result.

Theorem 2.7 (well-posedness of the mixed perturbed diffusion equation) *There exists a unique* $(\boldsymbol{\zeta}, \varphi) \in \mathbf{H}^4_{\mathrm{N}}(\mathrm{div}, \Omega) \times \mathrm{L}^2(\Omega)$ *such that*

$$a_{\widehat{\boldsymbol{\sigma}}}(\boldsymbol{\zeta}, \boldsymbol{\xi}) + b(\boldsymbol{\xi}, \varphi) = H(\boldsymbol{\xi}) \qquad \forall \boldsymbol{\xi} \in \mathbf{H}^4_{\mathrm{N}}(\mathrm{div}, \Omega), \tag{2.24a}$$
$$b(\boldsymbol{\zeta}, \psi) - c(\varphi, \psi) = I(\psi) \qquad \forall \psi \in \mathrm{L}^2(\Omega), \tag{2.24b}$$

and furthermore

$$\|\boldsymbol{\zeta}\|_{4,\mathrm{div};\Omega} + \|\varphi\|_{0,\Omega} \lesssim \|\ell\|_{0,\Omega} + \|\varphi_{\mathrm{D}}\|_{1/2,00;\Gamma_{\mathrm{D}}}.$$

Proof. The well-posedness follows from the properties of the forms $a(\bullet,\bullet)$, $b(\bullet,\bullet)$, and $c_{\widehat{\boldsymbol{\sigma}}}(\bullet,\bullet)$ established in Lemmas 2.2, 2.3, and 2.4 in combination with Theorem 2.5. □

2.3 Unique solvability of the coupled problem via fixed-point theory

We define the following map

$$\mathcal{J}^{\mathrm{Biot}} : \mathrm{L}^2(\Omega) \to \mathbb{V} \times \mathbf{Q}, \quad \widehat{\varphi} \mapsto \mathcal{J}^{\mathrm{Biot}}(\widehat{\varphi}) = ((\mathcal{J}^{\mathrm{Biot}}_1(\widehat{\varphi}), \mathcal{J}^{\mathrm{Biot}}_2(\widehat{\varphi})), \mathcal{J}^{\mathrm{Biot}}_3(\widehat{\varphi})) := ((\boldsymbol{\sigma}, p), \vec{\boldsymbol{u}}) = (\vec{\boldsymbol{\sigma}}, \vec{\boldsymbol{u}}),$$

where $(\vec{\boldsymbol{\sigma}}, \vec{\boldsymbol{u}}) \in \mathbb{V} \times \mathbf{Q}$ is the unique solution of the poroelasticity equations as stated in Theorem 2.6. In turn, we define the solution operator associated with the mixed diffusion equations as

$$\mathcal{J}^{\mathrm{diff}} : \mathbb{H}^{\mathrm{sym}}_{\mathrm{N}}(\mathbf{div}, \Omega) \to \mathbf{H}^4_{\mathrm{N}}(\mathrm{div}, \Omega) \times \mathrm{L}^2(\Omega), \quad \widehat{\boldsymbol{\sigma}} \mapsto \mathcal{J}^{\mathrm{diff}}(\widehat{\boldsymbol{\sigma}}) = (\mathcal{J}^{\mathrm{diff}}_1(\widehat{\boldsymbol{\sigma}}), \mathcal{J}^{\mathrm{diff}}_2(\widehat{\boldsymbol{\sigma}})) := (\boldsymbol{\zeta}, \varphi),$$

where $(\boldsymbol{\zeta}, \varphi)$ is the unique solution of the diffusion equations as stated in Theorem 2.7. These maps are well-defined and so it is the following one

$$\mathcal{J} : \mathrm{L}^2(\Omega) \to \mathrm{L}^2(\Omega), \quad \widehat{\varphi} \mapsto \mathcal{J}(\widehat{\varphi}) := \mathcal{J}^{\mathrm{diff}}_2(\mathcal{J}^{\mathrm{Biot}}_1(\widehat{\varphi})). \tag{2.25}$$

Finding a fixed point φ of $\mathcal{J}$ is therefore equivalent to solve (2.2). For this we use Banach fixed point theorem and start by considering, for a generic $r > 0$, the following closed ball

$$\mathrm{W} := \{\widehat{\varphi} \in \mathrm{L}^2(\Omega) : \|\widehat{\varphi}\|_{0,\Omega} \le r\},$$

and proceed next to show that $\mathcal{J}$ maps it to itself and that $\mathcal{J}$ is Lipschitz continuous.

Lemma 2.8 (ball mapping property) *Under the small data assumption*

$$\|\ell\|_{0,\Omega} + \|\varphi_{\mathrm{D}}\|_{1/2,00;\Gamma_{\mathrm{D}}} \le r, \tag{2.26}$$

it follows that $\mathcal{J}(\mathrm{W}) \subseteq \mathrm{W}$.

Proof. Given $\widehat{\varphi} \in \mathrm{W}$, by (2.25), (2.26) and the estimate given by Theorem 2.7 we have

$$\|\mathcal{J}(\widehat{\varphi})\|_{0,\Omega} = \|\mathcal{J}_2^{\mathrm{diff}}(\mathcal{J}_1^{\mathrm{Biot}}(\widehat{\varphi}))\|_{0,\Omega} \lesssim \|\ell\|_{0,\Omega} + \|\varphi_{\mathrm{D}}\|_{1/2,00;\Gamma_{\mathrm{D}}} \leq r,$$

which means that $\mathcal{J}\big(\mathrm{W}\big) \subseteq \mathrm{W}$. $\square$

We continue the analysis with the Lipschitz-continuity property of $\mathcal{J}$. To this end, we recall that Theorems 2.6 and 2.7 establish the existence of positive constants C_{B} and C_{D} such that

$$\sup_{\substack{(\vec{\boldsymbol{\tau}},\vec{\boldsymbol{v}})\in\mathbb{V}\times\mathbf{Q}\\(\vec{\boldsymbol{\tau}},\vec{\boldsymbol{v}})\neq\mathbf{0}}} \frac{A(\vec{\boldsymbol{\zeta}},\vec{\boldsymbol{\tau}}) + B(\vec{\boldsymbol{\tau}},\vec{\boldsymbol{w}}) + B(\vec{\boldsymbol{\zeta}},\vec{\boldsymbol{v}}) - C(\vec{\boldsymbol{w}},\vec{\boldsymbol{v}})}{\|(\vec{\boldsymbol{\tau}},\vec{\boldsymbol{v}})\|_{\mathbb{V}\times\mathbf{Q}}} \geq C_{\mathrm{B}}\|(\vec{\boldsymbol{\zeta}},\vec{\boldsymbol{w}})\|_{\mathbb{V}\times\mathbf{Q}} \;\forall\,(\vec{\boldsymbol{\zeta}},\vec{\boldsymbol{w}}) \in \mathbb{V}\times\mathbf{Q}, \tag{2.27a}$$

$$\begin{aligned}\sup_{\substack{(\boldsymbol{\xi},\psi)\in\mathbf{H}^4_{\mathrm{N}}(\mathrm{div},\Omega)\times\mathrm{L}^2(\Omega)\\(\boldsymbol{\xi},\psi)\neq\mathbf{0}}} &\frac{a_{\widehat{\boldsymbol{\sigma}}}(\boldsymbol{\zeta},\boldsymbol{\xi}) + b(\boldsymbol{\xi},\phi) + b(\boldsymbol{\zeta},\psi) - c(\phi,\psi)}{\|(\boldsymbol{\xi},\psi)\|_{\mathbf{H}^4_{\mathrm{N}}(\mathrm{div},\Omega)\times\mathrm{L}^2(\Omega)}}\\ &\geq C_{\mathrm{D}}\|(\boldsymbol{\zeta},\phi)\|_{\mathbf{H}^4_{\mathrm{N}}(\mathrm{div},\Omega)\times\mathrm{L}^2(\Omega)} \quad \forall\,(\boldsymbol{\zeta},\phi) \in \mathbf{H}^4_{\mathrm{N}}(\mathrm{div},\Omega)\times\mathrm{L}^2(\Omega).\end{aligned} \tag{2.27b}$$

Lemma 2.9 (Lipschitz continuity) *There exists a positive constant $L_{\mathcal{J}}$ such that*

$$\|\mathcal{J}(\varphi_1) - \mathcal{J}(\varphi_2)\|_{0,\Omega} \leq L_{\mathcal{J}}\|\varphi_1 - \varphi_2\|_{0,\Omega} \qquad \forall \varphi_1,\varphi_2 \in \mathrm{L}^2(\Omega). \tag{2.28}$$

Proof. Given $\varphi_1,\varphi_2 \in \mathrm{L}^2(\Omega)$, we let $\mathcal{J}^{\mathrm{Biot}}(\varphi_1) = (\vec{\boldsymbol{\sigma}}_1,\vec{\boldsymbol{u}}_1) \in \mathbb{V}\times\mathbf{Q}$ and $\mathcal{J}^{\mathrm{Biot}}(\varphi_2) = (\vec{\boldsymbol{\sigma}}_2,\vec{\boldsymbol{u}}_2) \in \mathbb{V}\times\mathbf{Q}$ be the unique solutions of (2.23). Then, applying the inf-sup condition (2.27a) with $(\vec{\boldsymbol{\zeta}},\vec{\boldsymbol{w}}) = (\vec{\boldsymbol{\sigma}}_1 - \vec{\boldsymbol{\sigma}}_2, \vec{\boldsymbol{u}}_1 - \vec{\boldsymbol{u}}_2)$, it follows that

$$\begin{aligned} C_{\mathrm{B}}\|(\vec{\boldsymbol{\sigma}}_1 - \vec{\boldsymbol{\sigma}}_2,\vec{\boldsymbol{u}}_1 - \vec{\boldsymbol{u}}_2)\|_{\mathbb{V}\times\mathbf{Q}} &\leq \sup_{\substack{(\vec{\boldsymbol{\tau}},\vec{\boldsymbol{v}})\in\mathbb{V}\times\mathbf{Q}\\(\vec{\boldsymbol{\tau}},\vec{\boldsymbol{v}})\neq\mathbf{0}}} \frac{A(\vec{\boldsymbol{\sigma}}_1 - \vec{\boldsymbol{\sigma}}_2,\vec{\boldsymbol{\tau}}) + B(\vec{\boldsymbol{\tau}},\vec{\boldsymbol{u}}_1 - \vec{\boldsymbol{u}}_2) + B(\vec{\boldsymbol{\sigma}}_1 - \vec{\boldsymbol{\sigma}}_2,\vec{\boldsymbol{v}}) - C(\vec{\boldsymbol{u}}_1 - \vec{\boldsymbol{u}}_2,\vec{\boldsymbol{v}})}{\|(\vec{\boldsymbol{\tau}},\vec{\boldsymbol{v}})\|_{\mathbb{V}\times\mathbf{Q}}}\\ &= \sup_{\substack{(\vec{\boldsymbol{\tau}},\vec{\boldsymbol{v}})\in\mathbb{V}\times\mathbf{Q}\\(\vec{\boldsymbol{\tau}},\vec{\boldsymbol{v}})\neq\mathbf{0}}} \frac{D(\varphi_1,\vec{\boldsymbol{\tau}}) - D(\varphi_2,\vec{\boldsymbol{\tau}})}{\|(\vec{\boldsymbol{\tau}},\vec{\boldsymbol{v}})\|_{\mathbb{V}\times\mathbf{Q}}}\\ &\leq \frac{(1+\alpha d)\beta}{2\mu + d\lambda}\|\varphi_1 - \varphi_2\|_{0,\Omega}. \end{aligned}$$

The bound above implies that

$$\|\mathcal{J}_1^{\mathrm{Biot}}(\varphi_1) - \mathcal{J}_1^{\mathrm{Biot}}(\varphi_2)\|_{4,\mathrm{div};\Omega} \leq \frac{(1+\alpha d)\beta}{C_{\mathrm{B}}(2\mu + d\lambda)}\|\varphi_1 - \varphi_2\|_{0,\Omega}. \tag{2.29}$$

On the other hand, given $\boldsymbol{\sigma}_1,\boldsymbol{\sigma}_2 \in \mathbb{H}^{\mathrm{sym}}_{\mathrm{N}}(\mathbf{div},\Omega)$, we let $\mathcal{J}^{\mathrm{diff}}(\boldsymbol{\sigma}_1) = (\boldsymbol{\zeta}_1,\varphi_1) \in \mathbf{H}^4_{\mathrm{N}}(\mathrm{div},\Omega)\times\mathrm{L}^2(\Omega)$ and $\mathcal{J}^{\mathrm{diff}}(\boldsymbol{\sigma}_2) = (\boldsymbol{\zeta}_2,\varphi_2) \in \mathbf{H}^4_{\mathrm{N}}(\mathrm{div},\Omega)\times\mathrm{L}^2(\Omega)$ be the unique solutions of (2.24). This means

$$\begin{aligned} a_{\boldsymbol{\sigma}_1}(\boldsymbol{\zeta}_1,\boldsymbol{\xi}) - a_{\boldsymbol{\sigma}_2}(\boldsymbol{\zeta}_2,\boldsymbol{\xi}) \quad &+ b(\boldsymbol{\xi},\varphi_1 - \varphi_2) &= 0 \qquad &\forall \boldsymbol{\xi} \in \mathbf{H}_{\mathrm{N}}(\mathrm{div},\Omega),\\ b(\boldsymbol{\zeta}_1 - \boldsymbol{\zeta}_2,\psi) \quad &- c(\varphi_1 - \varphi_2,\psi) &= 0 \qquad &\forall \psi \in \mathrm{L}^2(\Omega). \end{aligned}$$

Then, by adding and subtracting the term $a_{\boldsymbol{\sigma}_1}(\boldsymbol{\zeta}_2,\boldsymbol{\xi})$, it follows that

$$a_{\boldsymbol{\sigma}_1}(\boldsymbol{\zeta}_1 - \boldsymbol{\zeta}_2,\boldsymbol{\xi}) + b(\boldsymbol{\zeta}_1 - \boldsymbol{\zeta}_2,\psi) + b(\boldsymbol{\xi},\varphi_1 - \varphi_2) - c(\varphi_1 - \varphi_2,\psi) = a_{\boldsymbol{\sigma}_2}(\boldsymbol{\zeta}_2,\boldsymbol{\xi}) - c_{\boldsymbol{\sigma}_1}(\boldsymbol{\zeta}_2,\boldsymbol{\xi}).$$

Thus, from (2.27b) with $\widehat{\boldsymbol{\sigma}} = \boldsymbol{\sigma}_1$ and $(\boldsymbol{\zeta},\phi) = (\boldsymbol{\zeta}_1 - \boldsymbol{\zeta}_2, \varphi_1 - \varphi_2)$, and the assumptions for ϱ^{-1} (cf. (1.3)) we find that

$$\begin{aligned} \|\varphi_1 - \varphi_2\|_{0,\Omega} + \|\boldsymbol{\zeta}_1 - \boldsymbol{\zeta}_2\|_{4,\mathrm{div};\Omega} &\leq \frac{1}{C_{\mathrm{D}}} \sup_{\substack{(\boldsymbol{\xi},\psi)\in\mathbf{H}^4_{\mathrm{N}}(\mathrm{div},\Omega)\times\mathrm{L}^2(\Omega)\\(\boldsymbol{\xi},\psi)\neq\mathbf{0}}} \frac{|a_{\boldsymbol{\sigma}_2}(\boldsymbol{\zeta}_2,\boldsymbol{\xi}) - a_{\boldsymbol{\sigma}_1}(\boldsymbol{\zeta}_2,\boldsymbol{\xi})|}{\|(\boldsymbol{\xi},\psi)\|_{\mathbf{H}^4_{\mathrm{N}}(\mathrm{div},\Omega)\times\mathrm{L}^2(\Omega)}}\\ &\leq \frac{1}{C_{\mathrm{D}}} \sup_{\substack{(\boldsymbol{\xi},\psi)\in\mathbf{H}^4_{\mathrm{N}}(\mathrm{div},\Omega)\times\mathrm{L}^2(\Omega)\\(\boldsymbol{\xi},\psi)\neq\mathbf{0}}} \frac{\displaystyle\int_\Omega |(\varrho(\boldsymbol{\sigma}_2)^{-1} - \varrho(\boldsymbol{\sigma}_1)^{-1})\boldsymbol{\zeta}_2 \cdot \boldsymbol{\xi}|}{\|(\boldsymbol{\xi},\psi)\|_{\mathbf{H}^4_{\mathrm{N}}(\mathrm{div},\Omega)\times\mathrm{L}^2(\Omega)}} \end{aligned}$$

$$\leq \frac{L_\varrho}{C_{\mathrm{D}}}\|\boldsymbol{\sigma}_2-\boldsymbol{\sigma}_1\|_{0,\Omega}\|\boldsymbol{\zeta}_2\|_{0,4;\Omega}$$
$$\leq \frac{L_\varrho}{C_{\mathrm{D}}}(\|\ell\|_{0,\Omega}+\|\varphi_{\mathrm{D}}\|_{1/2,00;\Gamma_{\mathrm{D}}})\|\boldsymbol{\sigma}_2-\boldsymbol{\sigma}_1\|_{0,\Omega},$$

which implies that

$$\|\mathcal{J}_2^{\mathrm{diff}}(\boldsymbol{\sigma}_1)-\mathcal{J}_2^{\mathrm{diff}}(\boldsymbol{\sigma}_2)\|_{0,\Omega}\leq \frac{L_\varrho}{C_{\mathrm{D}}}(\|\ell\|_{0,\Omega}+\|\varphi_{\mathrm{D}}\|_{1/2,00;\Gamma_{\mathrm{D}}})\|\boldsymbol{\sigma}_1-\boldsymbol{\sigma}_2\|_{0,\Omega}. \tag{2.30}$$

Then, the estimate in (2.28) follows from the definition of $\mathcal{J}$ (cf. (2.25)), the Lipschitz-continuity of $\mathcal{J}_2^{\mathrm{diff}}$ (cf. (2.30)) and $\mathcal{J}_1^{\mathrm{Biot}}$ (cf. (2.29)) with

$$L_{\mathcal{J}}:=\frac{L_\varrho(1+\alpha d)\beta}{C_{\mathrm{B}}C_{\mathrm{D}}(2\mu+d\lambda)}(\|\ell\|_{0,\Omega}+\|\varphi_{\mathrm{D}}\|_{1/2,00;\Gamma_{\mathrm{D}}}). \tag{2.31}$$

□

Owing to the above analysis, we now establish the main result of this section.

Theorem 2.10 (well-posedness of the fully-coupled continuous problem) *Suppose that* $\|\ell\|_{0,\Omega}+\|\varphi_{\mathrm{D}}\|_{1/2,00;\Gamma_{\mathrm{D}}}\leq r$ *and* $L_{\mathcal{J}}<1$ *(cf. (2.31)). Then, the coupled problem (2.2) has a unique solution* $(\vec{\boldsymbol{\sigma}},\vec{\boldsymbol{u}})\in\mathbb{V}\times\mathbf{Q}$ *and* $(\boldsymbol{\zeta},\varphi)\in\mathbf{H}_{\mathrm{N}}^4(\mathrm{div},\Omega)\times\mathrm{L}^2(\Omega)$*. Moreover, we have*

$$\|(\vec{\boldsymbol{\sigma}},\vec{\boldsymbol{u}},\boldsymbol{\zeta},\varphi)\|_{\mathbb{V}\times\mathbf{Q}\times\mathbf{H}_{\mathrm{N}}^4(\mathrm{div},\Omega)\times\mathrm{L}^2(\Omega)}\lesssim\left(\frac{(1+\alpha d)\beta}{2\mu+d\lambda}+1\right)(\|\ell\|_{0,\Omega}+\|\varphi_{\mathrm{D}}\|_{1/2,00;\Gamma_{\mathrm{D}}})+\|\boldsymbol{f}\|_{0,\Omega}+\|g\|_{0,\Omega}$$
$$+\|\boldsymbol{u}_{\mathrm{D}}\|_{1/2,00;\Gamma_{\mathrm{D}}}+\|p_{\mathrm{D}}\|_{1/2,00;\Gamma_{\mathrm{D}}}. \tag{2.32}$$

Proof. We first recall that Lemma 2.8 guarantees that $\mathcal{J}$ maps W into itself. Then, bearing in mind the Lipschitz-continuity of $\mathcal{J}:\mathrm{W}\to\mathrm{W}$ given by Lemma 2.9 along with the fact that $L_{\mathcal{J}}<1$, a direct application of the classical Banach fixed-point Theorem yields the existence of a unique fixed point $\varphi\in\mathrm{W}$ of this operator, and hence a unique solution of (2.2). In addition, the *a priori* estimates provided by Theorem 2.6 and 2.7 yield (2.32), which completes the proof. □

3 Virtual element discretisation

This section introduces the VEM-based discrete formulation for the fully-coupled problem (2.1)-(2.2). We employ a VEM for both 2D/3D linear elasticity problems based on the Hellinger–Reissner variational principle (cf. (1.4a)-(1.4c)). The main advantage of this type of VE space is that it allows the symmetry of the discrete tensor to be enforced strongly. Moreover, its definition is unified in both 2D and 3D, taking into account that in 3D, facets correspond to the faces of the polyhedral element, while in 2D, they correspond to the edges of the polygonal element. On the other hand, the VEM employed here for mixed second order elliptic problems (corresponding to the equations (1.4d)-(1.4e) and (1.4f)-(1.4g)) requires separate definitions in 2D and 3D. In addition, we introduce appropriate polynomial projection, interpolation and stabilisation operators to guarantee computability of the discrete formulation.

We recall that the detailed construction, unisolvence in terms of the corresponding Degrees of Freedom (DoFs), additional properties of the VE spaces; as well with the properties of the polynomial spaces and the computability of the polynomial projection operators in terms of the (respective) DoFs presented in this section are provided in [2, 5, 6, 47].

Assumptions on the mesh. Let $\mathcal{T}_h$ be a collection of polygonal/polyhedral meshes on Ω and $\mathcal{F}_h$ be the set of all facets in 3D (edges in 2D). The diameter of a polygon/polyhedron K is represented by h_K and the length/area of a facet f is represented by h_f. The maximum diameter of elements in $\mathcal{T}_h$ is represented by h. It is assumed that there exists a uniform positive constant η such that

(A1) Every element K has a star-shaped interior with respect to a ball with a radius greater than ηh_K.

(A2) Every facet $f\in\partial K$ has a star-shaped interior with respect to a ball with a radius greater than ηh_K.

(A3) Every facet $f\in\partial K$ satisfies the inequality $h_f\geq\eta h_K$.

Polynomial spaces. In this paper, we consider an arbitrary polynomial degree $k \geq 1$. The space of polynomials of total degree at most k defined locally on $K \in \mathcal{T}_h$ (or facet $f \in \mathcal{F}_h$) is represented by $\mathrm{P}_k(K)$, and its vector and tensor counterparts are represented by $\mathbf{P}_k(K)$ and $\mathbb{P}_k(K)$, respectively. We also consider the standard notation $\mathrm{P}_{-1}(K) = \{0\}$.

The spaces $\mathbf{G}_k(K) := \nabla(\mathrm{P}_{k+1}(K))$ and $\mathbf{G}_k^{\oplus}(K)$ denote the gradients of polynomials of degree $\leq k+1$ on K and the complement of the space $\mathbf{G}_k(K)$ in the vector polynomial space $\mathbf{P}_k(K)$ such that the direct sum $\mathbf{P}_k(K) = \mathbf{G}_k(K) \oplus \mathbf{G}_k^{\oplus}(K)$ holds, respectively. In particular, we select $\mathbf{G}_k^{\oplus}(K) = \boldsymbol{x}^{\perp}\mathrm{P}_{k-1}(K)$ (resp. $\mathbf{G}_k^{\oplus}(K) := \boldsymbol{x} \wedge (\mathbf{P}_{k-1}(K))$ where $\boldsymbol{x}^{\perp} = (x_2, -x_1)^{\mathtt{t}}$ in 2D (resp. $\boldsymbol{x} := (x_1, x_2, x_3)^{\mathtt{t}}$ and $\wedge$ the usual external product in 3D).

Let $\boldsymbol{x}_K = (x_{1,K}, x_{2,K})^{\mathtt{t}}$ (resp. $\boldsymbol{x}_K = (x_{1,K}, x_{2,K}, x_{3,K})^{\mathtt{t}}$) denote the barycentre of K and let $\mathbf{M}_k(K)$ be the set of vector scaled monomials as

$$\mathbf{M}_k(K) := \left\{ \left(\frac{\boldsymbol{x} - \boldsymbol{x}_K}{h_K} \right)^{\boldsymbol{\alpha}} \in \mathbf{P}_k(K) : \ 0 \leq |\boldsymbol{\alpha}| \leq k \right\},$$

where $\boldsymbol{\alpha} = (\alpha_1, \alpha_2)^{\mathtt{t}}$ (resp. $\boldsymbol{\alpha} = (\alpha_1, \alpha_2, \alpha_3)^{\mathtt{t}}$) is a non-negative multi-index with $|\boldsymbol{\alpha}| = \alpha_1 + \alpha_2$ and $\boldsymbol{x}^{\boldsymbol{\alpha}} = x_1^{\alpha_1} x_2^{\alpha_2}$ in 2D (resp. $|\boldsymbol{\alpha}| = \alpha_1 + \alpha_2 + \alpha_3$ and $\boldsymbol{x}^{\boldsymbol{\alpha}} = x_1^{\alpha_1} x_2^{\alpha_2} x_3^{\alpha_3}$ in 3D), with analogous definition for the scalar and tensor version M_k and $\mathbb{M}_k$. Notice that the polynomial decompositions presented before hold also in terms of the scaled monomial. For example, in the 2D case, we can take the sets $\mathbf{G}_k(K)$ and $\mathbf{G}_k^{\oplus}(K)$ as $\mathbf{M}_k^{\nabla}(K) := \nabla \mathrm{M}_{k+1}(K) \setminus \{\mathbf{0}\}$ and $\mathbf{M}_k^{\oplus}(K) := \mathbf{m}^{\perp}\mathrm{M}_{k-1}(K)$, with $\mathbf{m}^{\perp} := (\frac{x_2 - x_{2,E}}{h_K}, \frac{x_{1,K} - x_1}{h_K})^{\mathtt{t}}$ and $\mathbf{m} := \frac{\boldsymbol{x} - \boldsymbol{x}_K}{h_K}$, respectively; and providing the decomposition $\mathbf{M}_k(K) = \mathbf{M}_k^{\nabla}(K) \oplus \mathbf{M}_k^{\oplus}(K)$.

The set of polynomials that solves locally the constitutive law in linear elasticity is defined as $\widetilde{\mathbb{M}}_k(K) := \{\widetilde{\mathbf{m}}_k \in \mathbb{M}_k(K) : \ \widetilde{\mathbf{m}}_k = \mathcal{C}\boldsymbol{\varepsilon}(\mathbf{m}_{k+1}) \text{ for some } \mathbf{m}_{k+1} \in \mathbf{M}_{k+1}(K)\}$. On the other hand, the set of scaled rigid body motions of an element K is given by

$$\mathbf{RBM}(K) := \begin{cases} \left\{ \begin{pmatrix} \frac{1}{h_E} \\ 0 \end{pmatrix}, \begin{pmatrix} 0 \\ \frac{1}{h_E} \end{pmatrix}, \begin{pmatrix} \frac{x_{2,E} - x_2}{h_E} \\ \frac{x_1 - x_{1,E}}{h_E} \end{pmatrix} \right\} & \text{in 2D,} \\ \left\{ \begin{pmatrix} \frac{1}{h_P} \\ 0 \\ 0 \end{pmatrix}, \begin{pmatrix} 0 \\ \frac{1}{h_P} \\ 0 \end{pmatrix}, \begin{pmatrix} 0 \\ 0 \\ \frac{1}{h_P} \end{pmatrix}, \begin{pmatrix} \frac{x_{2,P} - x_2}{h_P} \\ \frac{x_1 - x_{1,P}}{h_P} \\ 0 \end{pmatrix}, \begin{pmatrix} 0 \\ \frac{x_{3,P} - x_3}{h_P} \\ \frac{x_2 - x_{2,P}}{h_P} \end{pmatrix}, \begin{pmatrix} \frac{x_3 - x_{3,P}}{h_P} \\ 0 \\ \frac{x_{1,P} - x_1}{h_P} \end{pmatrix} \right\} & \text{in 3D.} \end{cases}$$

In this case, the polynomial decomposition $\mathbf{P}_k(K) = \mathbf{RBM}(K) \oplus \mathbf{RBM}_k^{\perp}(K)$, holds with

$$\mathbf{RBM}^{\perp}(K) := \left\{ \mathbf{m}_k \in \mathbf{M}_k : \int_K \mathbf{m}_k \cdot \mathbf{m}_{\mathbf{RBM}} = 0, \ \forall \mathbf{m}_{\mathbf{RBM}} \in \mathbf{RBM}(K) \right\}.$$

3.1 VEM for Hellinger–Reissner linear elasticity

The associated (conforming) VE space for $\mathbb{H}(\mathbf{div}, \Omega)$ in both 2D and 3D locally solves the constitutive law in linear elasticity [2, 47] and its defined by

$$\begin{aligned} \mathbb{S}^{h,k}(K) := \{ \boldsymbol{\tau}_h \in \mathbb{H}(\mathbf{div}, K) : \boldsymbol{\tau}_h \boldsymbol{n}|_f \in \mathbf{P}_k(f), \ \forall f \in \partial K, \\ \mathbf{div}\, \boldsymbol{\tau}_h \in \mathbf{P}_k(K), \ \boldsymbol{\tau}_h = \mathcal{C}\boldsymbol{\varepsilon}(\boldsymbol{v}^*) \text{ for some } \boldsymbol{v}^* \in \mathbf{H}^1(K) \}. \end{aligned}$$

Notice that the polynomial space $\widetilde{\mathbb{P}}_k(K) := \{ \widetilde{\mathbf{p}}_k \in \mathbb{P}_k(K) : \ \widetilde{\mathbf{p}}_k = \mathcal{C}\boldsymbol{\varepsilon}(\mathbf{p}_{k+1}) \text{ for some } \mathbf{p}_{k+1} \in \mathbf{P}_{k+1}(K) \} \subseteq \mathbb{S}^{h,k}(K)$. To define the global discrete spaces we patch together the local spaces in the following way

$$\begin{aligned} \mathbb{S}^{h,k} &:= \{ \boldsymbol{\tau}_h \in \mathbb{H}_{\mathrm{N}}^{\mathrm{sym}}(\mathbf{div}, \Omega) \colon \boldsymbol{\tau}_h|_K \in \mathbb{S}^{h,k}(K), \ \forall K \in \mathcal{T}_h \}, \\ \mathbf{U}^{h,k} &:= \{ \boldsymbol{v}_h \in \mathbf{L}^2(\Omega) \colon \boldsymbol{v}_h|_K \in \mathbf{P}_k(K), \ \forall K \in \mathcal{T}_h \}. \end{aligned}$$

The associated DoFs for $\boldsymbol{\tau}_h \in \mathbb{S}^{h,k}(K)$ and $\boldsymbol{v}_h \in \mathbf{U}^{h,k}(K) := \mathbf{P}_k(K)$ are given as follows

- $\displaystyle \frac{1}{h_f} \int_f \boldsymbol{\tau}_h \boldsymbol{n} \cdot \mathbf{m}_k, \quad \forall \mathbf{m}_k \in \mathbf{M}_k(f),$
- $\displaystyle \frac{1}{h_K} \int_K \mathbf{div}\, \boldsymbol{\tau}_h \cdot \mathbf{m}_{\mathbf{RBM}^{\perp}}, \quad \forall \mathbf{m}_{\mathbf{RBM}^{\perp}} \in \mathbf{RBM}^{\perp}(K),$
- $\displaystyle \frac{1}{h_K} \int_K \boldsymbol{v}_h \cdot \mathbf{m}_k, \quad \forall \mathbf{m}_k \in \mathbf{M}_k(K).$

3.2 VEM for perturbed mixed second-order elliptic problems

The conforming VE approximation for the space $\mathbf{H}(\mathrm{div},\Omega)$ in 2D is defined locally by solving a div-rot problem [6], as follows

$$\mathbf{V}^{h,k}_{2\mathrm{D}}(K) := \{\boldsymbol{\xi}_h \in \mathbf{H}(\mathrm{div},K)\cap\mathbf{H}(\mathrm{rot},K)\colon\ \boldsymbol{\xi}_h\cdot\boldsymbol{n}|_f \in \mathrm{P}_k(f),\ \forall f\subset\partial K,\\ \mathrm{div}\,\boldsymbol{\xi}_h \in \mathrm{P}_k(K),\ \mathrm{rot}\,\boldsymbol{\xi}_h \in \mathrm{P}_{k-1}(K)\}.$$

Observe that $\mathbf{P}_k(K)\subseteq \mathbf{V}^{h,k}_{2\mathrm{D}}(K)$. In turn, the global discrete space is defined as

$$\mathbf{V}^{h,k}_{2\mathrm{D}} := \{\boldsymbol{\xi}_h \in \mathbf{H}_{\mathrm{N}}(\mathrm{div},\Omega)\colon \boldsymbol{\xi}_h|_K \in \mathbf{V}^{h,k}_{2\mathrm{D}}(K),\ \forall K\in\mathcal{T}_h\}.$$

We consider the following DoFs for $\boldsymbol{\xi}_h \in \mathbf{V}^{h,k}_{2\mathrm{D}}(K)$:

- The values of $\boldsymbol{\xi}_h\cdot\boldsymbol{n}$ at the $k+1$ Gauss–Lobatto quadrature points of each edge of K,
- $\dfrac{1}{h_K}\displaystyle\int_K \boldsymbol{\xi}_h\cdot\mathbf{m}^{\nabla}_{k-1},\quad \forall\mathbf{m}^{\nabla}_{k-1}\in\mathbf{M}^{\nabla}_{k-1}(K),$
- $\dfrac{1}{h_K}\displaystyle\int_K \boldsymbol{\xi}_h\cdot\mathbf{m}^{\oplus}_{k},\quad \forall\mathbf{m}^{\oplus}_{k}\in\mathbf{M}^{\oplus}_{k}(K).$

In contrast, the 3D version of the conforming VE approximation for the space $\mathbf{H}(\mathrm{div},\Omega)$ locally solves a $\nabla(\mathrm{div})$–$\mathbf{curl}\,\mathbf{curl}$ problem [5] and it is defined as

$$\mathbf{V}^{h,k+1}_{3\mathrm{D}}(K) := \{\boldsymbol{\xi}_h \in \mathbf{H}(\mathrm{div},K)\cap\mathbf{H}(\mathbf{curl},K)\colon\ \boldsymbol{\xi}_h\cdot\boldsymbol{n}|_f \in \mathrm{P}_{k+1}(f),\ \forall f\in\partial K,\\ \nabla(\mathrm{div}\,\boldsymbol{\xi}_h) \in \mathbf{G}_{k-1}(K),\ \mathbf{curl}\,\mathbf{curl}\,\boldsymbol{\xi}_h \in \mathbf{P}_{k}(K)\}.$$

Note that $\mathbf{P}_{k+1}(K)\subseteq \mathbf{V}^{h,k+1}_{3\mathrm{D}}(K)$. Then, the discrete global spaces are defined by

$$\mathbf{V}^{h,k+1}_{3\mathrm{D}} := \{\boldsymbol{\xi}_h \in \mathbf{H}_{\mathrm{N}}(\mathrm{div},\Omega)\colon \boldsymbol{\xi}_h|_K \in \mathbf{V}^{h,k+1}_{3\mathrm{D}}(K),\ \forall K\in\mathcal{T}_h\}.$$

The set of DoFs for $\boldsymbol{\xi}_h \in \mathbf{V}^{h,k+1}_{3\mathrm{D}}(K)$ is provided next

- The values of $\boldsymbol{\xi}_h\cdot\boldsymbol{n}$ at the $k+2$ quadrature points on each face of K,
- $\dfrac{1}{h_K}\displaystyle\int_K \boldsymbol{\xi}_h\cdot\mathbf{m}^{\nabla}_{k-1},\quad \forall\mathbf{m}^{\nabla}_{k-1}\in\mathbf{M}^{\nabla}_{k-1}(K),$
- $\dfrac{1}{h_K}\displaystyle\int_K \boldsymbol{\xi}_h\cdot\mathbf{m}^{\oplus}_{k+1},\quad \forall\mathbf{m}^{\oplus}_{k+1}\in\mathbf{M}^{\oplus}_{k+1}(K).$

Finally, the global discrete space for the space $\mathrm{L}^2(\Omega)$ is defined in general for 2D and 3D as

$$\mathrm{Q}^{h,k} := \{\psi_h \in \mathrm{L}^2(\Omega)\colon \psi_h|_K \in \mathrm{P}_k(K),\ \forall K\in\mathcal{T}_h\},$$

and, for a given $\psi_h \in \mathrm{Q}^{h,k}(K) := \mathrm{P}_k(K)$, the DoFs for the space above are defined by

- $\dfrac{1}{h_K}\displaystyle\int_K \psi_h m_k,\quad \forall m_k\in\mathrm{M}_k(K).$

3.3 Polynomial projection and interpolation operators

For each element K, we introduce the following local polynomial projection operators:

- The $\mathcal{C}$-energy projection is defined as $\sqcap^{\mathcal{C},K}_k : \widetilde{\mathbb{S}}(K)\to\widetilde{\mathbb{M}}_k(K)$ by

$$\int_K \mathcal{C}^{-1}\left(\boldsymbol{\tau}-\sqcap^{\mathcal{C},K}_k\boldsymbol{\tau}\right) : \widetilde{\mathbf{m}}_k = 0,\quad \forall\boldsymbol{\tau}\in\widetilde{\mathbb{S}}(K),\ \forall\widetilde{\mathbf{m}}_k\in\widetilde{\mathbb{M}}_k(K), \tag{3.1}$$

where $\widetilde{\mathbb{S}}(K) := \{\boldsymbol{\tau}\in\mathbb{H}(\mathbf{div},K):\ \boldsymbol{\tau}=\mathcal{C}\boldsymbol{\varepsilon}(\boldsymbol{v})\text{ for some }\boldsymbol{v}\in\mathbf{H}^1(K)\}.$

- The $\mathbf{L}^2$ projection is defined by $\mathbf{\Pi}_k^{0,K} : \mathbf{L}^2(K) \to \mathbf{M}_k(K)$ where

$$\int_K \left(\boldsymbol{\xi} - \mathbf{\Pi}_k^{0,K}\boldsymbol{\xi}\right) \cdot \mathbf{m}_k = 0, \ \forall \boldsymbol{\xi} \in \mathbf{L}^2(K), \ \forall \mathbf{m}_k \in \mathbf{M}_k(K), \tag{3.2}$$

with an analogous definition for scalar functions.

The detailed proof of computability of these operators in terms of the respective DoFs can be found in [2, 5, 6, 47]. In addition, we state a result involving classical polynomial approximation theory [13]. The estimate is presented for scalar functions, but it also holds in general for vector and tensor functions.

Proposition 3.1 (polynomial approximation) *Given $K \in \mathcal{T}_h$, assume that $v \in \mathrm{H}^{\overline{s}}(K)$, with $1 \leq \overline{s} \leq k+1$. Then, there exist $v_\pi \in \mathrm{P}_k(K)$ and a positive constant that depends only on η (cf. (A1)-(A3)) such that for $0 \leq \overline{r} \leq \overline{s}$ the following estimate holds*

$$|v - v_\pi|_{\overline{r},K} \lesssim h_K^{\overline{s}-\overline{r}} |v|_{\overline{s},K}.$$

Next, the nature of the space defined in Section 3.1 allow us to define locally the Fortin–like interpolation operator $\mathbb{F}^{k,K} : \mathbb{H}^1(K) \to \mathbb{S}^{h,k}(K)$ through the associated DoFs in a unified way for an element K (cf. [11]). Whereas, following Section 3.2, the Fortin–like interpolation operators $\mathbf{F}_{2\mathrm{D}}^{k,K} : \mathbf{H}^1(K) \to \mathbf{V}_{2\mathrm{D}}^{h,k}(K)$ and $\mathbf{F}_{3\mathrm{D}}^{k+1,K} : \mathbf{H}^1(K) \to \mathbf{V}_{3\mathrm{D}}^{h,k+1}(K)$ are defined by their associated DoFs, taking into account that the element K refers to a polygon in 2D and a polyhedral in 3D. See, e.g., [6, Section 3.2] and [7, Section 4.1] for their respective constructions. Moreover, the associated commutative property holds for each operator as follows: for each $K \in \mathcal{T}_h$, we have

$$\mathbf{div}(\mathbb{F}^{k,K}\boldsymbol{\tau}) = \mathbf{\Pi}_k^{0,K}(\mathbf{div}\,\boldsymbol{\tau}), \quad \mathrm{div}(\mathbf{F}_{2\mathrm{D}}^{k,K}\boldsymbol{\xi}) = \Pi_k^{0,K}(\mathrm{div}\,\boldsymbol{\xi}), \quad \mathrm{div}(\mathbf{F}_{3\mathrm{D}}^{k+1,K}\boldsymbol{\xi}) = \Pi_k^{0,K}(\mathrm{div}\,\boldsymbol{\xi}). \tag{3.3}$$

Proposition 3.2 (Hellinger–Reissner VEM interpolation estimates) *Given $K \in \mathcal{T}_h$, assume that $\boldsymbol{\tau} \in \mathbb{H}(\mathbf{div}, K) \cap \mathbb{H}^{\overline{s}}(K)$, with $1 \leq \overline{s} \leq k+1$. Then, there exists a positive constant that depends only on η (cf. (A1)-(A3)) such that, for $0 \leq \overline{r} \leq \overline{s}$, the following estimate holds*

$$|\boldsymbol{\tau} - \mathbb{F}^{k,K}\boldsymbol{\tau}|_{\overline{r},K} \lesssim h_K^{\overline{s}-\overline{r}} |\boldsymbol{\tau}|_{\overline{s},K}.$$

Proposition 3.3 (mixed VEM interpolation estimates) *Given $K \in \mathcal{T}_h$ and $1 \leq \overline{s} \leq k+1$, there exist positive constants that depend only on η (cf. (A1)-(A3)) such that for $0 \leq \overline{r} \leq \overline{s}$ the following estimates hold*

$$\|\boldsymbol{\xi} - \mathbf{F}_{2\mathrm{D}}^{k,K}\boldsymbol{\xi}\|_{0,\overline{l};K} \lesssim h_K^{\overline{s}-\overline{r}} |\boldsymbol{\xi}|_{\overline{s},\overline{l};K}, \qquad \|\boldsymbol{\xi} - \mathbf{F}_{3\mathrm{D}}^{k+1,K}\boldsymbol{\xi}\|_{0,\overline{l};K} \lesssim h_K^{\overline{s}-\overline{r}} |\boldsymbol{\xi}|_{\overline{l},\overline{s};K} \qquad \forall \boldsymbol{\xi} \in \mathbf{W}^{\overline{s},\overline{l}}(K).$$

Remark 3.1 *Typically, one also requires an interpolation property for the divergence part of the flux (or stress) space to obtain error estimates (see, for example, [30–32] for mixed VEM in the L^p context). Such a property calls for additional regularity for the divergence part, for example (using the notation from Proposition 3.3 in the 2D case)*

$$\|\,\mathrm{div}(\boldsymbol{\xi} - \mathbf{F}_{2\mathrm{D}}^{k,K}\boldsymbol{\xi})\|_{0,K} \lesssim h_K^{\overline{s}-\overline{r}} |\,\mathrm{div}\,\boldsymbol{\xi}|_{\overline{s},K} \qquad \forall \boldsymbol{\xi} \in \mathbf{W}^{1,1}(K) \text{ such that } \mathrm{div}\,\boldsymbol{\xi} \in \mathrm{H}^{\overline{s}}(K).$$

Here we proceed differently and derive estimates involving the divergence by simply using the commutativity property (3.3) and applying Proposition 3.1. This avoids the assumption of more regularity for the divergence, but rather asking it for the concentration.

3.4 Discrete problem

Without losing generality we denote by $\mathbf{V}^{h,\overline{k}}$ the global discrete spaces defined in Section 3.2, i.e., $\mathbf{V}^{h,\overline{k}} = \mathbf{V}_{2\mathrm{D}}^{h,k}$ (resp. $\mathbf{V}^{h,\overline{k}} = \mathbf{V}_{3\mathrm{D}}^{h,k+1}$) for polygonal elements (resp. polyhedral elements), we also introduce the discrete product spaces $\mathbb{V}^{h,k} := \mathbb{S}^{h,k} \times \mathrm{Q}^{h,k}$ and $\mathbf{Q}^{h,k} := \mathrm{U}^{h,k} \times \mathbf{V}^{h,\overline{k}}$, and note that the space $\widetilde{\mathbf{V}}^{h,\overline{k}} := \mathbf{V}^{h,\overline{k}} \cap \mathbf{H}_{\mathrm{N}}^4(\mathrm{div}, \Omega)$ consists of the discrete space $\mathbf{V}^{h,\overline{k}}$ equipped with the norm $\|\cdot\|_{4,\mathrm{div};\Omega}$. For brevity, (and wherever needed) the polynomial projections of $\boldsymbol{\sigma}_h \in \mathbb{S}^{h,k}$, $\boldsymbol{z}_h \in \mathbf{V}^{h,\overline{k}}$ and $\boldsymbol{\zeta}_h \in \widetilde{\mathbf{V}}^{h,\overline{k}}$ are denoted by $\boldsymbol{\sigma}_h^{\sqcap} := \sqcap_k^{\mathcal{C},K}\boldsymbol{\sigma}_h$, $\boldsymbol{z}_h^{\mathbf{\Pi}} := \mathbf{\Pi}_{\overline{k}}^{0,K}\boldsymbol{z}_h$ and $\boldsymbol{\zeta}_h^{\mathbf{\Pi}} := \mathbf{\Pi}_{\overline{k}}^{0,K}\boldsymbol{\zeta}_h$, respectively, where the projection $\boldsymbol{\Pi}^{0,K}_{\overline{k}}$ refers to $\boldsymbol{\Pi}^{0,K}_{k}$ in the two dimensional setting (resp. $\boldsymbol{\Pi}^{0,K}_{k+1}$ in the three dimensional setting). We recall that the computability of the discrete formulation (introduced below) follows directly from the computability of the projection operators discussed in Section 3.3.

Given $\vec{\boldsymbol{\sigma}}_h := (\boldsymbol{\sigma}_h, p_h)$, $\vec{\boldsymbol{\tau}}_h := (\boldsymbol{\tau}_h, q_h) \in \mathbb{V}^{h,k}$, $\vec{\boldsymbol{u}}_h := (\boldsymbol{u}_h, \boldsymbol{z}_h)$, $\vec{\boldsymbol{v}}_h := (\boldsymbol{v}_h, \boldsymbol{w}_h) \in \mathbf{Q}^{h,k}$, and a fixed polynomial $\widehat{\boldsymbol{\sigma}}^{\Pi}_h \in \widetilde{\mathbb{M}}_k(K)$, the computable discrete bilinear forms $A_h : \mathbb{V}^{h,k} \times \mathbb{V}^{h,k} \to \mathbb{R}$, $B : \mathbb{V}^{h,k} \times \mathbf{Q}^{h,k} \to \mathbb{R}$, $C_h : \mathbf{Q}^{h,k} \times \mathbf{Q}^{h,k} \to \mathbb{R}$, $D_h : \mathrm{Q}^{h,k} \times \mathbb{V}^{h,k} \to \mathbb{R}$, $a_{h,\widehat{\boldsymbol{\sigma}}^{\Pi}_h} : \widetilde{\mathbf{V}}^{h,\overline{k}} \times \widetilde{\mathbf{V}}^{h,\overline{k}} \to \mathbb{R}$, $b : \mathrm{Q}^{h,k} \times \widetilde{\mathbf{V}}^{h,\overline{k}} \to \mathbb{R}$, and $c : \mathrm{Q}^{h,k} \times \mathrm{Q}^{h,k} \to \mathbb{R}$, are defined as

$$
\begin{aligned}
A_h(\vec{\boldsymbol{\sigma}}_h, \vec{\boldsymbol{\tau}}_h) &= \sum_{K\in\mathcal{T}_h} A_h^K(\vec{\boldsymbol{\sigma}}_h, \vec{\boldsymbol{\tau}}_h) \\
&:= \sum_{K\in\mathcal{T}_h} \Big[(\mathcal{C}^{-1}(\Pi^{\mathcal{C},K}_k \boldsymbol{\sigma}_h), \Pi^{\mathcal{C},K}_k \boldsymbol{\tau}_h)_K + S_1^{\mathcal{C},K}((\mathbb{1} - \Pi^{\mathcal{C},K}_k)\boldsymbol{\sigma}_h, (\mathbb{1} - \Pi^{\mathcal{C},K}_k)\tau_h) \\
&\qquad + \big(\frac{\alpha p_h}{2\mu + d\lambda}, \operatorname{tr}(\Pi^{\mathcal{C},K}_k \boldsymbol{\tau}_h)\big)_K + \big(\frac{\alpha q_h}{2\mu + d\lambda}, \operatorname{tr}(\Pi^{\mathcal{C},K}_k \boldsymbol{\sigma}_h)\big)_K + \big[s_0 + \frac{d\alpha^2}{2\mu + d\lambda}\big](p_h, q_h)_K \Big], \\
B(\vec{\boldsymbol{\tau}}_h, \vec{\boldsymbol{v}}_h) &= \sum_{K\in\mathcal{T}_h} B^K(\vec{\boldsymbol{\tau}}_h, \vec{\boldsymbol{v}}_h) := \sum_{K\in\mathcal{T}_h} \Big[(\boldsymbol{v}_h, \mathbf{div}\, \boldsymbol{\tau}_h)_K + (q_h, \operatorname{div} \boldsymbol{w}_h)_K \Big], \\
C_h(\vec{\boldsymbol{u}}_h, \vec{\boldsymbol{v}}_h) &= \sum_{K\in\mathcal{T}_h} C_h^K(\vec{\boldsymbol{u}}_h, \vec{\boldsymbol{v}}_h) \\
&:= \sum_{K\in\mathcal{T}_h} \Big[(\boldsymbol{\kappa}^{-1}(\boldsymbol{\Pi}^{0,K}_{\overline{k}} \boldsymbol{z}_h), \boldsymbol{\Pi}^{0,K}_{\overline{k}} \boldsymbol{w}_h)_K + S_2^{0,K}((\mathbf{1} - \boldsymbol{\Pi}^{0,K}_{\overline{k}})\boldsymbol{z}_h, (\mathbf{1} - \boldsymbol{\Pi}^{0,K}_{\overline{k}})\boldsymbol{w}_h) \Big], \\
D_h(\psi_h, \vec{\boldsymbol{\tau}}_h) &= \sum_{K\in\mathcal{T}_h} D_h(\psi_h, \vec{\boldsymbol{\tau}}_h) := \sum_{K\in\mathcal{T}_h} (\frac{\beta\psi_h}{2\mu + d\lambda}, \operatorname{tr}(\Pi^{\mathcal{C},K}_k \boldsymbol{\tau}_h) + \alpha d q_h)_K, \\
a_{h,\widehat{\boldsymbol{\sigma}}^{\Pi}_h}(\boldsymbol{\zeta}_h, \boldsymbol{\xi}_h) &= \sum_{K\in\mathcal{T}_h} a^K_{h,\widehat{\boldsymbol{\sigma}}^{\Pi}_h}(\boldsymbol{\zeta}_h, \boldsymbol{\xi}_h) \\
&:= \sum_{K\in\mathcal{T}_h} \Big[(\varrho(\widehat{\boldsymbol{\sigma}}^{\Pi}_h)^{-1}(\boldsymbol{\Pi}^{0,K}_{\overline{k}} \boldsymbol{\zeta}_h), \boldsymbol{\Pi}^{0,K}_{\overline{k}} \boldsymbol{\xi}_h)_K + S_3^{0,\boldsymbol{\sigma}^{\Pi}_h,K}((\mathbf{1} - \boldsymbol{\Pi}^{0,K}_{\overline{k}})\boldsymbol{\zeta}_h, (\mathbf{1} - \boldsymbol{\Pi}^{0,K}_{\overline{k}})\boldsymbol{\xi}_h) \Big], \\
b(\boldsymbol{\xi}_h, \psi_h) &= \sum_{K\in\mathcal{T}_h} b^K(\boldsymbol{\xi}_h, \psi_h) := -\sum_{K\in\mathcal{T}_h} (\operatorname{div} \boldsymbol{\xi}_h, \psi_h)_K, \\
c(\varphi_h, \psi_h) &= \sum_{K\in\mathcal{T}_h} c^K(\varphi_h, \psi_h) := \sum_{K\in\mathcal{T}_h} (\varphi_h, \psi_h)_K.
\end{aligned}
$$

The stabilisation terms $S_1^{\mathcal{C},K} : \mathbb{V}^{h,k} \times \mathbb{V}^{h,k} \to \mathbb{R}$, $S_2^{0,K} : \mathbf{Q}^{h,k} \times \mathbf{Q}^{h,k} \to \mathbb{R}$, and $S_3^{0,K} : \widetilde{\mathbf{V}}^{h,\overline{k}} \times \widetilde{\mathbf{V}}^{h,\overline{k}} \to \mathbb{R}$ are assumed to be any positive semi-definite inner products satisfying the following condition: for each $K \in \mathcal{T}_h$, there exist positive constants $C_{s_1}, C_{s_2}, C_{s_3}$ (independent of h and K) such that

$$
\begin{aligned}
C_{s1}^{-1}(\mathcal{C}^{-1}\boldsymbol{\tau}_h, \boldsymbol{\tau}_h)_K &\le S_1^{\mathcal{C},K}(\boldsymbol{\tau}_h, \boldsymbol{\tau}_h) \le C_{s1}(\mathcal{C}^{-1}\boldsymbol{\tau}_h, \boldsymbol{\tau}_h)_K \qquad \forall \boldsymbol{\tau}_h \in \ker(\Pi^{\mathcal{C},K}_k), &\text{(3.4a)} \\
C_{s2}^{-1}(\boldsymbol{\kappa}^{-1}\boldsymbol{w}_h, \boldsymbol{w}_h)_K &\le S_2^{0,K}(\boldsymbol{w}_h, \boldsymbol{w}_h) \le C_{s2}(\boldsymbol{\kappa}^{-1}\boldsymbol{w}_h, \boldsymbol{w}_h)_K \qquad \forall \boldsymbol{w}_h \in \ker(\boldsymbol{\Pi}^{0,K}_{\overline{k}}), &\text{(3.4b)} \\
C_{s3}^{-1}(\varrho(\widehat{\boldsymbol{\sigma}}^{\Pi}_h)^{-1}\boldsymbol{\xi}_h, \boldsymbol{\xi}_h)_K &\le S_3^{0,K}(\boldsymbol{\xi}_h, \boldsymbol{\xi}_h) \le C_{s3}(\varrho(\widehat{\boldsymbol{\sigma}}^{\Pi}_h)^{-1}\boldsymbol{\xi}_h, \boldsymbol{\xi}_h)_K \quad \forall \boldsymbol{\xi}_h \in \ker(\boldsymbol{\Pi}^{0,K}_{\overline{k}}). &\text{(3.4c)}
\end{aligned}
$$

Finally, the computable linear functionals $F : \mathbb{V}^{h,k} \to \mathbb{R}$, $G : \mathbf{Q}^{h,k} \to \mathbb{R}$, $H : \widetilde{\mathbf{V}}^{h,\overline{k}} \to \mathbb{R}$, and $I_h : \mathrm{Q}^{k,k} \to \mathbb{R}$ are given by

$$
\begin{aligned}
F(\vec{\boldsymbol{\tau}}_h) &= \sum_{K\in\mathcal{T}_h} F^K(\vec{\boldsymbol{\tau}}_h) := \sum_{K\in\mathcal{T}_h} \Big[\sum_{F\in\partial K\cap\Gamma_{\mathrm{D}}} \langle \boldsymbol{u}_{\mathrm{D}}, \boldsymbol{\tau}_h \boldsymbol{n} \rangle_F + (g, q_h)_K \Big], \\
G(\vec{\boldsymbol{v}}_h) &= \sum_{K\in\mathcal{T}_h} G^K(\vec{\boldsymbol{v}}_h) := -\sum_{K\in\mathcal{T}_h} \Big[(\boldsymbol{f}, \boldsymbol{v}_h)_K + \sum_{F\in\partial K\cap\Gamma_{\mathrm{D}}} \langle p_{\mathrm{D}}, \boldsymbol{w}_h \cdot \boldsymbol{n} \rangle_F \Big], \\
H(\boldsymbol{\xi}_h) &= \sum_{K\in\mathcal{T}_h} H^K(\boldsymbol{\xi}_h) := -\sum_{K\in\mathcal{T}_h} \sum_{F\in\partial K\cap\Gamma_{\mathrm{D}}} \langle \varphi_{\mathrm{D}}, \boldsymbol{\xi}_h \cdot \boldsymbol{n} \rangle_F,
\end{aligned}
$$

$$I(\psi_h) = \sum_{K\in\mathcal{T}_h} I^K(\psi_h) := -\sum_{K\in\mathcal{T}_h} (\ell,\psi_h)_K.$$

The discrete version of (2.2) is defined next: find $(\vec{\boldsymbol{\sigma}}_h, \vec{\boldsymbol{u}}_h) \in \mathbb{V}^{h,k} \times \mathbf{Q}^{h,k}$ and $(\varphi_h, \boldsymbol{\zeta}_h) \in \mathrm{Q}^{h,k} \times \widetilde{\mathbf{V}}^{h,\bar{k}}$, such that

$$\begin{aligned}
A_h(\vec{\boldsymbol{\sigma}}_h,\vec{\boldsymbol{\tau}}_h) + B(\vec{\boldsymbol{\tau}}_h,\vec{\boldsymbol{u}}_h) + D_h(\varphi_h,\vec{\boldsymbol{\tau}}_h) &= F(\vec{\boldsymbol{\tau}}_h) && \forall \vec{\boldsymbol{\tau}}_h \in \mathbb{V}^{h,k}, && (3.5a)\\
B(\vec{\boldsymbol{\sigma}}_h,\vec{\boldsymbol{v}}_h) - C_h(\vec{\boldsymbol{u}}_h,\vec{\boldsymbol{v}}_h) &= G(\vec{\boldsymbol{v}}_h) && \forall \vec{\boldsymbol{v}}_h \in \mathbf{Q}^{h,k}, && (3.5b)\\
a_{h,\boldsymbol{\sigma}_h^{\mathbb{\Pi}}}(\boldsymbol{\zeta}_h,\boldsymbol{\xi}_h) + b(\boldsymbol{\xi}_h,\varphi_h) &= H(\boldsymbol{\xi}_h) && \forall \boldsymbol{\xi}_h \in \widetilde{\mathbf{V}}^{h,\bar{k}}, && (3.5c)\\
b(\boldsymbol{\zeta}_h,\psi_h) - c(\varphi_h,\psi_h) &= I(\psi_h) && \forall \psi_h \in \mathrm{Q}^{h,k}. && (3.5d)
\end{aligned}$$

4 Discrete well-posedness analysis

This section extends the results shown in Section 2 to the VEM formulation proposed in (3.5). Following the analysis for the continuous problem, we employ a discrete fixed-point argument to state the well-posedness of the fully-coupled discrete problem. We recall that, thanks to stabilisation, the discrete operators inherit the properties presented in Section 2.1.

4.1 Properties of the discrete operators

Note that, for each $K \in \mathcal{T}_h$, given $\vec{\boldsymbol{\tau}}_h \in \mathbb{V}^{h,k}$ and $\vec{\boldsymbol{v}}_h \in \mathbf{Q}^{h,k}$, we have that $\mathbf{div}\,\boldsymbol{\tau}_h \in \mathbf{P}_k(K)$, $\mathrm{div}\,\boldsymbol{w}_h \in \mathrm{P}_k(K)$ (see also the definition of the 2D (resp. 3D) VEM space in Section 3.2 (resp. [5, Theorem 8.2])), $q_h \in \mathrm{P}_k(K)$, and $\boldsymbol{v}_h \in \mathbf{P}_k(K)$. Hence, the the following characterisations hold:

$$\begin{aligned}
\mathbb{V}_0^h := \ker(\mathbf{B}|_{\mathbb{V}^{h,k}}) &= \{\vec{\boldsymbol{\tau}}_h \in \mathbb{V}^{h,k} :\ B(\vec{\boldsymbol{\tau}}_h,\vec{\boldsymbol{v}}_h) = 0,\ \forall \vec{\boldsymbol{v}}_h \in \mathbf{Q}^{h,k}\}\\
&= \mathbb{V}_{01}^h \times \mathbb{V}_{02}^h \equiv \{\boldsymbol{\tau}_h \in \mathbb{S}^{h,k} :\ \mathbf{div}\,\boldsymbol{\tau}_h|_K = \mathbf{0},\ \forall K \in \mathcal{T}_h\} \times \{0\}, && (4.1a)\\
\mathbf{Q}_0^h := \ker(\mathbf{B}^*|_{\mathbf{Q}^{h,k}}) &= \{\vec{\boldsymbol{v}}_h \in \mathbf{Q}^{h,k} :\ B(\vec{\boldsymbol{\tau}}_h,\vec{\boldsymbol{v}}_h) = 0,\ \forall \vec{\boldsymbol{\tau}}_h \in \mathbb{V}^{h,k}\}\\
&= \mathbf{Q}_{01}^h \times \mathbf{Q}_{02}^h \equiv \{\mathbf{0}\} \times \{\boldsymbol{w}_h \in \mathbf{V}^{h,\bar{k}} :\ \mathrm{div}\,\boldsymbol{w}_h|_K = 0,\ \forall K \in \mathcal{T}_h\}. && (4.1b)
\end{aligned}$$

On the other hand, the orthogonal spaces $(\mathbb{V}_0^h)^\perp = (\mathbb{V}_{01}^h)^\perp \times (\mathbb{V}_{02}^h)^\perp$ and $(\mathbf{Q}_0^h)^\perp = (\mathbf{Q}_{01}^h)^\perp \times (\mathbf{Q}_{02}^h)^\perp$ are closed subspaces of $\mathbb{V}^{h,k}$ and $\mathbf{Q}^{h,k}$, where

$$\begin{gathered}
(\mathbb{V}_{01}^h)^\perp \equiv \{\boldsymbol{\sigma}_h \in \mathbb{S}^{h,k} :\ (\boldsymbol{\sigma}_h,\boldsymbol{\tau}_h)_K = 0,\ \forall \boldsymbol{\tau}_h \in \mathbb{V}_{01}^h,\ \forall K \in \mathcal{T}_h\}, \quad (\mathbb{V}_{02}^h)^\perp \equiv \mathrm{Q}^{h,k},\\
(\mathbf{Q}_{01}^h)^\perp \equiv \mathbf{Q}^{h,k}, \quad \text{and} \quad (\mathbf{Q}_{02}^h)^\perp \equiv \{\boldsymbol{z}_h \in \mathbf{V}^{h,\bar{k}} :\ (\boldsymbol{z}_h,\boldsymbol{w}_h)_K = 0,\ \forall \boldsymbol{w}_h \in \mathbf{Q}_{02}^h,\ \forall K \in \mathcal{T}_h\}.
\end{gathered}$$

In what follows, we prove some key properties of the discrete bilinear forms.

Lemma 4.1 (symmetry and positive semi-definiteness of discrete diagonal forms) *The bilinear forms $A_h(\bullet,\bullet)$ and $C_h(\bullet,\bullet)$ are symmetric and positive semi-definite; and (for a given $\widehat{\boldsymbol{\sigma}}_h^{\mathbb{\Pi}} := \mathbb{\Pi}_k^{\mathcal{C},K}\widehat{\boldsymbol{\sigma}}_h$) $a_{h,\widehat{\boldsymbol{\sigma}}_h^{\mathbb{\Pi}}}(\bullet,\bullet)$ is positive semi-definite.*

Proof. The proof reduces to employ the arguments in Lemma 2.2 together with the properties of the stabilisation operators in (3.4). Indeed, we can extend (2.4) for all $\vec{\boldsymbol{\tau}}_h \in \mathbb{V}^{h,k}$ as follows

$$\begin{aligned}
A_h(\vec{\boldsymbol{\tau}}_h,\vec{\boldsymbol{\tau}}_h) \geq{}& \frac{1}{2\mu}\|(\mathbb{\Pi}_k^{\mathcal{C},K}\boldsymbol{\tau}_h)^{\mathtt{d}}\|_{0,\Omega}^2 + S_1^{\mathcal{C},K}((\mathbb{1}-\mathbb{\Pi}_k^{\mathcal{C},K})\boldsymbol{\tau}_h,(\mathbb{1}-\mathbb{\Pi}_k^{\mathcal{C},K})\boldsymbol{\tau}_h)\\
&+ \frac{s_0}{2}\|q_h\|_{0,\Omega}^2 + \frac{s_0}{d(s_0(2\mu+d\lambda)+2d\alpha^2)}\|\operatorname{tr}(\mathbb{\Pi}_k^{\mathcal{C},K}\boldsymbol{\tau}_h)\|_{0,\Omega}^2 \geq 0. \qquad (4.2)
\end{aligned}$$

In addition, for a given $\widehat{\boldsymbol{\sigma}}_h^{\mathbb{\Pi}}$, we have

$$a_{h,\widehat{\boldsymbol{\sigma}}_h^{\mathbb{\Pi}}}(\boldsymbol{\xi}_h,\boldsymbol{\xi}_h) \geq \varrho_1\|\boldsymbol{\Pi}_k^{0,K}\boldsymbol{\xi}_h\|_{0,\Omega}^2 + S_3^{0,K}((\mathbf{1}-\boldsymbol{\Pi}_k^{0,K})\boldsymbol{\xi}_h,(\mathbf{1}-\boldsymbol{\Pi}_k^{0,K})\boldsymbol{\xi}_h) \geq 0,$$

thanks to the positive semi-definitess of $S_1^{\mathcal{C},K}(\bullet,\bullet)$ and $S_3^{0,K}(\bullet,\bullet)$. $\square$

Lemma 4.2 (coercivity for the main discrete diagonal forms) *There exist constants $\overline{\alpha}_A, \overline{\alpha}_a > 0$ such that*

$$A_h(\vec{\boldsymbol{\tau}}_h, \vec{\boldsymbol{\tau}}_h) \geq \overline{\alpha}_A \|\vec{\boldsymbol{\tau}}_h\|^2_{\mathbb{V}} \quad \forall\, \vec{\boldsymbol{\tau}}_h \in \mathbb{V}^h_0, \tag{4.3a}$$

$$c(\psi_h, \psi_h) \geq \overline{\alpha}_c \|\psi_h\|^2_{0,\Omega} \quad \forall\, \psi_h \in \mathrm{Q}^{h,k}. \tag{4.3b}$$

Proof. Note that (4.2) and (3.4a) imply that for all $\vec{\boldsymbol{\tau}}_h \in \mathbb{V}^h_0$

$$A_h(\vec{\boldsymbol{\tau}}_h, \vec{\boldsymbol{\tau}}_h) \geq \min\{\frac{1}{2\mu}, C_{s1}^{-1}\}\|\boldsymbol{\tau}_h^{\mathtt{d}}\|^2_{0,\Omega} + \frac{s_0}{2}\|q_h\|^2_{0,\Omega} + \min\{\frac{s_0}{d(s_0(2\mu + d\lambda) + 2d\alpha^2)}, C_{s1}^{-1}\}\|\operatorname{tr}\boldsymbol{\tau}_h\|^2_{0,\Omega}. \tag{4.4}$$

Thus, applying (2.5) and (2.6) to $\boldsymbol{\tau}_h$, there exist $\overline{C}_1, \overline{C}_2 > 0$ such that $A_h(\vec{\boldsymbol{\tau}}_h, \vec{\boldsymbol{\tau}}_h) \geq \overline{\alpha}_A \|\vec{\boldsymbol{\tau}}_h\|^2_{\mathbf{div},\Omega}$, where $\overline{\alpha}_A = \frac{\overline{C}_1 \overline{C}_2}{4\mu}\min\{1, C_{s1}^{-1}\}$. Finally, in a similar manner to Lemma 2.3, we obtain that (4.3b) holds with $\overline{\alpha}_c = 1$. □

Lemma 4.3 (discrete inf-sup conditions) *There exist positive constants $\overline{\beta}_B, \overline{\beta}_b$ such that*

$$\sup_{\vec{\boldsymbol{\tau}}_h \in \mathbb{V}^{h,k}\setminus\{\mathbf{0}\}} \frac{B(\vec{\boldsymbol{\tau}}_h, \vec{\boldsymbol{v}}_h)}{\|\vec{\boldsymbol{\tau}}_h\|_{\mathbb{V}}} \geq \overline{\beta}_B \|\vec{\boldsymbol{v}}_h\|_{\mathbf{Q}} \qquad \forall\, \vec{\boldsymbol{v}}_h \in [\ker(\mathbf{B}_h^*)]^{\perp}, \tag{4.5a}$$

$$\sup_{\psi_h \in \mathrm{Q}^{h,k}\setminus\{0\}} \frac{b(\boldsymbol{\xi}_h, \psi_h)}{\|\psi_h\|_{0,\Omega}} \geq \overline{\beta}_b \|\boldsymbol{\xi}_h\|_{4,\mathrm{div};\Omega} \qquad \forall\, \boldsymbol{\xi}_h \in \widetilde{\mathbf{V}}^{h,\overline{k}}. \tag{4.5b}$$

Proof. We start by recalling from [1, Proposition 5.6] the following discrete inf-sup condition

$$\sup_{\boldsymbol{\tau} \in \mathbb{S}^{h,k}\setminus\{\mathbf{0}\}} \frac{(\boldsymbol{v}_h, \mathbf{div}\,\boldsymbol{\tau}_h)}{\|\boldsymbol{\tau}_h\|_{\mathbf{div},\Omega}} \geq \overline{\beta}_1 \|\boldsymbol{v}_h\|_{0,\Omega} \quad \forall\, \boldsymbol{v}_h \in (\mathbf{Q}^h_{01})^{\perp}. \tag{4.6}$$

Similarly to [8, Proposition 5.4.2], given that $\operatorname{div}\boldsymbol{w}_h \in \mathbf{P}_k(K)$ for all $K \in \mathcal{T}_h$, $\boldsymbol{w}_h \in (\mathbf{Q}^h_{02})^{\perp} \subseteq \mathbf{H}_{\mathrm{N}}(\operatorname{div}, \Omega)$, and the definition of $\Pi_k^{0,K}$ in (3.2), we have that

$$\sup_{q_h \in \mathrm{Q}^{h,k}\setminus\{0\}} \frac{(q_h, \operatorname{div}\boldsymbol{w}_h)}{\|q_h\|_{0,\Omega}} \geq \sup_{q \in \mathrm{L}^2(\Omega)\setminus\{0\}} \frac{(\Pi_k^0 q, \operatorname{div}\boldsymbol{w}_h)}{\|\Pi_k^0 q\|_{0,\Omega}} \geq \sup_{q \in \mathrm{L}^2(\Omega)\setminus\{0\}} \frac{(q, \operatorname{div}\boldsymbol{w}_h)}{C_\pi \|q\|_{0,\Omega}} \geq \overline{\beta}_2 \|\boldsymbol{w}_h\|_{\mathrm{div},\Omega}, \tag{4.7}$$

where in the last inequality we have used the continuous inf-sup condition (2.9b). Here $\overline{\beta}_2 = \frac{\beta_2}{C_\pi}$, $\Pi_k^0 q := \Pi_k^{0,K} q|_K$ for all $K \in \mathcal{T}_h$, and C_π being the associated continuity constant of Π_k^0 in the L^2-norm. Therefore, the bounds in (4.6)-(4.7) yields (4.5a) with $\overline{\beta}_B = \frac{\overline{\beta}_1 + \overline{\beta}_2}{4}$. Much in the same way, (3.2) and the continuous inf-sup condition (2.8b) lead to

$$\sup_{\psi_h \in \mathrm{Q}^{h,k}\setminus\{0\}} \frac{-(\psi_h, \operatorname{div}\boldsymbol{\xi}_h)}{\|\psi_h\|_{0,\Omega}} \geq \sup_{\psi \in \mathrm{L}^2(\Omega)\setminus\{0\}} \frac{-(\Pi_k^0 \psi, \operatorname{div}\boldsymbol{\xi}_h)}{\|\Pi_k^0 \psi\|_{0,\Omega}} \geq \sup_{\psi \in \mathrm{L}^2(\Omega)\setminus\{0\}} \frac{-(\psi, \operatorname{div}\boldsymbol{\xi}_h)}{C_\pi \|\psi\|_{0,\Omega}} \geq \overline{\beta}_b \|\boldsymbol{\xi}_h\|_{4,\mathrm{div};\Omega},$$

for all $\boldsymbol{\xi}_h \in \widetilde{\mathbf{V}}^{h,\overline{k}} \subseteq \mathbf{H}^4_{\mathrm{N}}(\operatorname{div}, \Omega)$. Thus, (4.5b) holds with $\overline{\beta}_b = \frac{\beta_b}{C_\pi}$. □

4.2 Unique solvability of the discrete coupled problem

We follow the analysis in Section 2.2-2.3 to derive the unique solvability of the discrete problem (3.5). Given two computable prescribed functions $\widehat{\varphi}_h \in \mathrm{Q}^{h,k}$ and $\widehat{\boldsymbol{\sigma}}_h^{\sqcap} \in \mathbb{S}^{h,k}$, the following results imply the well-posedness of the decoupled equations corresponding to the discrete Biot equations (3.5a)-(3.5b) and the discrete mixed perturbed diffusion equation (3.5c)-(3.5d). The proof follows as in the continuous case by employing Lemmas 4.1-4.3, and the discrete versions of [8, Theorem 4.3.1] and Theorem 2.5.

Theorem 4.4 (well-posedness of the discrete Biot equations) *There exists a unique $(\vec{\boldsymbol{\sigma}}_h, \vec{\boldsymbol{u}}_h) \in \mathbb{V}^{h,k} \times \mathbf{Q}^{h,k}$ such that*

$$A_h(\vec{\boldsymbol{\sigma}}_h, \vec{\boldsymbol{\tau}}_h) + B(\vec{\boldsymbol{\tau}}_h, \vec{\boldsymbol{u}}_h) = -D_h(\widehat{\varphi}_h, \vec{\boldsymbol{\tau}}_h) + F(\vec{\boldsymbol{\tau}}_h) \qquad \forall \vec{\boldsymbol{\tau}}_h \in \mathbb{V}^{h,k}, \tag{4.8a}$$

$$B(\vec{\boldsymbol{\sigma}}_h, \vec{\boldsymbol{v}}_h) - C_h(\vec{\boldsymbol{u}}_h, \vec{\boldsymbol{v}}_h) = G(\vec{\boldsymbol{v}}_h) \qquad \forall \vec{\boldsymbol{v}}_h \in \mathbf{Q}^{h,k}. \tag{4.8b}$$

Moreover,

$$\|(\vec{\boldsymbol{\sigma}}_h, \vec{\boldsymbol{u}}_h)\|_{\mathbb{V}\times\mathbf{Q}} \lesssim \frac{(1+\alpha d)\beta}{2\mu + d\lambda}\|\widehat{\varphi}_h\|_{0,\Omega} + \|\boldsymbol{f}\|_{0,\Omega} + \|\boldsymbol{u}_{\mathrm{D}}\|_{1/2,00;\Gamma_{\mathrm{D}}} + \|g\|_{0,\Omega} + \|p_{\mathrm{D}}\|_{1/2,00;\Gamma_{\mathrm{D}}}.$$

Theorem 4.5 (well-posedness of the discrete mixed perturbed diffusion equation) *There exists a unique* $(\boldsymbol{\zeta}_h, \varphi_h) \in \widetilde{\mathbf{V}}^{k,\overline{k}} \times \mathrm{Q}^{h,k}$ *such that*

$$a_{h,\widehat{\boldsymbol{\sigma}}_h^{\Pi}}(\boldsymbol{\zeta}_h, \boldsymbol{\xi}_h) + b(\boldsymbol{\xi}_h, \phi_h) = H(\boldsymbol{\xi}_h) \qquad \forall \boldsymbol{\xi}_h \in \widetilde{\mathbf{V}}^{h,\overline{k}}, \tag{4.9a}$$

$$b(\boldsymbol{\zeta}_h, \psi_h) - c(\varphi_h, \psi_h) = I(\psi_h) \qquad \forall \psi_h \in \mathrm{Q}^{h,k}. \tag{4.9b}$$

Moreover ,

$$\|\boldsymbol{\zeta}_h\|_{4,\mathrm{div};\Omega} + \|\varphi_h\|_{0,\Omega} \lesssim \|\ell\|_{0,\Omega} + \|\varphi_{\mathrm{D}}\|_{1/2,00;\Gamma_{\mathrm{D}}}.$$

Next, we define the following discrete maps

$$\mathcal{J}_h^{\mathrm{Biot}} : \mathrm{Q}^{h,k}(\Omega) \to \mathbb{V}^{h,k} \times \mathbf{Q}^{h,k},$$
$$\widehat{\varphi}_h \mapsto \mathcal{J}_h^{\mathrm{Biot}}(\widehat{\varphi}_h) = ((\mathcal{J}_{1h}^{\mathrm{Biot}}(\widehat{\varphi}_h), \mathcal{J}_{2h}^{\mathrm{Biot}}(\widehat{\varphi}_h)), \mathcal{J}_{3h}^{\mathrm{Biot}}(\widehat{\varphi})) := ((\boldsymbol{\sigma}_h, p_h), \vec{\boldsymbol{u}}_h) = (\vec{\boldsymbol{\sigma}}_h, \vec{\boldsymbol{u}}_h),$$

where $(\vec{\boldsymbol{\sigma}}_h, \vec{\boldsymbol{u}}_h) \in \mathbb{V}^{h,k} \times \mathbf{Q}^{h,k}$ is given by Theorem 4.4; and

$$\mathcal{J}_h^{\mathrm{diff}} : \mathbb{S}^{h,k} \to \widetilde{\mathbf{V}}^{h,\overline{k}} \times \mathrm{Q}^{h,k},$$
$$\widehat{\boldsymbol{\sigma}}_h \mapsto \mathcal{J}_h^{\mathrm{diff}}(\widehat{\boldsymbol{\sigma}}_h) = (\mathcal{J}_{1h}^{\mathrm{diff}}(\widehat{\boldsymbol{\sigma}}_h), \mathcal{J}_{2h}^{\mathrm{diff}}(\widehat{\boldsymbol{\sigma}}_h)) := (\boldsymbol{\zeta}_h, \varphi_h),$$

with $(\boldsymbol{\zeta}_h, \varphi_h)$ provided by Theorem 4.5. These maps are well-defined, along with the discrete solution operator defined next

$$\mathcal{J}_h : \mathrm{Q}^{h,k} \to \mathrm{Q}^{h,k},$$
$$\widehat{\varphi}_h \mapsto \mathcal{J}_h(\widehat{\varphi}_h) := \mathcal{J}_{2h}^{\mathrm{diff}}(\mathcal{J}_{1h}^{\mathrm{Biot}}(\widehat{\varphi}_h)). \tag{4.10}$$

In what follows, we show well-posedness of the fully-coupled discrete problem (3.5) through the equivalent fixed-point formulation $\mathcal{J}_h(\varphi_h) = \varphi_h$. First, we define the discrete closed ball for some $r > 0$

$$\mathrm{W}_h := \{\widehat{\varphi}_h \in \mathrm{Q}^{h,k} : \|\widehat{\varphi}_h\|_{0,\Omega} \leq r\}.$$

Next, we prove that $\mathcal{J}_h$ maps W_h into itself and show the Lipschitz continuity of $\mathcal{J}_h$.

Lemma 4.6 (discrete ball mapping property) *Under the small data assumption in (2.26), it follows that* $\mathcal{J}(\mathrm{W}_h) \subseteq \mathrm{W}_h$.

Proof. Given $\widehat{\varphi}_h \in \mathrm{W}_h$, the definition (4.10), (2.26) and the estimate given by Theorem 4.5 provide that

$$\|\mathcal{J}_h(\widehat{\varphi}_h)\|_{0,\Omega} = \|\mathcal{J}_{2h}^{\mathrm{diff}}(\mathcal{J}_{1h}^{\mathrm{Biot}}(\widehat{\varphi}_h))\|_{0,\Omega} \lesssim \|\ell\|_{0,\Omega} + \|\varphi_{\mathrm{D}}\|_{1/2,00;\Gamma_{\mathrm{D}}} \leq r.$$

□

Lemma 4.7 (discrete Lipschitz continuity) *There exists a positive constant* $L_{\mathcal{J}_h}$ *such that*

$$\|\mathcal{J}_h(\varphi_{1h}) - \mathcal{J}_h(\varphi_{2h})\|_{0,\Omega} \leq L_{\mathcal{J}_h}\|\varphi_{1h} - \varphi_{2h}\|_{0,\Omega} \qquad \forall \varphi_{1h}, \varphi_{2h} \in \mathrm{Q}^{h,k}. \tag{4.11}$$

Proof. Given $\varphi_{1h}, \varphi_{2h} \in \mathrm{Q}^{h,k}$, we let $\mathcal{J}_h^{\mathrm{Biot}}(\varphi_{1h}) = (\vec{\boldsymbol{\sigma}}_{1h}, \vec{\boldsymbol{u}}_{1h}) \in \mathbb{V}^{h,k} \times \mathbf{Q}^{h,k}$ and $\mathcal{J}_h^{\mathrm{Biot}}(\varphi_{2h}) = (\vec{\boldsymbol{\sigma}}_{2h}, \vec{\boldsymbol{u}}_{2h}) \in \mathbb{V}^{h,k} \times \mathbf{Q}^{h,k}$ be the unique solutions of (4.8). Then, applying the discrete version of the inf-sup condition (2.27a) with $(\vec{\boldsymbol{\zeta}}_h, \vec{\boldsymbol{w}}_h) = (\vec{\boldsymbol{\sigma}}_{1h} - \vec{\boldsymbol{\sigma}}_{2h}, \vec{\boldsymbol{u}}_{1h} - \vec{\boldsymbol{u}}_{2h})$, imply that $\overline{C}_{\mathrm{B}}\|(\vec{\boldsymbol{\zeta}}_h, \vec{\boldsymbol{w}}_h)\|_{\mathbb{V}^{h,k}\times\mathbf{Q}^{h,k}}$ is bounded by

$$\sup_{(\vec{\boldsymbol{\tau}}_h, \vec{\boldsymbol{v}}_h)\in(\mathbb{V}^{h,k}\times\mathbf{Q}^{h,k})\setminus\{(\mathbf{0},\mathbf{0})\}} \frac{A_h(\vec{\boldsymbol{\sigma}}_{1h} - \vec{\boldsymbol{\sigma}}_{2h}, \vec{\boldsymbol{\tau}}_h) + B(\vec{\boldsymbol{\tau}}_h, \vec{\boldsymbol{u}}_{1h} - \vec{\boldsymbol{u}}_{2h}) + B(\vec{\boldsymbol{\sigma}}_{1h} - \vec{\boldsymbol{\sigma}}_{2h}, \vec{\boldsymbol{v}}_h) - C_h(\vec{\boldsymbol{u}}_{1h} - \vec{\boldsymbol{u}}_{2h}, \vec{\boldsymbol{v}}_h)}{\|(\vec{\boldsymbol{\tau}}_h, \vec{\boldsymbol{v}}_h)\|_{\mathbb{V}\times\mathbf{Q}}}$$
$$= \sup_{(\vec{\boldsymbol{\tau}}_h, \vec{\boldsymbol{v}}_h)\in(\mathbb{V}^{h,k}\times\mathbf{Q}^{h,k})\setminus\{(\mathbf{0},\mathbf{0})\}} \frac{D_h(\varphi_{1h}, \vec{\boldsymbol{\tau}}_h) - D_h(\varphi_{2h}, \vec{\boldsymbol{\tau}}_h)}{\|(\vec{\boldsymbol{\tau}}_h, \vec{\boldsymbol{v}}_h)\|_{\mathbb{V}\times\mathbf{Q}}} \leq \frac{(1+\alpha d)\beta}{2\mu + d\lambda}\|\varphi_{1h} - \varphi_{2h}\|_{0,\Omega}.$$

Thus,

$$\|\mathcal{J}_{1h}^{\mathrm{Biot}}(\varphi_{1h}) - \mathcal{J}_{1h}^{\mathrm{Biot}}(\varphi_{2h})\|_{4,\mathrm{div};\Omega} \leq \frac{(1+\alpha d)\beta}{\overline{C}_{\mathrm{B}}(2\mu + d\lambda)}\|\varphi_{1h} - \varphi_{2h}\|_{0,\Omega}. \tag{4.12}$$

Similarly, let $\boldsymbol{\sigma}_{1h}, \boldsymbol{\sigma}_{2h} \in \mathbb{S}^{h,k}$, such that $\mathcal{J}^{\rm diff}(\boldsymbol{\sigma}_{1h}) = (\varphi_{1h}, \boldsymbol{\zeta}_{1h}) \in \mathrm{Q}^{h,k} \times \widetilde{\mathbf{V}}^{h,\overline{k}}$ and $\mathcal{J}^{\rm diff}(\boldsymbol{\sigma}_{2h}) = (\varphi_{2h}, \boldsymbol{\zeta}_{2h}) \in \mathrm{Q}^{h,k} \times \widetilde{\mathbf{V}}^{h,\overline{k}}$ be the unique solutions of (4.9). Equivalently, we have

$$
\begin{aligned}
a_{h,\boldsymbol{\sigma}_{1h}^{\sqcap}}(\boldsymbol{\zeta}_{1h}, \boldsymbol{\xi}_h) + a_{h,\boldsymbol{\sigma}_{2h}^{\sqcap}}(\boldsymbol{\zeta}_{2h}, \boldsymbol{\xi}_h) + b_h(\boldsymbol{\xi}_h, \varphi_{1h} - \varphi_{2h}) &= 0 \quad \forall \psi_h \in \mathrm{Q}^{h,k}, \\
b_h(\boldsymbol{\zeta}_{1h} - \boldsymbol{\zeta}_{2h}, \psi_h) - c_h(\varphi_{1h} - \varphi_{2h}, \psi_h) &= 0 \quad \forall \boldsymbol{\xi}_h \in \widetilde{\mathbf{V}}^{h,\overline{k}},
\end{aligned}
$$

and from here we add and subtract the term $a_{\boldsymbol{\sigma}_{1h}^{\Pi}}(\boldsymbol{\zeta}_{2h}, \boldsymbol{\xi}_h)$ to obtain

$$
a_{h,\boldsymbol{\sigma}_{1h}^{\sqcap}}(\boldsymbol{\zeta}_{1h} - \boldsymbol{\zeta}_{2h}, \boldsymbol{\xi}_h) + b(\boldsymbol{\zeta}_{1h} - \boldsymbol{\zeta}_{2h}, \psi_h) + b(\boldsymbol{\xi}_h, \varphi_{1h} - \varphi_{2h}) - c(\varphi_{1h} - \varphi_{2h}, \psi) = a_{\boldsymbol{\sigma}_{1h}^{\sqcap}}(\boldsymbol{\zeta}_{2h}, \boldsymbol{\xi}_h) - a_{\boldsymbol{\sigma}_{2h}^{\sqcap}}(\boldsymbol{\zeta}_{2h}, \boldsymbol{\xi}_h).
$$

Then, the discrete version of (2.27b) with $\widehat{\boldsymbol{\sigma}} = \boldsymbol{\sigma}_{1h}^{\sqcap}$ and $(\boldsymbol{\zeta}, \phi) = (\boldsymbol{\zeta}_{1h} - \boldsymbol{\zeta}_{2h}, \varphi_{1h} - \varphi_{2h})$, together with the assumptions on $\varrho^{-1}(\bullet)$ (cf. (1.3)), allow us to readily see that

$$
\begin{aligned}
\overline{C}_{\rm D}(\|\boldsymbol{\zeta}_{1h} - \boldsymbol{\zeta}_{2h}\|_{4,{\rm div};\Omega} + \|\varphi_{1h} - \varphi_{2h}\|_{0,\Omega}) &\leq \sup_{(\boldsymbol{\xi}_h,\psi_h)\in(\widetilde{\mathbf{V}}^{h,\overline{k}}\times \mathrm{Q}^{h,k})\setminus\{(\mathbf{0},\mathbf{0})\}} \frac{|a_{\boldsymbol{\sigma}_{1h}^{\sqcap}}(\boldsymbol{\zeta}_{2h}, \boldsymbol{\xi}_h) - a_{\boldsymbol{\sigma}_{2h}^{\sqcap}}(\boldsymbol{\zeta}_{2h}, \boldsymbol{\xi}_h)|}{\|(\boldsymbol{\xi}_h, \psi_h)\|_{\mathrm{L}^2(\Omega)\times \mathbf{H}^4_{\rm N}({\rm div},\Omega)}} \\
&\leq \sup_{(\boldsymbol{\xi}_h,\psi_h)\in(\widetilde{\mathbf{V}}^{h,\overline{k}}\times \mathrm{Q}^{h,k})\setminus\{(\mathbf{0},\mathbf{0})\}} \frac{\displaystyle\int_\Omega |(\varrho(\boldsymbol{\sigma}_{2h}^{\sqcap})^{-1} - \varrho(\boldsymbol{\sigma}_{1h}^{\sqcap})^{-1})\boldsymbol{\zeta}_{2h}\cdot \boldsymbol{\xi}_h|}{\|(\boldsymbol{\xi}_h, \psi_h)\|_{\mathrm{L}^2(\Omega)\times \mathbf{H}^4_{\rm N}({\rm div},\Omega)}} \\
&\leq L_\varrho \|\boldsymbol{\sigma}_{2h}^{\sqcap} - \boldsymbol{\sigma}_{1h}^{\sqcap}\|_{0,\Omega}\|\boldsymbol{\zeta}_{2h}\|_{0,4;\Omega} \\
&\leq L_\varrho \overline{C}_\pi(\|\ell\|_{0,\Omega} + \|\varphi_{\rm D}\|_{1/2,00;\Gamma_{\rm D}})\|\boldsymbol{\sigma}_{2h} - \boldsymbol{\sigma}_{1h}\|_{0,\Omega},
\end{aligned}
$$

where $\overline{C}_\pi$ is the continuity constant of the projection operator $\sqcap_k^{\mathcal{C},K}$ in the $\mathbb{L}^2$-norm, which implies that

$$
\|\mathcal{J}_{2h}^{\rm diff}(\boldsymbol{\sigma}_{1h}) - \mathcal{J}_{2h}^{\rm diff}(\boldsymbol{\sigma}_{2h})\|_{0,\Omega} \leq \frac{L_\varrho \overline{C}_\pi}{\overline{C}_{\rm D}}(\|\ell\|_{0,\Omega} + \|\varphi_{\rm D}\|_{1/2,00;\Gamma_{\rm D}})\|\boldsymbol{\sigma}_{1h} - \boldsymbol{\sigma}_{2h}\|_{0,\Omega}. \tag{4.13}
$$

Then, the estimate (4.11) follows from the definition of $\mathcal{J}_h$ (4.10), the Lipschitz-continuity of $\mathcal{J}_{2h}^{\rm diff}$ (4.13) and that of $\mathcal{J}_{1h}^{\rm Biot}$ (4.12), with

$$
L_{\mathcal{J}_h} := \frac{L_\varrho \overline{C}_\pi (1 + \alpha d)\beta}{\overline{C}_{\rm B}\overline{C}_{\rm D}(2\mu + d\lambda)}(\|\ell\|_{0,\Omega} + \|\varphi_{\rm D}\|_{1/2,00;\Gamma_{\rm D}}). \tag{4.14}
$$

□

We are ready to state the main result of this section which is a consequence of Lemmas 4.6-4.7 together with the Banach fixed-point theorem.

Theorem 4.8 (well-posedness of the fully-coupled discrete problem) *Suppose that $\|\ell\|_{0,\Omega} + \|\varphi_{\rm D}\|_{1/2,00;\Gamma_{\rm D}} \leq r$ and $L_{\mathcal{J}_h} < 1$ (cf. (4.14)). Then, the coupled problem (3.5) has a unique solution $(\vec{\boldsymbol{\sigma}}_h, \vec{\boldsymbol{u}}_h) \in \mathbb{V}^{h,k} \times \mathbf{Q}^{h,k}$ and $(\boldsymbol{\zeta}_h, \varphi_h) \in \widetilde{\mathbf{V}}^{h,\overline{k}} \times \mathrm{Q}^{h,k}$. Moreover, and similarly to the continuous case, we have*

$$
\begin{aligned}
\|(\vec{\boldsymbol{\sigma}}_h, \vec{\boldsymbol{u}}_h, \boldsymbol{\zeta}_h, \varphi_h)\|_{\mathbb{V}\times\mathbf{Q}\times\mathbf{H}^4_{\rm N}({\rm div},\Omega)\times\mathrm{L}^2(\Omega)} &\lesssim \left(\frac{(1 + \alpha d)\beta}{2\mu + d\lambda} + 1\right)\left(\|\ell\|_{0,\Omega} + \|\varphi_{\rm D}\|_{1/2,00;\Gamma_{\rm D}}\right) + \|\boldsymbol{f}\|_{0,\Omega} + \|g\|_{0,\Omega} \\
&\quad + \|\boldsymbol{u}_{\rm D}\|_{1/2,00;\Gamma_{\rm D}} + \|p_{\rm D}\|_{1/2,00;\Gamma_{\rm D}}.
\end{aligned} \tag{4.15}
$$

5 A priori error analysis

This section is devoted to deriving the optimal a priori error estimate. The first step is to establish the Strang-type inequalities which are formulated in the theorem below.

Theorem 5.1 (quasi-optimality) *In addition to the assumptions of Theorems 2.10 and 4.8, let $(\vec{\boldsymbol{\sigma}}, \vec{\boldsymbol{u}}, \boldsymbol{\zeta}, \varphi) \in \mathbb{V} \times \mathbf{Q} \times \mathbf{H}^4_{\rm N}({\rm div}, \Omega) \times \mathrm{L}^2(\Omega)$ and $(\vec{\boldsymbol{\sigma}}_h, \vec{\boldsymbol{u}}_h, \boldsymbol{\zeta}_h, \varphi_h) \in \mathbb{V}^{h,k} \times \mathbf{Q}^{h,k} \times \widetilde{\mathbf{V}}^{h,\overline{k}} \times \mathrm{Q}^{h,k}$ be the unique solutions to (2.2) and (3.5), respectively. Under these conditions, the following error estimates hold:*

$$
\|(\vec{\boldsymbol{\sigma}} - \vec{\boldsymbol{\sigma}}_h, \vec{\boldsymbol{u}} - \vec{\boldsymbol{u}}_h)\|_{\mathbb{V}\times\mathbf{Q}} \lesssim \|\vec{\boldsymbol{\sigma}} - \vec{\boldsymbol{\sigma}}_h^{\sqcap}\|_{\mathbb{V}} + \|\vec{\boldsymbol{\sigma}} - \vec{\boldsymbol{\sigma}}_h^{\mathbb{F}}\|_{\mathbb{V}} + \|\vec{\boldsymbol{u}} - \vec{\boldsymbol{u}}_h^{\mathbf{\Pi}}\|_{\mathbb{V}} + \|\vec{\boldsymbol{u}} - \vec{\boldsymbol{u}}_h^{\mathbf{F}}\|_{\mathbf{Q}}
$$

$$
+\ \frac{(1+\alpha d)\beta}{2\mu+d\lambda}\|\varphi-\varphi_h\|_{0,\Omega}, \tag{5.1}
$$

$$
\|(\boldsymbol{\zeta}-\boldsymbol{\zeta}_h,\varphi-\varphi_h)\|_{\mathbf{H}^4_{\mathrm{N}}(\mathrm{div},\Omega)\times \mathrm{L}^2(\Omega)} \lesssim \|\boldsymbol{\zeta}-\mathbf{F}_d^{\bar{k},K}\boldsymbol{\zeta}\|_{4,\mathrm{div};\Omega}+\|\boldsymbol{\zeta}-\boldsymbol{\Pi}_{\bar{k}}^{0,K}\boldsymbol{\zeta}\|_{4,\mathrm{div};\Omega}+\|\varphi-\Pi_k^{0,K}\varphi\|_{0,\Omega}
$$
$$
+\ L_\varrho(\|\ell\|_{0,\Omega}+\|\varphi_{\mathrm{D}}\|_{1/2,00;\Gamma_{\mathrm{D}}})\|\boldsymbol{\sigma}-\boldsymbol{\sigma}_h^{\Pi}\|_{\mathbb{V}}, \tag{5.2}
$$

where $\vec{\boldsymbol{\sigma}}_h^{\mathbb{F}} := (\mathbb{F}^{k,K}\boldsymbol{\sigma},\Pi_k^{0,K}p)$, $\vec{\boldsymbol{\sigma}}_h^{\Pi} := (\boldsymbol{\sigma}_h^{\Pi},p_h)$, $\vec{\boldsymbol{u}}_h^{\mathbf{F}} := (\boldsymbol{\Pi}_k^{0,K}\boldsymbol{u},\mathbf{F}_d^{\bar{k},K}\boldsymbol{z})$, $\vec{\boldsymbol{u}}_h^{\boldsymbol{\Pi}} := (\boldsymbol{u}_h,\boldsymbol{\Pi}_{\bar{k}}^{0,K}\boldsymbol{z})$*, and by* $\mathbf{F}_d^{\bar{k},K}$ *we represent the Fortin operators either* $\mathbf{F}_{2\mathrm{D}}^{k,K}$ *or* $\mathbf{F}_{3\mathrm{D}}^{k+1,K}$*, depending on the spatial dimension under consideration.*

Proof. We proceed in a similar way as in [37], noting from (2.2) and (3.5) that $(\vec{\boldsymbol{\sigma}}_h-\vec{\boldsymbol{\sigma}}_h^{\mathbb{F}},\vec{\boldsymbol{u}}_h-\vec{\boldsymbol{u}}_h^{\mathbf{F}})\in\mathbb{V}^{h,k}\times\mathbf{Q}^{h,k}$ is the unique solution to

$$
\begin{aligned}
A_h(\vec{\boldsymbol{\sigma}}_h-\vec{\boldsymbol{\sigma}}_h^{\mathbb{F}},\vec{\boldsymbol{\tau}}_h)+\ B(\vec{\boldsymbol{\tau}}_h,\vec{\boldsymbol{u}}_h-\vec{\boldsymbol{u}}_h^{\mathbf{F}}) &= \widetilde{F}_1(\vec{\boldsymbol{\tau}}_h) && \forall\vec{\boldsymbol{\tau}}_h\in\mathbb{V}^{h,k},\\
B(\vec{\boldsymbol{\sigma}}_h-\vec{\boldsymbol{\sigma}}_h^{\mathbb{F}},\vec{\boldsymbol{v}}_h)-\ C_h(\vec{\boldsymbol{u}}_h-\vec{\boldsymbol{u}}_h^{\mathbf{F}},\vec{\boldsymbol{v}}_h) &= \widetilde{G}_1(\vec{\boldsymbol{v}}_h) && \forall\vec{\boldsymbol{v}}_h\in\mathbf{Q}^{h,k},
\end{aligned}
$$

where

$$
\begin{aligned}
\widetilde{F}_1(\vec{\boldsymbol{\tau}}_h) &:= A(\vec{\boldsymbol{\sigma}},\vec{\boldsymbol{\tau}}_h)-A_h(\vec{\boldsymbol{\sigma}}_h^{\mathbb{F}},\vec{\boldsymbol{\tau}}_h)+B(\vec{\boldsymbol{\tau}}_h,\vec{\boldsymbol{u}}-\vec{\boldsymbol{u}}_h^{\mathbf{F}})+D_h(\varphi-\varphi_h,\vec{\boldsymbol{\tau}}_h),\\
\widetilde{G}_1(\vec{\boldsymbol{v}}_h) &:= B(\vec{\boldsymbol{\sigma}}-\vec{\boldsymbol{\sigma}}_h^{\mathbb{F}},\vec{\boldsymbol{v}}_h)-C(\vec{\boldsymbol{u}},\vec{\boldsymbol{v}}_h)+C_h(\vec{\boldsymbol{u}}_h^{\mathbf{F}},\vec{\boldsymbol{v}}_h).
\end{aligned}
$$

By exploiting the continuous dependence on data established in Theorem 4.4, we can deduce that

$$
\|(\vec{\boldsymbol{\sigma}}_h-\vec{\boldsymbol{\sigma}}_h^{\mathbb{F}},\vec{\boldsymbol{u}}_h-\vec{\boldsymbol{u}}_h^{\mathbf{F}})\|_{\mathbb{V}\times\mathbf{Q}}\lesssim\|\widetilde{F}_1\|_{\mathbb{V}'}+\|\widetilde{G}_1\|_{\mathbf{Q}'}. \tag{5.3}
$$

Now, noting that $A_h(\vec{\boldsymbol{\sigma}}_h^{\Pi},\vec{\boldsymbol{\tau}}_h)=A(\vec{\boldsymbol{\sigma}}_h^{\Pi},\vec{\boldsymbol{\tau}}_h)$, by applying the continuity of the bilinear forms $A(\bullet,\bullet)$, $A_h(\bullet,\bullet)$, $B(\bullet,\bullet)$, $D(\bullet,\bullet)$, $C(\bullet,\bullet)$, and $C_h(\bullet,\bullet)$, as well as using the triangle inequality, it is possible to deduce that

$$
|A(\vec{\boldsymbol{\sigma}},\vec{\boldsymbol{\tau}}_h)-A_h(\vec{\boldsymbol{\sigma}}_h^{\mathbb{F}},\vec{\boldsymbol{\tau}}_h)|\lesssim(\|\vec{\boldsymbol{\sigma}}-\vec{\boldsymbol{\sigma}}_h^{\Pi}\|_{\mathbb{V}}+\|\vec{\boldsymbol{\sigma}}_h^{\Pi}-\vec{\boldsymbol{\sigma}}_h^{\mathbb{F}}\|_{\mathbb{V}})\|\boldsymbol{\tau}_h\|_{\mathbb{V}}\lesssim(\|\vec{\boldsymbol{\sigma}}-\vec{\boldsymbol{\sigma}}_h^{\Pi}\|_{\mathbb{V}}+\|\vec{\boldsymbol{\sigma}}-\vec{\boldsymbol{\sigma}}_h^{\mathbb{F}}\|_{\mathbb{V}})\|\boldsymbol{\tau}_h\|_{\mathbb{V}}, \tag{5.4a}
$$
$$
|B(\vec{\boldsymbol{\tau}}_h,\vec{\boldsymbol{u}}-\vec{\boldsymbol{u}}_h^{\mathbf{F}})|\lesssim\|\vec{\boldsymbol{u}}-\vec{\boldsymbol{u}}_h^{\mathbf{F}}\|_{\mathbf{Q}}\|\boldsymbol{\tau}_h\|_{\mathbb{V}}, \tag{5.4b}
$$
$$
|D_h(\varphi-\varphi_h,\vec{\boldsymbol{\tau}}_h)|\lesssim\frac{(1+\alpha d)\beta}{2\mu+d\lambda}\|\varphi-\varphi_h\|_{0,\Omega}\|\boldsymbol{\tau}_h\|_{\mathbb{V}}, \tag{5.4c}
$$
$$
|B(\vec{\boldsymbol{\sigma}}-\vec{\boldsymbol{\sigma}}_h^{\mathbb{F}},\vec{\boldsymbol{v}}_h)|\lesssim\|\vec{\boldsymbol{\sigma}}-\vec{\boldsymbol{\sigma}}_h^{\mathbb{F}}\|_{\mathbb{V}}\|\boldsymbol{v}_h\|_{\mathbf{Q}}, \tag{5.4d}
$$
$$
|C_h(\vec{\boldsymbol{u}}_h^{\mathbf{F}},\vec{\boldsymbol{v}}_h)-C(\vec{\boldsymbol{u}},\vec{\boldsymbol{v}}_h)|\lesssim(\|\vec{\boldsymbol{u}}-\vec{\boldsymbol{u}}_h^{\boldsymbol{\Pi}}\|_{\mathbf{Q}}+\|\vec{\boldsymbol{u}}_h^{\mathbf{F}}-\vec{\boldsymbol{u}}_h^{\boldsymbol{\Pi}}\|_{\mathbf{Q}})\|\boldsymbol{v}_h\|_{\mathbf{Q}}\lesssim\|(\vec{\boldsymbol{u}}-\vec{\boldsymbol{u}}_h^{\boldsymbol{\Pi}}\|_{\mathbf{Q}}+\|\vec{\boldsymbol{u}}-\vec{\boldsymbol{u}}_h^{\mathbf{F}}\|_{\mathbf{Q}})\|\boldsymbol{v}_h\|_{\mathbf{Q}}. \tag{5.4e}
$$

Upon substitution of (5.4) into (5.3), and invoking the triangle inequality, the result (5.1) follows. Conversely, for the diffusivity problem, it follows once more from (2.2) and (3.5) that $(\boldsymbol{\zeta}_h-\mathbf{F}_d^{\bar{k},K}\boldsymbol{\zeta},\varphi_h-\Pi_k^{0,K}\varphi)\in\widetilde{\mathbf{V}}^{h,\bar{k}}\times\mathrm{Q}^{h,k}$ constitutes the unique solution of

$$
\begin{aligned}
a_{h,\boldsymbol{\sigma}_h^{\Pi}}(\boldsymbol{\zeta}_h-\mathbf{F}_d^{\bar{k},K}\boldsymbol{\zeta},\boldsymbol{\xi}_h)+b(\boldsymbol{\xi}_h,\varphi_h-\Pi_k^{0,K}\varphi) &= \widetilde{F}_2(\boldsymbol{\xi}_h) && \forall\boldsymbol{\xi}_h\in\widetilde{\mathbf{V}}^{h,\bar{k}}, && \text{(5.5a)}\\
b(\boldsymbol{\zeta}_h-\mathbf{F}_d^{\bar{k},K}\boldsymbol{\zeta},\psi_h)-c(\varphi_h-\Pi_k^{0,K}\varphi,\psi_h) &= \widetilde{G}_2(\psi_h) && \forall\psi_h\in\mathrm{Q}^{h,k}, && \text{(5.5b)}
\end{aligned}
$$

where

$$
\begin{aligned}
\widetilde{F}_2(\boldsymbol{\xi}_h) &:= a_{\boldsymbol{\sigma}}(\boldsymbol{\zeta},\boldsymbol{\xi}_h)-a_{h,\boldsymbol{\sigma}_h^{\Pi}}(\mathbf{F}_d^{\bar{k},K}\boldsymbol{\zeta},\boldsymbol{\xi}_h)+b(\boldsymbol{\xi}_h,\varphi-\Pi_k^{0,K}\varphi),\\
\widetilde{G}_2(\psi_h) &:= b(\boldsymbol{\zeta}-\mathbf{F}_d^{\bar{k},K}\boldsymbol{\zeta},\psi_h)-c(\varphi-\Pi_k^{0,K}\varphi,\psi_h).
\end{aligned}
$$

The continuous dependence on data shows

$$
\|(\boldsymbol{\zeta}_h-\mathbf{F}_d^{\bar{k},K}\boldsymbol{\zeta},\varphi_h-\Pi_k^{0,K}\varphi)\|_{\mathbf{H}^4_{\mathrm{N}}(\mathrm{div},\Omega)\times\mathrm{L}^2(\Omega)}\lesssim\|\widetilde{F}_2\|_{\mathbf{H}^4_{\mathrm{N}}(\mathrm{div},\Omega)'}+\|\widetilde{G}_2\|_{\mathrm{L}^2(\Omega)'}. \tag{5.6}
$$

After adding and subtracting suitable terms, applying the continuity of the bilinear forms $a_{\boldsymbol{\sigma}}(\bullet,\bullet)$, $a_{h,\boldsymbol{\sigma}_h}(\bullet,\bullet)$, $b(\bullet,\bullet)$, and $c(\bullet,\bullet)$, and invoking the triangle inequality, we can deduce that

$$
|a_{\boldsymbol{\sigma}}(\boldsymbol{\zeta},\boldsymbol{\xi}_h)-a_{h,\boldsymbol{\sigma}_h^{\Pi}}(\mathbf{F}_d^{\bar{k},K}\boldsymbol{\zeta},\boldsymbol{\xi}_h)|\lesssim(\|\boldsymbol{\zeta}-\mathbf{F}_d^{\bar{k},K}\boldsymbol{\zeta}\|_{4,\mathrm{div};\Omega}+\|\boldsymbol{\zeta}-\boldsymbol{\Pi}_{\bar{k}}^{0,K}\boldsymbol{\zeta}\|_{4,\mathrm{div};\Omega})\|\boldsymbol{\xi}_h\|_{4,\mathrm{div};\Omega}
$$

$$+ L_\varrho(\|\ell\|_{0,\Omega} + \|\varphi_{\mathrm{D}}\|_{1/2,00;\Gamma_{\mathrm{D}}})\|\boldsymbol{\sigma} - \boldsymbol{\sigma}_h^{\sqcap}\|_{\mathbb{V}}\|\boldsymbol{\xi}_h\|_{4,\mathrm{div};\Omega}, \tag{5.7a}$$

$$|b(\boldsymbol{\xi}_h, \varphi - \Pi_k^{0,K}\varphi)| \lesssim \|\varphi - \Pi_k^{0,K}\varphi\|_{0,\Omega}\|\boldsymbol{\xi}_h\|_{4,\mathrm{div};\Omega}, \tag{5.7b}$$

$$|b(\boldsymbol{\zeta} - \mathbf{F}_d^{\overline{k},K}\boldsymbol{\zeta}, \psi_h)| \lesssim \|\boldsymbol{\zeta} - \mathbf{F}_d^{\overline{k},K}\boldsymbol{\zeta}\|_{4,\mathrm{div};\Omega}\|\psi_h\|_{0,\Omega}, \tag{5.7c}$$

$$|c(\varphi - \Pi_k^{0,K}\varphi, \psi_h)| \lesssim \|\varphi - \Pi_k^{0,K}\varphi\|_{0,\Omega}\|\psi_h\|_{0,\Omega}. \tag{5.7d}$$

Finally, proceeding as in the previous case, the substitution of (5.7) into (5.6), combined with the triangle inequality, yields the estimate (5.2). □

Theorem 5.2 (convergence rates) *In addition to the hypotheses of Theorem 5.1, assume that*

$$\frac{(1+\alpha d)\beta}{2\mu + d\lambda} + L_\varrho(\|\ell\|_{0,\Omega} + \|\varphi_{\mathrm{D}}\|_{1/2,00;\Gamma_{\mathrm{D}}}) < \frac{1}{2}.$$

Additionally, suppose that there exist $s \in [1, k+1]$ and $\overline{s} \in [1, \overline{k}+1]$ such that $\boldsymbol{\sigma} \in \mathbb{H}^s(\Omega), p \in \mathrm{H}^s(\Omega), \boldsymbol{u} \in \mathbf{H}^s(\Omega), \boldsymbol{z} \in \mathbf{H}^{\overline{s}}(\Omega), \boldsymbol{\zeta} \in \mathbf{H}^{\overline{s}}(\Omega)$ and $\varphi \in \mathrm{H}^s(\Omega)$. Then, there holds

$$\mathrm{e}_h \lesssim h^{\min\{s,\overline{s}\}}\left(\|\boldsymbol{\sigma}\|_{s,\Omega} + \|p\|_{s,\Omega} + \|\boldsymbol{u}\|_{s,\Omega} + \|\boldsymbol{z}\|_{\overline{s},\Omega} + \|\boldsymbol{\zeta}\|_{\overline{s},\Omega} + \|\varphi\|_{s,\Omega}\right), \tag{5.8}$$

where $\mathrm{e}_h := \|\vec{\boldsymbol{\sigma}} - \vec{\boldsymbol{\sigma}}_h\|_{\mathbb{V}} + \|\vec{\boldsymbol{u}} - \vec{\boldsymbol{u}}_h\|_{\mathbf{Q}} + \|\boldsymbol{\zeta} - \boldsymbol{\zeta}_h\|_{4,\mathrm{div};\Omega} + \|\varphi - \varphi_h\|_{0,\Omega}$.

Proof. The proof relies on estimates (5.1) and (5.2), in conjunction with the smallness assumption and the approximation properties of the spaces stated in Propositions 3.1, 3.2, 3.3, and in [13]. □

6 Numerical results

In this section we illustrate the accuracy and performance of the proposed scheme (cf. Section 3) through several numerical experiments. We show the optimal behaviour of the method under different polytopal meshes. Finally, we simulate an application-oriented problem.

We define the total computable error via the local polynomial approximation of the discrete solutions as $\bar{\mathrm{e}}_h^2 := \bar{\mathrm{e}}^2_{\boldsymbol{\sigma}_h^{\sqcap}} + \bar{\mathrm{e}}^2_{\boldsymbol{u}_h} + \bar{\mathrm{e}}^2_{\boldsymbol{z}_h^{\Pi}} + \bar{\mathrm{e}}^2_{p_h} + \bar{\mathrm{e}}^2_{\boldsymbol{\zeta}_h^{\Pi}} + \bar{\mathrm{e}}^2_{\varphi_h}$, with

$$\begin{aligned}
\bar{\mathrm{e}}^2_{\boldsymbol{\sigma}_h^{\sqcap}} &:= \|\boldsymbol{\sigma} - \sqcap_k^{\mathcal{C},K}\boldsymbol{\sigma}_h\|^2_{0,\Omega} + \|\,\mathbf{div}\,\boldsymbol{\sigma} - \mathbf{div}\,\boldsymbol{\sigma}_h\|^2_{0,\Omega}, \quad \bar{\mathrm{e}}^2_{\boldsymbol{u}_h} := \|\boldsymbol{u} - \boldsymbol{u}_h\|^2_{0,\Omega},\\
\bar{\mathrm{e}}^2_{\boldsymbol{z}_h^{\Pi}} &:= \|\boldsymbol{z} - \boldsymbol{\Pi}_{\overline{k}}^{0,K}\boldsymbol{z}_h\|^2_{0,\Omega} + \|\,\mathrm{div}\,\boldsymbol{z} - \mathrm{div}\,\boldsymbol{z}_h\|^2_{0,\Omega}, \quad \bar{\mathrm{e}}^2_{p_h} := \|p - p_h\|^2_{0,\Omega},\\
\bar{\mathrm{e}}^2_{\boldsymbol{\zeta}_h^{\Pi}} &:= \|\boldsymbol{\zeta} - \boldsymbol{\Pi}_{\overline{k}}^{0,K}\boldsymbol{\zeta}_h\|^2_{4,0;\Omega} + \|\,\mathrm{div}\,\boldsymbol{\zeta} - \mathrm{div}\,\boldsymbol{\zeta}_h\|^2_{0,\Omega}, \quad \bar{\mathrm{e}}^2_{\varphi_h} := \|\varphi - \varphi_h\|^2_{0,\Omega}.
\end{aligned}$$

The experimental rate of convergence $r(\cdot)$ applied to the total error $\bar{\mathrm{e}}_h$ (or to any of its components) in the refinement $1 \leq j$ is computed from the formula $r(\bar{\mathrm{e}}_h)^{j+1} = \log(\bar{\mathrm{e}}_h^{j+1}/\bar{\mathrm{e}}_h^{j})/\log(h^{j+1}/h^j)$, where h^j denotes the mesh size in the refinement j. The fixed-point algorithm has stopping criterion driven based on the ℓ^2-norm of the increments (i.e., the difference between the DoFs at the iteration i and $i-1$ of the fixed-point algorithm) with a tolerance of 5×10^{-6}. We stress that these experiments were implemented in the library `VEM++` [21].

Finally, following [2, 47], we define the stabilisation term $S_1^{\mathcal{C},K}(\boldsymbol{\sigma}_h, \boldsymbol{\tau}_h) := (h_K \operatorname{tr}(\mathcal{C})/2)\int_{\partial K}\boldsymbol{\sigma}_h\boldsymbol{n}\cdot\boldsymbol{\tau}_h\boldsymbol{n}$, while $S_2^{0,K}(\cdot,\cdot)$ and $S_3^{0,\boldsymbol{\sigma}_h^{\sqcap},K}(\cdot,\cdot)$ are given by a scaled `DOFI-DOFI` stabilisation (see [37]), with respective scaling factors given by $\left\|\int_K \boldsymbol{\kappa}^{-1}\right\|_F$ and $|\int_K \varrho^{-1}(\boldsymbol{\sigma}_h^{\sqcap})|$, where $\|\cdot\|_F$ denotes the Frobenius norm of the matrix.

6.1 Convergence rates under uniform refinement: 2D case

For this test, the modulation parameter is prescribed as $\eta_1 = 10^{-3}$ (cf. (1.2)), whereas all remaining model parameters are fixed to unity. The smooth manufactured solutions are defined as follows

$$\boldsymbol{u}(x_1, x_2) = \left(\cos(4\pi x_1)\cos(4\pi x_2) + e^{-x_1}, \sin(4\pi x_1)\sin(4\pi x_2) + e^{-x_2}\right)^{\mathtt{t}},$$

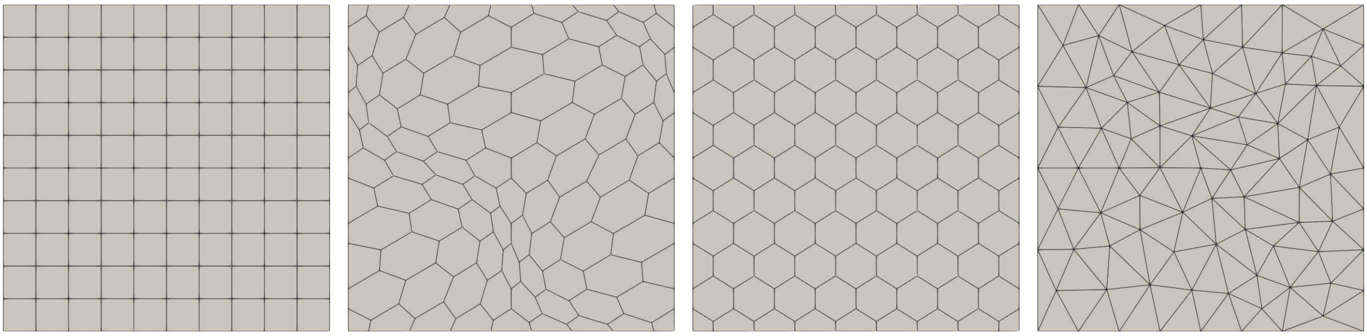

(a) Quadrilateral (b) Distorted (c) Hexahedral (d) Triangular

Figure 6.1: Example 1. Variety of 2D meshes used in the uniform refinement convergence test.

$$p(x_1,x_2) = \cos(2\pi x_1)\cos(2\pi x_2) + e^{x_2}, \quad \varphi(x_1,x_2) = \sin(2\pi x_1)\sin(2\pi x_2) + e^{x_1},$$

in the unit square domain $\Omega = (0,1)^2$ with the polygonal discretisations depicted in Figure 6.1, the boundary conditions are defined in the following sets: $\Gamma_{\mathrm{N}} = \{(x_1,x_2) \in \partial\Omega : x_1 = 0 \text{ or } x_2 = 0\}$ and $\Gamma_{\mathrm{D}} = \partial\Omega \setminus \Gamma_{\mathrm{N}}$. In particular, the right-hand sides functions ($\mathbf{f}$, g and ℓ) and the stress-dependent diffusivity (cf. (1.2)) are sufficiently smooth, as they are derived from the prescribed manufactured solutions. We recall that the polynomial order in two dimensions is given by k for both the Hellinger–Reissner VEM space and the mixed VEM space.

The error history is reported in Table 1. Here, we observe optimal rate of convergence $O(h^k)$ ($k = 1, 2$) as predicted by Corollary 5.2 for all the meshes listed in Figure 6.1. Moreover, we provided in detail the computable error for the variables of interest, obtaining their expected optimal convergence rates. The number of iterations required by the fixed-point algorithm to convergence are displayed in the last column. Snapshots of the variables of interest are shown in Figure 6.2 for the Hexahedral mesh (see Figure 6.1(c)) in the last refinement step with polynomial degree $k = 2$.

Finally, Table 2 illustrates the performance of the scheme under large variations of the physical parameters. The test considers nearly incompressible materials ($\lambda = 10^6$), very small storativity ($s_0 = 10^{-8}$), and weak Biot–Willis coupling ($\alpha = 10^{-6}$). The mesh is fixed to the Hexahedral case (cf. Figure 6.1(c)) and we set the polynomial degree $k = 1$. Once again, we observe the expected optimal convergence rates, confirming the robustness of the method in these extreme settings.

6.2 Convergence rates under uniform refinement: 3D case

We extend Example 6.1 by consider the unit cube domain $\Omega = (0,1)^3$ discretised using the polyhedral meshes illustrated in Figure 6.3, the sub-boundaries are defined by the sets $\Gamma_{\mathrm{N}} = \{(x_1,x_2,x_3) \in \partial\Omega : x_1 = 0 \text{ or } x_2 = 0 \text{ or } x_3 = 0\}$ and $\Gamma_{\mathrm{D}} = \partial\Omega \setminus \Gamma_{\mathrm{N}}$. We set unity model parameters and define the manufactured solutions by

$$\begin{gathered}\boldsymbol{u}(x_1,x_2,x_3) = \left(\cos(4\pi x_2)\cos(4\pi x_3) + e^{x_1}, \sin(4\pi x_1)\sin(4\pi x_3) + e^{x_2}, cos(4\pi x_3)sin(4\pi x_1) + e^{x_3}\right)^{\mathtt{t}}, \\ p(x_1,x_2,x_3) = \sin(2\pi x_2)\sin(2\pi x_3) + e^{x_1}, \quad \varphi(x_1,x_2,x_3) = \cos(2\pi x_1)\cos(2\pi x_2) + e^{x_3},\end{gathered}$$

where the polynomial order in this case is given by k for the Hellinger–Reissner and $k+1$ for the mixed VEM spaces. One more time, all the model parameters are fixed to unity except for the modulation parameter which now given by $\eta_1 = 10^{-5}$.

In three dimensions, the computational cost increases substantially, even in the lowest-case order $k = 1$; for example, the Hellinger–Reissner subsystem alone yields a linear system of dimension $542{,}925 \times 542{,}925$, with $100{,}405{,}246$ nonzero entries in the last refinement step of the Voronoi mesh (cf. Figure 6.3(c)). Such system sizes would normally pose a considerable challenge, both in terms of memory requirements and solution time. However, `VEM++` exploits parallelisation through `MPI` and its interface with `PETSc-MUMPS` (see [4,42]), which allows distributed assembly and the efficient solution of large-scale sparse systems. For this study, computations were performed on the NCI Gadi HPC cluster using the hugemem queue (1,5 TB of RAM per node with 48 CPUs), with 16 CPUs for the first two refinements, 32 CPUs for the third, and 64 CPUs for the final refinement, demonstrating both the scalability of the implementation and its robustness in handling high-dimensional three-dimensional problems.

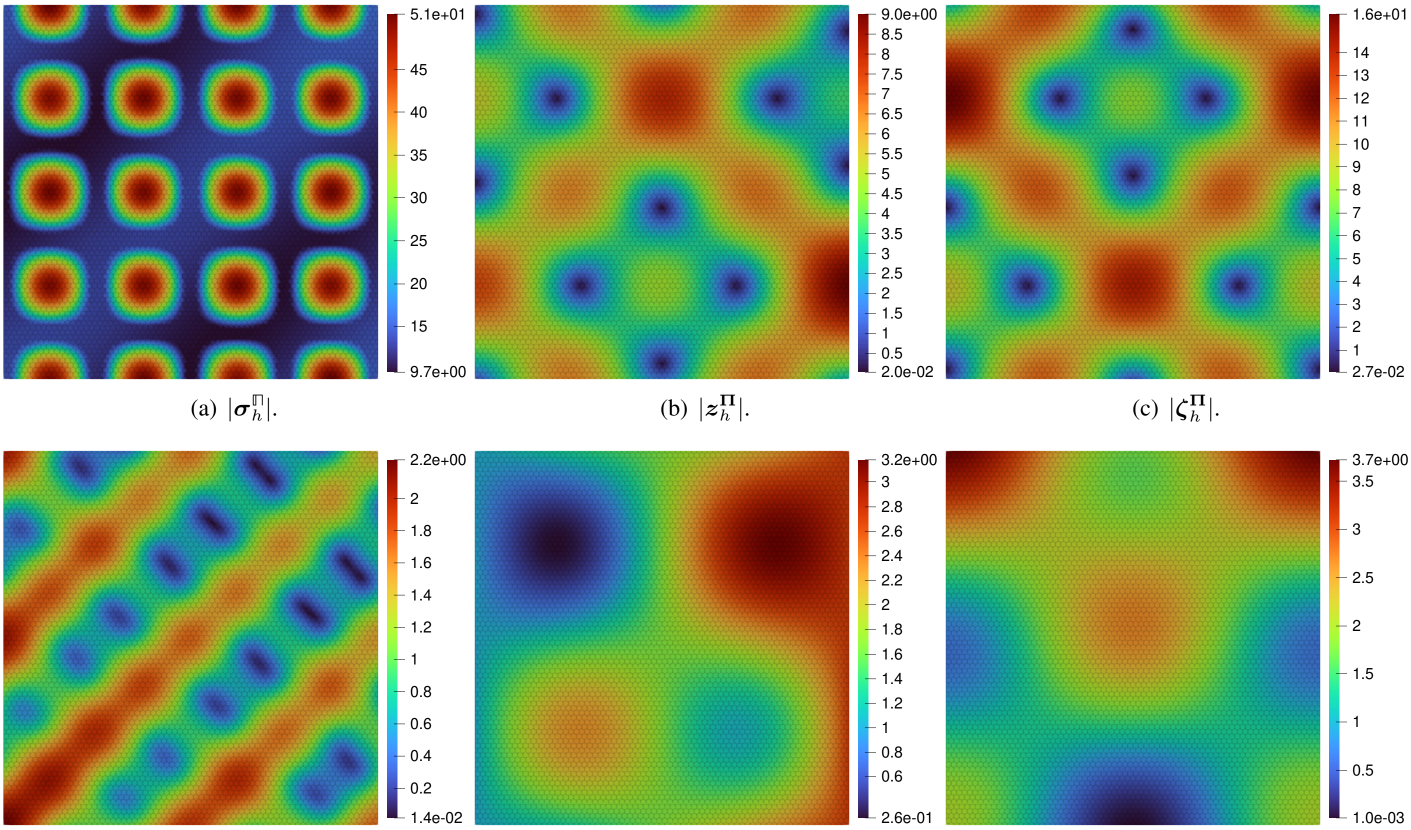

(a) $|\boldsymbol{\sigma}_h^{\Pi}|$. (b) $|\boldsymbol{z}_h^{\Pi}|$. (c) $|\boldsymbol{\zeta}_h^{\Pi}|$.

(d) $|\boldsymbol{u}_h|$. (e) p_h. (f) φ_h.

Figure 6.2: Example 1. Snapshots of the variables of interest for the Hexahedral mesh in the last refinement step with $k = 2$. The parameters are set to unity, except for $\eta_1 = 10^{-3}$.

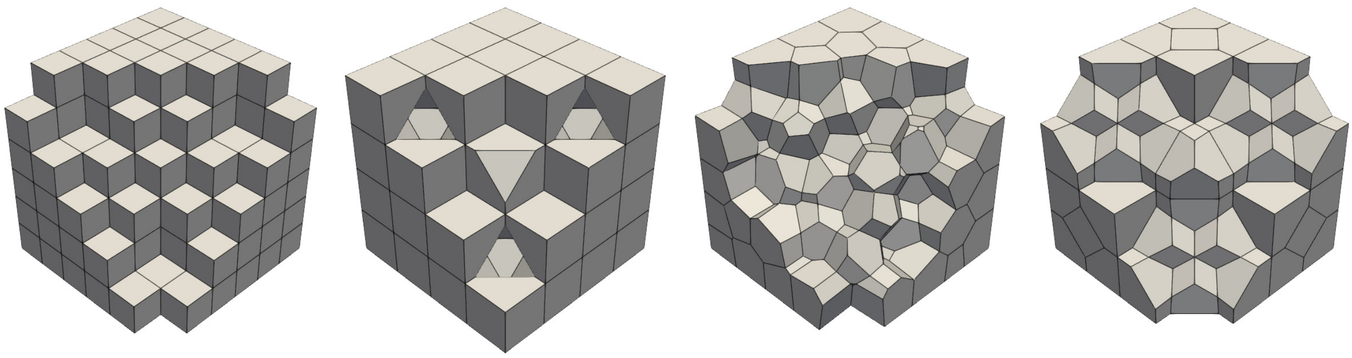

(a) Cubical (b) Octahedral (c) Voronoi (d) Nonahedral

Figure 6.3: Example 2. Cross-section of a variety of 3D meshes used in the uniform refinement convergence test.

We summarise the error history in Table 3. One more time, the prediction provided by Corollary 5.2 holds for all the meshes listed in Figure 6.3, we observe optimal rate of convergence $O(h^2)$. Snapshots of the variables of interest are shown in Figure 6.4 for the Voronoi mesh with 4,000 elements (last refinement step).

6.3 Sleep-driven molecular clearance within brain tissue

Neurodegenerative diseases such as Alzheimer's and dementia are linked to the accumulation of proteins (functional molecules) and metabolites (intermediate or residual products of metabolism) within brain tissue. To mitigate this, the brain enhances its clearance mechanisms during sleep. Studies indicate that sleep deprivation impairs molecular clearance, and this effect cannot be compensated for by an extra night's sleep [24]. Moreover, it has been shown that the cortical

k	$\mathcal{T}_h$	h	$\bar{e}_h$	$r(\bar{e}_h)$	$\bar{e}_{\boldsymbol{\sigma}_h^{\Pi}}$	$r(\bar{e}_{\boldsymbol{\sigma}_h^{\Pi}})$	$\bar{e}_{\boldsymbol{u}_h}$	$r(\bar{e}_{\boldsymbol{u}_h})$	$\bar{e}_{\boldsymbol{z}_h^{\Pi}}$	$r(\bar{e}_{\boldsymbol{z}_h^{\Pi}})$	$\bar{e}_{p_h}$	$r(\bar{e}_{p_h})$	$\bar{e}_{\zeta_h^{\Pi}}$	$r(\bar{e}_{\zeta_h^{\Pi}})$	$\bar{e}_{\varphi_h}$	$r(\bar{e}_{\varphi_h})$	it
1	Quadrilateral	1.00e-01	3.31e+01	*	3.29e+01	*	5.28e-01	*	1.66e+00	*	1.92e-02	*	2.90e+00	*	1.95e-02	*	3
		5.00e-02	8.65e+00	1.93	8.61e+00	1.93	7.61e-02	2.79	4.15e-01	2.00	4.85e-03	1.99	7.46e-01	1.96	4.88e-03	2.00	3
		2.50e-02	2.19e+00	1.99	2.17e+00	1.99	1.14e-02	2.74	1.00e-01	2.05	1.22e-03	2.00	1.97e-01	1.92	1.22e-03	2.00	3
		1.25e-02	5.48e-01	2.00	5.45e-01	2.00	2.06e-03	2.46	2.45e-02	2.03	3.04e-04	2.00	5.59e-02	1.82	3.05e-04	2.00	4
	Distorted	1.03e-01	4.07e+01	*	4.04e+01	*	9.22e-01	*	1.97e+00	*	2.42e-02	*	3.74e+00	*	2.54e-02	*	3
		5.07e-02	1.03e+01	1.93	1.03e+01	1.93	1.15e-01	2.93	4.64e-01	2.04	5.70e-03	2.04	8.95e-01	2.01	5.99e-03	2.04	3
		2.66e-02	2.79e+00	2.02	2.78e+00	2.02	1.81e-02	2.87	1.23e-01	2.06	1.53e-03	2.03	2.38e-01	2.05	1.59e-03	2.06	3
		1.32e-02	6.90e-01	2.00	6.87e-01	2.00	2.90e-03	2.63	3.00e-02	2.02	3.77e-04	2.01	5.88e-02	2.00	3.89e-04	2.01	3
	Hexahedral	1.03e-01	3.18e+01	*	3.16e+01	*	7.09e-01	*	1.49e+00	*	1.81e-02	*	2.83e+00	*	1.90e-02	*	3
		5.07e-02	7.79e+00	1.98	7.75e+00	1.98	8.71e-02	2.95	3.48e-01	2.04	4.32e-03	2.02	6.63e-01	2.04	4.44e-03	2.05	3
		2.66e-02	2.07e+00	2.05	2.06e+00	2.05	1.35e-02	2.88	9.16e-02	2.07	1.15e-03	2.05	1.74e-01	2.07	1.16e-03	2.07	3
		1.32e-02	5.11e-01	2.01	5.09e-01	2.01	2.16e-03	2.63	2.27e-02	2.00	2.84e-04	2.00	4.28e-02	2.01	2.86e-04	2.01	3
	Triangular	4.36e-02	8.51e+00	*	8.47e+00	*	6.32e-02	*	3.96e-01	*	4.44e-03	*	7.12e-01	*	4.74e-03	*	3
		2.55e-02	2.92e+00	1.99	2.91e+00	1.99	1.48e-02	2.70	1.42e-01	1.90	1.58e-03	1.92	2.44e-01	1.99	1.61e-03	2.00	3
		1.79e-02	1.46e+00	1.96	1.45e+00	1.96	6.15e-03	2.47	7.18e-02	1.93	7.97e-04	1.93	1.22e-01	1.94	8.08e-04	1.95	3
		1.39e-02	8.82e-01	1.98	8.78e-01	1.98	3.38e-03	2.37	4.36e-02	1.97	4.82e-04	1.99	7.33e-02	2.02	4.85e-04	2.02	3
2	Quadrilateral	1.00e-01	6.68e+00	*	6.66e+00	*	2.23e-01	*	1.98e-01	*	1.94e-03	*	3.32e-01	*	2.16e-03	*	3
		5.00e-02	8.71e-01	2.94	8.70e-01	2.94	1.47e-02	3.92	2.40e-02	3.05	2.45e-04	2.99	4.20e-02	2.98	2.72e-04	2.99	3
		2.50e-02	1.10e-01	2.99	1.10e-01	2.99	9.68e-04	3.92	2.70e-03	3.15	3.07e-05	3.00	5.25e-03	3.00	3.41e-05	3.00	3
		1.25e-02	1.38e-02	3.00	1.38e-02	3.00	7.12e-05	3.77	3.18e-04	3.09	3.84e-06	3.00	6.56e-04	3.00	4.27e-06	3.00	4
	Distorted	1.03e-01	9.66e+00	*	9.63e+00	*	4.39e-01	*	2.70e-01	*	2.87e-03	*	4.73e-01	*	3.16e-03	*	3
		5.07e-02	1.20e+00	2.94	1.20e+00	2.94	2.64e-02	3.96	3.34e-02	2.94	3.35e-04	3.03	5.62e-02	3.00	3.70e-04	3.02	3
		2.66e-02	1.67e-01	3.05	1.67e-01	3.05	1.98e-03	4.01	4.71e-03	3.03	4.62e-05	3.07	7.78e-03	3.06	5.11e-05	3.07	3
		1.32e-02	2.05e-02	3.01	2.04e-02	3.01	1.31e-04	3.89	5.88e-04	2.98	5.64e-06	3.01	9.53e-04	3.01	6.25e-06	3.01	3
	Hexahedral	1.03e-01	5.91e+00	*	5.89e+00	*	2.68e-01	*	1.58e-01	*	1.71e-03	*	2.80e-01	*	1.84e-03	*	3
		5.07e-02	7.02e-01	3.00	7.01e-01	3.00	1.52e-02	4.04	1.88e-02	3.00	1.98e-04	3.04	3.20e-02	3.05	2.09e-04	3.06	3
		2.66e-02	9.53e-02	3.09	9.52e-02	3.09	1.11e-03	4.06	2.54e-03	3.10	2.66e-05	3.11	4.36e-03	3.09	2.84e-05	3.09	3
		1.32e-02	1.17e-02	3.01	1.17e-02	3.01	7.39e-05	3.88	3.15e-04	3.00	3.25e-06	3.01	5.28e-04	3.02	3.45e-06	3.02	4
	Triangular	4.36e-02	8.58e-01	*	8.56e-01	*	1.29e-02	*	3.27e-02	*	2.54e-04	*	5.41e-02	*	3.42e-04	*	3
		2.55e-02	1.71e-01	3.00	1.71e-01	3.00	1.57e-03	3.91	6.21e-03	3.09	4.86e-05	3.07	1.03e-02	3.08	6.50e-05	3.09	3
		1.79e-02	6.39e-02	2.78	6.37e-02	2.78	4.19e-04	3.71	2.27e-03	2.83	1.77e-05	2.85	3.79e-03	2.82	2.39e-05	2.82	3
		1.39e-02	2.93e-02	3.08	2.93e-02	3.08	1.62e-04	3.75	1.05e-03	3.06	8.27e-06	3.01	1.72e-03	3.12	1.08e-05	3.13	4

Table 1: Example 1. Convergence history and fixed-point iteration count for a variety of 2D meshes with polynomial degrees $k = 1, 2$. The parameters are set to unity, except for $\eta_1 = 10^{-3}$.

	h	$\bar{e}_h$	$r(\bar{e}_h)$	$\bar{e}_{\boldsymbol{\sigma}_h^{\Pi}}$	$r(\bar{e}_{\boldsymbol{\sigma}_h^{\Pi}})$	$\bar{e}_{\boldsymbol{u}_h}$	$r(\bar{e}_{\boldsymbol{u}_h})$	$\bar{e}_{\boldsymbol{z}_h^{\Pi}}$	$r(\bar{e}_{\boldsymbol{z}_h^{\Pi}})$	$\bar{e}_{p_h}$	$r(\bar{e}_{p_h})$	$\bar{e}_{\zeta_h^{\Pi}}$	$r(\bar{e}_{\zeta_h^{\Pi}})$	$\bar{e}_{\varphi_h}$	$r(\bar{e}_{\varphi_h})$	it
$\lambda = 10^6$	1.03e-01	7.52e+02	*	7.22e+02	*	2.11e+02	*	1.43e+00	*	1.81e-02	*	1.50e+00	*	1.90e-02	*	1
	5.07e-02	1.61e+02	2.17	1.59e+02	2.13	2.30e+01	3.12	3.43e-01	2.01	4.32e-03	2.02	3.53e-01	2.04	4.44e-03	2.05	1
	2.66e-02	4.29e+01	2.05	4.27e+01	2.04	3.19e+00	3.06	9.12e-02	2.05	1.15e-03	2.05	9.26e-02	2.07	1.16e-03	2.07	1
	1.32e-02	1.04e+01	2.03	1.04e+01	2.03	3.85e-01	3.03	2.26e-02	2.00	2.84e-04	2.00	2.28e-02	2.01	2.86e-04	2.01	1
$s_0 = 10^{-8}$	1.03e-01	3.18e+01	*	3.16e+01	*	7.09e-01	*	1.49e+00	*	1.81e-02	*	2.83e+00	*	1.90e-02	*	3
	5.07e-02	7.79e+00	1.98	7.75e+00	1.98	8.71e-02	2.95	3.48e-01	2.04	4.32e-03	2.02	6.63e-01	2.04	4.44e-03	2.05	3
	2.66e-02	2.07e+00	2.05	2.06e+00	2.05	1.35e-02	2.88	9.16e-02	2.07	1.15e-03	2.05	1.74e-01	2.07	1.16e-03	2.07	3
	1.32e-02	5.11e-01	2.01	5.09e-01	2.01	2.16e-03	2.63	2.27e-02	2.00	2.84e-04	2.00	4.28e-02	2.01	2.86e-04	2.01	3
$\alpha = 10^{-6}$	1.03e-01	3.18e+01	*	3.16e+01	*	7.08e-01	*	1.43e+00	*	1.81e-02	*	2.91e+00	*	1.90e-02	*	3
	5.07e-02	7.79e+00	1.98	7.75e+00	1.98	8.70e-02	2.95	3.43e-01	2.01	4.32e-03	2.02	6.83e-01	2.04	4.44e-03	2.05	3
	2.66e-02	2.07e+00	2.05	2.06e+00	2.05	1.35e-02	2.88	9.12e-02	2.05	1.15e-03	2.05	1.79e-01	2.07	1.16e-03	2.07	3
	1.32e-02	5.11e-01	2.01	5.09e-01	2.01	2.16e-03	2.63	2.26e-02	2.00	2.84e-04	2.00	4.41e-02	2.01	2.86e-04	2.01	3

Table 2: Example 1. Convergence history and fixed-point iteration counts are shown for the Hexahedral mesh with polynomial degree $k = 1$ and extreme values for the parameters λ, s_0, and α. In each test, the remaining parameters are set to unity, except $\eta_1 = 10^{-3}$.

interstitial space in mice (the narrow, irregularly shaped region between neurons and blood vessels in the cerebral cortex) increases by more than 60% during sleep, resulting in more efficient clearance [48].

Experimentally, MRI scans can visualise the distribution of the fluorescent cerebrospinal fluid (CSF) tracer Gadobutrol within brain tissue under various conditions, including sleep and awake states [24] (see Figure 6.5). In this example,

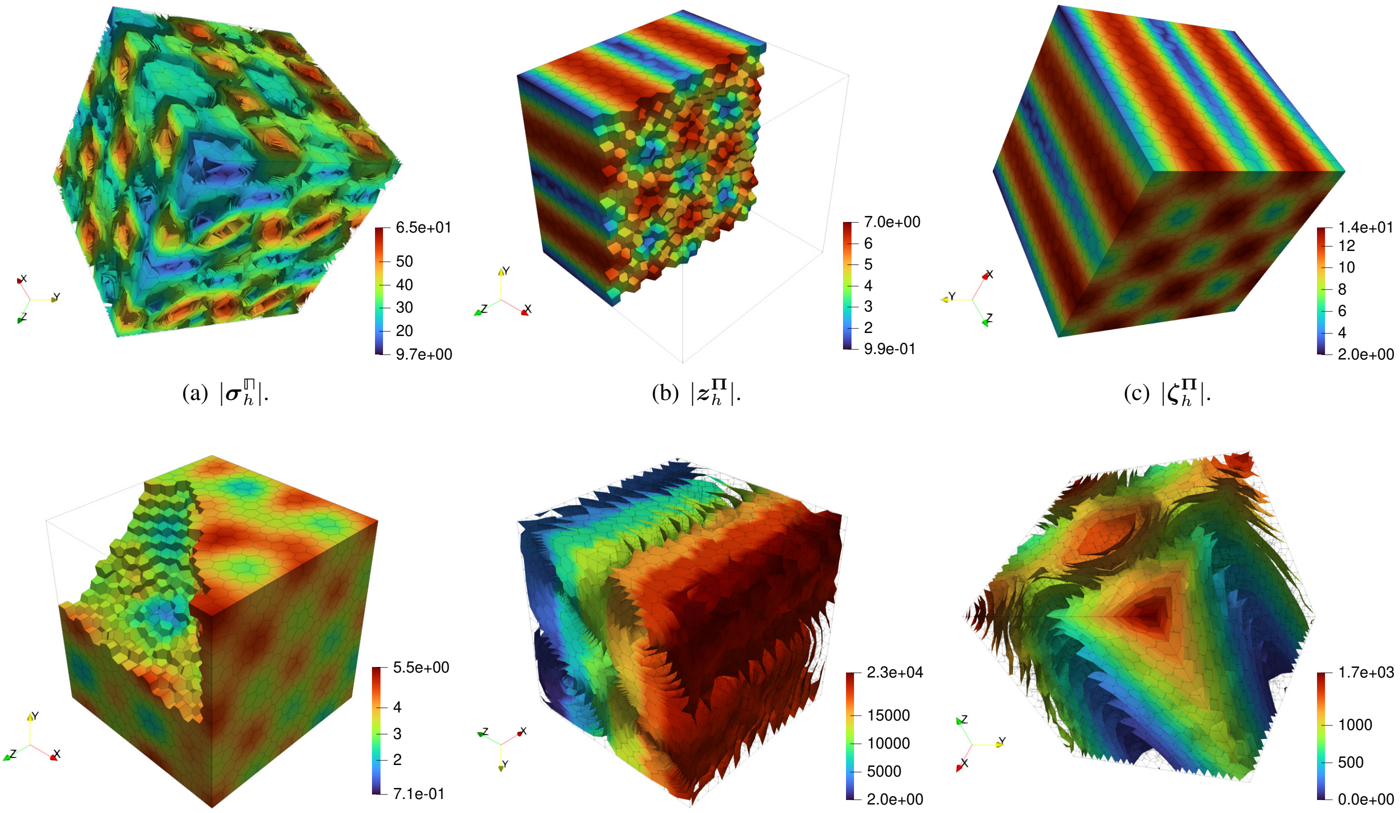

(a) $|\boldsymbol{\sigma}_h^{\sqcap}|$. (b) $|\boldsymbol{z}_h^{\boldsymbol{\Pi}}|$. (c) $|\zeta_h^{\boldsymbol{\Pi}}|$.

(d) $|\boldsymbol{u}_h|$. (e) p_h. (f) φ_h.

Figure 6.4: Example 2. Snapshots of the variables of interest for the Voronoi mesh in the last refinement step with $k = 1$. The modulation parameter is set to $\eta_1 = 10^{-5}$, while the remaining parameters are set to unity.

$\mathcal{T}_h$	h	$\bar{\mathrm{e}}_h$	$r(\bar{\mathrm{e}}_h)$	$\bar{\mathrm{e}}_{\boldsymbol{\sigma}_h^{\sqcap}}$	$r(\bar{\mathrm{e}}_{\boldsymbol{\sigma}_h^{\sqcap}})$	$\bar{\mathrm{e}}_{\boldsymbol{u}_h}$	$r(\bar{\mathrm{e}}_{\boldsymbol{u}_h})$	$\bar{\mathrm{e}}_{\boldsymbol{z}_h^{\boldsymbol{\Pi}}}$	$r(\bar{\mathrm{e}}_{\boldsymbol{z}_h^{\boldsymbol{\Pi}}})$	$\bar{\mathrm{e}}_{p_h}$	$r(\bar{\mathrm{e}}_{p_h})$	$\bar{\mathrm{e}}_{\zeta_h^{\boldsymbol{\Pi}}}$	$r(\bar{\mathrm{e}}_{\zeta_h^{\boldsymbol{\Pi}}})$	$\bar{\mathrm{e}}_{\varphi_h}$	$r(\bar{\mathrm{e}}_{\varphi_h})$	it
Cubical	2.17e-01	6.07e+01	*	6.04e+01	*	3.14e-01	*	2.36e+00	*	2.97e-02	*	4.69e+00	*	2.98e-02	*	2
	1.44e-01	2.84e+01	1.87	2.83e+01	1.87	1.05e-01	2.71	1.06e+00	1.97	1.34e-02	1.97	2.11e+00	1.97	1.34e-02	1.97	2
	1.08e-01	1.63e+01	1.94	1.62e+01	1.93	5.44e-02	2.29	6.01e-01	1.98	7.56e-03	1.98	1.19e+00	1.99	7.57e-03	1.99	2
	8.66e-02	1.05e+01	1.96	1.05e+01	1.96	3.40e-02	2.11	3.85e-01	1.99	4.85e-03	1.99	7.65e-01	1.99	4.85e-03	1.99	2
Octahedral	2.08e-01	5.81e+01	*	5.79e+01	*	2.88e-01	*	2.22e+00	*	2.78e-02	*	4.39e+00	*	2.79e-02	*	2
	1.04e-01	1.53e+01	1.93	1.52e+01	1.93	5.07e-02	2.50	5.67e-01	1.97	7.08e-03	1.98	1.12e+00	1.98	7.08e-03	1.98	2
	8.33e-02	9.85e+00	1.96	9.82e+00	1.96	3.18e-02	2.09	3.66e-01	1.96	4.54e-03	1.99	7.16e-01	1.99	4.54e-03	1.99	3
	6.94e-02	6.87e+00	1.97	6.85e+00	1.97	2.19e-02	2.04	2.56e-01	1.96	3.16e-03	1.99	4.98e-01	1.99	3.16e-03	1.99	2
Voronoi	3.59e-01	1.43e+02	*	1.42e+02	*	1.50e+00	*	6.94e+00	*	8.81e-02	*	1.33e+01	*	8.53e-02	*	2
	1.80e-01	4.39e+01	1.70	4.38e+01	1.70	1.91e-01	2.98	1.63e+00	2.09	2.04e-02	2.11	3.21e+00	2.05	2.04e-02	2.07	2
	8.98e-02	1.12e+01	1.97	1.11e+01	1.97	3.71e-02	2.36	4.33e-01	1.91	5.16e-03	1.98	8.13e-01	1.98	5.16e-03	1.98	2
	7.19e-02	7.21e+00	1.97	7.18e+00	1.97	2.35e-02	2.05	2.85e-01	1.87	3.31e-03	1.99	5.21e-01	2.00	3.31e-03	1.99	4
Nonahedral	3.46e-01	1.27e+02	*	1.27e+02	*	1.41e+00	*	5.54e+00	*	7.01e-02	*	1.08e+01	*	6.99e-02	*	2
	1.73e-01	3.64e+01	1.81	3.63e+01	1.80	1.59e-01	3.15	1.42e+00	1.97	1.77e-02	1.99	2.66e+00	2.03	1.69e-02	2.05	2
	1.37e-01	2.32e+01	1.95	2.32e+01	1.95	8.70e-02	2.60	8.90e-01	2.01	1.10e-02	2.04	1.68e+00	1.98	1.07e-02	1.98	2
	1.09e-01	1.48e+01	1.97	1.47e+01	1.97	5.12e-02	2.29	5.67e-01	1.95	6.90e-03	2.03	1.07e+00	1.97	6.78e-03	1.97	2

Table 3: Example 2. Convergence history and fixed-point iteration count for a variety of 3D meshes for the lowest-case order $k = 1$. We considered unit parameters except for $\eta_1 = 10^{-5}$.

we focus on the mathematical modelling of this process by tracking the concentration of the CSF tracer under sleep and awake states in coronal slices of the brain. The mesh originally introduced in [9] provides the geometry of the coronal slice boundary. We extend this geometry by including the left, right, and bottom ventricles, and employ the capabilities of `PolyMesher` [43] to discretise the domain with 19,999 Voronoi cells.

Following [33], we neglect convection and assume that stress-dependent diffusion is the dominant transport mechanism. This assumption is supported by experimental data indicating that transport within brain tissue occurs $5-26\%$ faster than

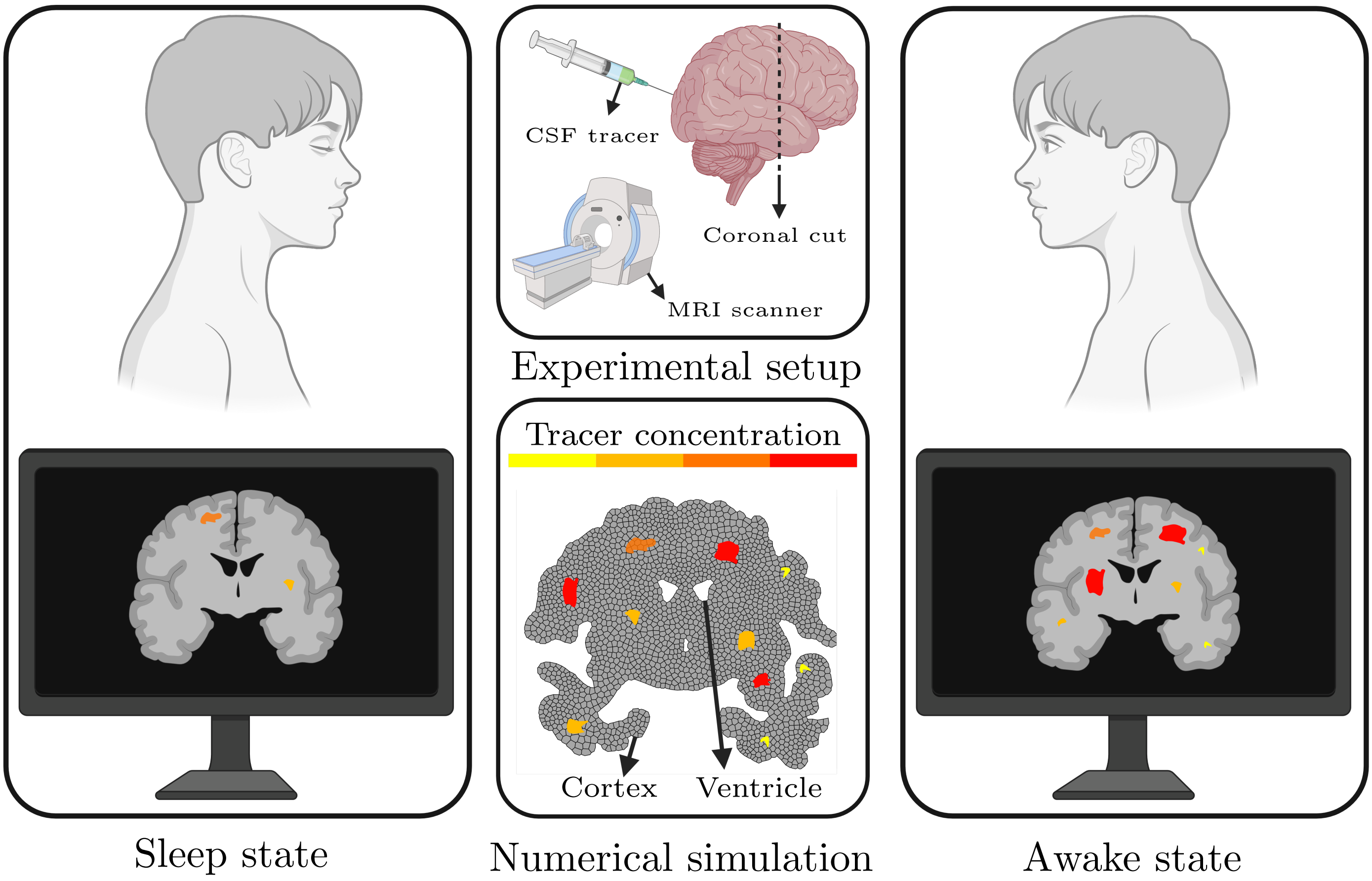

Figure 6.5: Example 3. Two-dimensional schematic illustration of molecular clearance in brain tissue of a fluorescent CSF tracer. The experimental setup is shown at the top middle. The MRI scans for the sleep and awake states are shown on the left and right pannels. The bottom middle panels show the expected CSF tracer concentration computational simulations in a polytopal mesh of a coronal slice of the brain with 1,999 Voronoi cells.

predicted by Fickian diffusion [45]. The expansion of the cortical interstitial space during sleep leads to an increase in the volume fraction of brain tissue [48]. This can be measured as a porosity of $\phi = 0.14$ in the awake state and $\phi = 0.23$ in the sleep state.

We imposed a compression condition $\boldsymbol{\sigma}\boldsymbol{n} = -(p_0\pi/2)\boldsymbol{n}$ on the brain cortex and clamped the brain tissue along the three ventricles. In addition, a ventricular pressure of $p_D = p_0$ is prescribed, while no filtration flux is imposed in the cortex. The initial concentration of the CSF tracer Gadobutrol is assumed to be uniformly distributed within the brain cortex, with a value of $\varphi_0 = 6.05 \times 10^{-4}\mathrm{g/mm^3}$. We adimensionalise the concentration using this quantity and set the boundary condition $\varphi_D = 1$; no CSF tracer flux is allowed through the ventricles. Finally, we assume that no external forces act in the simulation; that is, the right-hand sides $\boldsymbol{f}$, g, and ℓ are set to zero.

The stress-assisted diffusion coefficient is modified from (1.2) and now takes the form

$$\varrho(\boldsymbol{\sigma}) = \frac{\varrho_0}{\varphi_0\phi}\left(1 + \exp(-\eta[\mathrm{tr}\,\boldsymbol{\sigma}]^2)\right),$$

where $\varrho_0 = 5.30 \times 10^{-2}\mathrm{mm^3/s}$ and $\eta = 2.00 \times 10^{-1}$. The coupling parameters are set to $\alpha = 1$, $\beta = 0.35$. Relevant parameters associated with the brain transport problem including mechanical properties of brain tissue are given next (see [14, 20, 46]):

$$E = 8.00 \times 10^2\mathrm{g/mm\,s^2}, \quad \nu = 0.495, \quad \lambda = \frac{E\nu}{(1+\nu)(1-2\nu)}, \quad \mu = \frac{E}{2(1+\nu)},$$
$$\kappa_0 = 1.43 \times 10^{-5}\mathrm{g\,mm/s^3}, \quad \boldsymbol{\kappa} = \kappa_0\mathbb{I}, \quad s_0 = 2.00 \times 10^{-8}\mathrm{mm\,s^2/g}.$$

We report snapshots of the approximated variables of interest φ_h, $\boldsymbol{u}_h$, $\boldsymbol{\sigma}_h^{\Pi}$, and $\boldsymbol{z}_h^{\boldsymbol{\Pi}}$ for the lowest order VEM scheme (cf. Section 3) in Figure 6.6. The sleep state is displayed in the left column, and the awake state in the middle column.

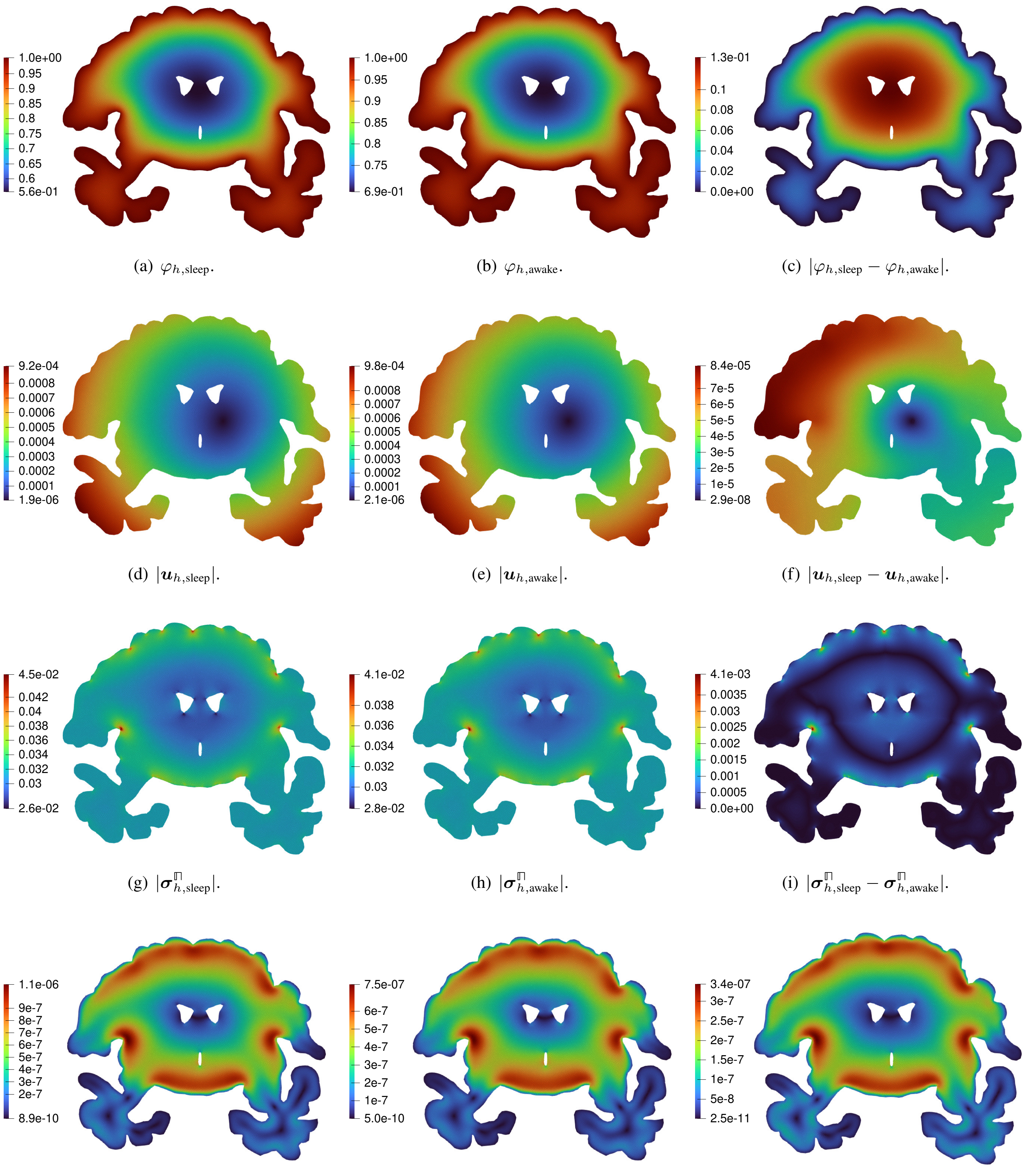

(a) $\varphi_{h,\text{sleep}}$. (b) $\varphi_{h,\text{awake}}$. (c) $|\varphi_{h,\text{sleep}} - \varphi_{h,\text{awake}}|$.

(d) $|\boldsymbol{u}_{h,\text{sleep}}|$. (e) $|\boldsymbol{u}_{h,\text{awake}}|$. (f) $|\boldsymbol{u}_{h,\text{sleep}} - \boldsymbol{u}_{h,\text{awake}}|$.

(g) $|\boldsymbol{\sigma}^{\Pi}_{h,\text{sleep}}|$. (h) $|\boldsymbol{\sigma}^{\Pi}_{h,\text{awake}}|$. (i) $|\boldsymbol{\sigma}^{\Pi}_{h,\text{sleep}} - \boldsymbol{\sigma}^{\Pi}_{h,\text{awake}}|$.

(j) $|\boldsymbol{z}^{\Pi}_{h,\text{sleep}}|$. (k) $|\boldsymbol{z}^{\Pi}_{h,\text{awake}}|$. (l) $|\boldsymbol{z}^{\Pi}_{h,\text{sleep}} - \boldsymbol{z}^{\Pi}_{h,\text{awake}}|$.

Figure 6.6: Example 3. Snapshots of the variables of interest for the sleep-driven metabolite clearance within brain tissue simulation. The geometry of the human brain is discretised with 19,999 Voronoi cells and the polynomial degree for the VEM scheme is set to $k = 1$.

The right column illustrates the difference between the two states. The simulation results indicate that the CSF tracer concentration is approximately 13% higher in the awake state, particularly in the region adjacent to the ventricles. The computational results reproduce the experimentally observed differences in CSF tracer concentration clearance between the awake and sleep states, indicating that stress-dependent diffusion can play a key role in this process.

Acknowledgements

We are thankful to Abner J. Salgado for pointing out a potential issue in the regularity of the auxiliary problem needed in Lemma 2.4. We also thank Michele Visinoni for his support in several aspects regarding the VEM implementation for the Hellinger–Reissner subproblem, and Miroslav Kuchta for providing the brain geometries used in our last example.

This work has been supported by the Australian Research Council through the Future Fellowship grant FT220100496 and Discovery Project grant DP22010316; and by Vicerrectoría de Investigación project C3088, Sede de Occidente, Universidad de Costa Rica. Computational resources were provided by Monash eResearch, in partnership with the Faculties of Science, Engineering and IT, through the Monash allocation scheme on the National Computational Infrastructure (NCI), Australia (2025).

References

[1] E. Artioli, S. De Miranda, C. Lovadina, and L. Patruno, *A stress/displacement virtual element method for plane elasticity problems*, Computer Methods in Applied Mechanics and Engineering, 325 (2017), pp. 155–174.

[2] ——, *A family of virtual element methods for plane elasticity problems based on the Hellinger–Reissner principle*, Computer Methods in Applied Mechanics and Engineering, 340 (2018), pp. 978–999.

[3] ——, *A dual hybrid virtual element method for plane elasticity problems*, ESAIM: Mathematical Modelling and Numerical Analysis, 54 (2020), pp. 1725–1750.

[4] S. Balay, S. Abhyankar, M. F. Adams, S. Benson, J. Brown, P. Brune, K. Buschelman, E. M. Constantinescu, L. Dalcin, A. Dener, et al., *Petsc/tao users manual revision 3.23*, tech. rep., Argonne National Laboratory (ANL), Argonne, IL (United States), 03 2025.

[5] L. Beirão da Veiga, F. Brezzi, L. D. Marini, and A. Russo, *H(div) and H(curl)-conforming VEM*, Numerische Mathematik, 133 (2016), p. 303–332.

[6] ——, *Mixed virtual element methods for general second order elliptic problems on polygonal meshes*, ESAIM: Mathematical Modelling and Numerical Analysis, 50 (2016), pp. 727–747.

[7] L. Beirão da Veiga, L. Mascotto, and J. Meng, *Interpolation and stability estimates for edge and face virtual elements of general order*, Mathematical Models and Methods in Applied Sciences, 32 (2022), pp. 1589–1631.

[8] D. Boffi, F. Brezzi, and M. Fortin, *Mixed Finite Element Methods and Applications*, vol. 44, Springer-Verlag, Berlin, 2013.

[9] W. M. Boon, M. Hornkjøl, M. Kuchta, K.-A. Mardal, and R. Ruiz-Baier, *Parameter-robust methods for the Biot–Stokes interfacial coupling without Lagrange multipliers*, Journal of Computational Physics, 467 (2022), pp. e111464(1–25).

[10] L. Botti, M. Botti, and D. A. Di Pietro, *A Hybrid High-Order method for multiple-network poroelasticity*, in Polyhedral Methods in Geosciences, Springer, 2021, pp. 227–258.

[11] M. Botti, L. Mascotto, G. Vacca, and M. Visinoni, *Stability and interpolation estimates of Hellinger-Reissner virtual element spaces*, arXiv preprint, 2502.06286 (2025). Available at https://arxiv.org/abs/2502.06286.

[12] M. Botti, D. Prada, A. Scotti, and M. Visinoni, *Fully-mixed virtual element method for the biot problem*, arXiv preprint, 2504.17729 (2025). Available at https://arxiv.org/abs/2504.17729.

[13] S. Brenner and R. Scott, *The mathematical theory of finite element methods*, Springer, 2008.

[14] S. Budday, R. Nay, R. de Rooij, P. Steinmann, T. Wyrobek, T. C. Ovaert, and E. Kuhl, *Mechanical properties of gray and white matter brain tissue by indentation*, Journal of the Mechanical Behavior of Biomedical Materials, 46 (2015), pp. 318–330.

[15] J. Camaño, G. N. Gatica, R. Oyarzúa, R. Ruiz-Baier, and P. Venegas, *New fully-mixed finite element methods for the Stokes-Darcy coupling*, Computer Methods in Applied Mechanics and Engineering, 295 (2015), pp. 362–395.

[16] J. Careaga, G. N. Gatica, C. Inzunza, and R. Ruiz-Baier, *New Banach spaces-based mixed finite element methods for the coupled poroelasticity and heat equations*, IMA Journal of Numerical Analysis, 45 (2025), pp. 1936–1984.

[17] S. Carrasco, S. Caucao, and G. N. Gatica, *A twofold perturbed saddle point-based fully mixed finite element method for the coupled Brinkman–Forchheimer/Darcy problem*, Tech. Rep. Preprint 2024-25, Centro de Investigación en Ingeniería Matemática (CI²MA), Universidad de Concepción, 2025. Available at https://www.ci2ma.udec.cl/publicaciones/prepublicaciones.

[18] E. Colmenares, G. N. Gatica, and S. Moraga, *A Banach spaces-based analysis of a new fully-mixed finite element method for the Boussinesq problem*, ESAIM: Mathematical Modelling and Numerical Analysis, 54 (2020), pp. 1525–1568.

[19] C. I. Correa and G. N. Gatica, *On the continuous and discrete well-posedness of perturbed saddle-point formulations in Banach spaces*, Computers & Mathematics with Applications. An International Journal, 117 (2022), pp. 14–23.

[20] M. Corti, P. F. Antonietti, L. Dede', and A. M. Quarteroni, *Numerical modeling of the brain poromechanics by high-order discontinuous Galerkin methods*, Mathematical Models and Methods in Applied Sciences, 33 (2023), pp. 1577–1609.

[21] F. Dassi, *VEM++, a C++ library to handle and play with the virtual element method*, Numer. Algor., (2025).

[22] F. Dassi, C. Lovadina, and M. Visinoni, *A three-dimensional Hellinger-Reissner virtual element method for linear elasticity problems*, Computer Methods in Applied Mechanics and Engineering, 364 (2020), p. 112910.

[23] J. Droniou, G. Enchéry, I. Faille, A. Haidar, and R. Masson, *A bubble VEM-fully discrete polytopal scheme for mixed-dimensional poromechanics with frictional contact at matrix–fracture interfaces*, Computer Methods in Applied Mechanics and Engineering, 422 (2024), p. 116838.

[24] P. K. Eide, V. Vinje, A. H. Pripp, K.-A. Mardal, and G. Ringstad, *Sleep deprivation impairs molecular clearance from the human brain*, Brain, 144 (2021), pp. 863–874.

[25] A. Ern and J.-L. Guermond, *Finite elements II—Galerkin approximation, elliptic and mixed PDEs*, vol. 73 of Texts in Applied Mathematics, Springer, Cham, (2021).

[26] G. N. Gatica and L. F. Gatica, *On the a priori and a posteriori error analysis of a two-fold saddle-point approach for nonlinear incompressible elasticity*, International Journal for Numerical Methods in Engineering, 68 (2006), pp. 861–892.

[27] G. N. Gatica, B. Gómez-Vargas, and R. Ruiz-Baier, *Analysis and mixed-primal finite element discretisations for stress-assisted diffusion problems*, Computer Methods in Applied Mechanics and Engineering, 337 (2018), pp. 411–438.

[28] ——, *Formulation and analysis of fully-mixed finite element methods for stress-assisted diffusion problems*, Computers & Mathematics with Applications, 77 (2019), pp. 1312–1330.

[29] ——, *A posteriori error analysis of mixed finite element methods for stress-assisted diffusion problems*, Journal of Computational and Applied Mathematics, 409 (2022), pp. e114144(1–23).

[30] G. N. Gatica and F. A. Sequeira, *An L^p spaces-based mixed virtual element method for the two-dimensional Navier–Stokes equations*, Mathematical Models and Methods in Applied Sciences, 31 (2021), pp. 2937–2977.

[31] Z. Gharibi, *Mixed virtual element approximation for the five-field formulation of the steady Boussinesq problem with temperature-dependent parameters*, Journal of Scientific Computing, 102 (2025), p. 4.

[32] Z. Gharibi, M. Dehghan, and R. Ruiz-Baier, *A stabilization-free mixed virtual element approximation for unsteady non-Newtonian pseudoplastic Stokes flows*, Mathematical Models and Methods in Applied Sciences, (2025), p. to appear.

[33] B. Gómez-Vargas, K.-A. Mardal, R. Ruiz-Baier, and V. Vinje, *Twofold saddle-point formulation of Biot poroelasticity with stress-dependent diffusion*, SIAM Journal on Numerical Analysis, 63 (2023), pp. 1449–1481.

[34] J. Guo and M. Feng, *A robust and mass conservative virtual element method for linear three-field poroelasticity*, Journal of Scientific Computing, 92 (2022), p. 95.

[35] D. Jerison and C. E. Kenig, *The inhomogeneous Dirichlet problem in Lipschitz domains*, Journal of Functional Analysis, 130 (1995), pp. 161–219.

[36] A. Khan, B. P. Lamichhane, R. Ruiz-Baier, and S. Villa-Fuentes, *A priori and a posteriori error bounds for the fully mixed FEM formulation of poroelasticity with stress-dependent permeability*, IMA Journal of Numerical Analysis, in press (2025).

[37] R. Khot, A. E. Rubiano, and R. Ruiz-Baier, *Robust virtual element methods for coupled stress-assisted diffusion problems*, SIAM Journal on Scientific Computing, 47 (2025), pp. A497–A526.

[38] S. Kumar, D. Mora, R. Ruiz-Baier, and N. Verma, *Numerical solution of the Biot/elasticity interface problem using virtual element methods*, Journal of Scientific Computing, 98 (2024), p. 53.

[39] B. P. Lamichhane, R. Ruiz-Baier, and S. Villa-Fuentes, *New twofold saddle-point formulations for Biot poroelasticity with porosity-dependent permeability*, Results in Applied Mathematics, 21 (2024), pp. e100438(1–22).

[40] H. Liang and H. Rui, *A parameter robust reconstruction nonconforming virtual element method for the incompressible poroelasticity model*, Applied Numerical Mathematics, 202 (2024), pp. 127–142.

[41] X. Liu and Z. Chen, *A virtual element method for overcoming locking phenomena in Biot's consolidation model*, ESAIM: Mathematical Modelling and Numerical Analysis, 57 (2023), pp. 3007–3027.

[42] Message Passing Interface Forum, *MPI: A Message-Passing Interface Standard Version 4.1*, November 2023.

[43] C. Talischi, G. H. Paulino, A. Pereira, and I. F. M. Menezes, *Polymesher: a general-purpose mesh generator for polygonal elements written in matlab*, Structural and Multidisciplinary Optimization, 45 (2012), pp. 309–328.

[44] X. Tang, Z. Liu, B. Zhang, and M. Feng, *On the locking-free three-field virtual element methods for Biot's consolidation model in poroelasticity*, ESAIM: Mathematical Modelling and Numerical Analysis, 55 (2021), pp. S909–S939.

[45] L. M. Valnes, S. K. Mitusch, G. Ringstad, P. K. Eide, S. W. Funke, and K.-A. Mardal, *Apparent diffusion coefficient estimates based on 24 hours tracer movement support glymphatic transport in human cerebral cortex*, Scientific Reports, 10 (2020), p. 9176.

[46] V. Vinje, A. Eklund, K.-A. Mardal, M. E. Rognes, and K.-H. Støverud, *Intracranial pressure elevation alters csf clearance pathways*, Fluids and Barriers of the CNS, 17 (2020), p. 29.

[47] M. Visinoni, *A family of three-dimensional virtual elements for Hellinger-Reissner elasticity problems*, Computers & Mathematics with Applications, 155 (2024), pp. 97–109.

[48] L. Xie, H. Kang, Q. Xu, M. J. Chen, Y. Liao, M. Thiyagarajan, J. O'Donnell, D. J. Christensen, C. Nicholson, J. J. Iliff, T. Takano, R. Deane, and M. Nedergaard, *Sleep drives metabolite clearance from the adult brain*, Science, 342 (2013), pp. 373–377.